

# **Exploring Graphene Oxide in Environmentally Altered Graphite: A Link Between Chemistry and Archaeology**

by

©Amir Joorab Doozha

A Dissertation submitted to the School of Graduate Studies in partial fulfillment of the requirements for the degree of

**Ph.D.**

**Department of Chemistry**

Memorial University of Newfoundland

**November 2019**

St. John's

Newfoundland

# Abstract

Graphene oxide (GO) has drawn a great deal of attention, in a laboratory setting, due to its ability to stay suspended in water more easily for solution processing of graphene. In an outdoor setting, it is possible that GO is formed as graphite degrades over time in charred carbon-rich materials such as archaeological charcoal. This GO could be used as a valuable source for radiocarbon dating because its carbon would have the same age as the graphitic carbon that is traditionally extracted for dating. Before radiocarbon dating, graphitic samples are cleaned using a series of strong acid and base treatments to remove contaminants. However, this cleaning procedure can break down some graphite-based samples, leaving no graphite for  $^{14}\text{C}$  dating. In those situations, we suspect that GO is cleaned away along with the unwanted contaminants. Our studies are the first to consider whether GO exists in archaeological charcoal and if it can be separated effectively from carbon-containing contaminants. These findings will be particularly useful for chemists and environmental scientists who work with natural sources of graphite in which oxidized graphenic materials may be present.

Here, we show that a mixture of oxidized graphenic material with different degrees of oxidation, and fluorescent carbon-based materials, can be present in archaeological charcoal. We also develop a straightforward protocol that separates a simple test case of a lab-prepared mixture of these components. Our results help to explain why a significant amount of archaeological charcoal is sometimes lost during aqueous

cleaning treatments at different pH values.

The fluorescent carbon-based materials described above could originate from either the original graphite (in the form of highly oxidized pieces, called oxidative debris (OD)) or from contaminants (such as humic acid (HA)). The fluorescent materials stay suspended in alkaline aqueous solutions. Although UV-Vis data of base-treated archaeological charcoal shows evidence of oxidized carbon, it is not informative enough to study a mixture of oxidized graphite, OD, and HA. Therefore, we monitor UV absorption at specific wavelengths as a function of retention time using size exclusion chromatography (SEC). Our results demonstrate that distinguishing oxidized graphite, OD, and HA from each other is very challenging. Based on SEC results, we identify materials in archaeological charcoal that have similar UV excitation responses and similar retention time (size) to a common HA standard, as well as other components with similar UV excitation responses at longer retention times (smaller sizes).

# Acknowledgements

I would love to thank my supervisor Dr. Kristin M. Poduska for her great support and exceptional advice during my Ph.D. period.

I would like to thank my friends for their collaboration and brilliant ideas. I would also love to express my appreciation for my beloved wife, Nastaran Hosseinsarraf, who has supported me during these years to make such an impressive achievement.

This project would have been impossible without financial support from my supervisor's NSERC grants. Moreover, I especially want to thank the Chemistry Department at Memorial University for providing excellent resources to support my research.

# Table of Contents

<b>Abstract</b>	<b>ii</b>
<b>Acknowledgments</b>	<b>iv</b>
<b>List of Tables</b>	<b>ix</b>
<b>List of Figures</b>	<b>xvi</b>
<b>List of Abbreviations and Symbols</b>	<b>xvii</b>
<b>1 Introduction</b>	<b>1</b>
1.1 Graphenic carbon materials . . . . .	2
1.1.1 Graphite . . . . .	2
1.1.2 Graphene . . . . .	3
1.1.3 Graphene Oxide (GO) . . . . .	4
1.1.4 Oxidative debris (OD) . . . . .	6
1.2 Radiocarbon dating ( $^{14}\text{C}$ ) . . . . .	7
1.2.1 $^{14}\text{C}$ production and decay . . . . .	8
1.2.2 $^{14}\text{C}$ measurement . . . . .	8
1.3 Radiocarbon samples . . . . .	9
1.3.1 Carbonaceous contaminants . . . . .	10

1.3.2	Graphite sample cleaning for radiocarbon dating . . . . .	11
1.4	Thesis objectives . . . . .	14
1.5	Copyright and authorship statement . . . . .	16
	Bibliography . . . . .	17
<b>2</b>	<b>Materials and Methods</b>	<b>26</b>
2.1	Materials . . . . .	26
2.1.1	Graphite flakes . . . . .	27
2.1.2	As-prepared oxidized graphite (aOG) . . . . .	27
2.1.3	Modern charcoal . . . . .	27
2.1.4	Archaeological charcoal . . . . .	27
2.1.5	Coal . . . . .	28
2.1.6	Humic acid (HA) . . . . .	28
2.2	Sample separation methods . . . . .	28
2.2.1	Separation of GO and OD from aOG . . . . .	29
2.2.2	ABA treatment . . . . .	29
2.2.3	Water-Sonication-Base-Acid (WSBA) . . . . .	30
2.3	Characterization methods . . . . .	30
2.3.1	Raman spectroscopy . . . . .	31
2.3.2	IR spectroscopy . . . . .	33
2.3.3	pH measurements . . . . .	35
2.3.4	UV-Vis spectroscopy . . . . .	35
2.3.5	Size exclusion chromatography (SEC) . . . . .	37
2.3.6	Optical microscopy . . . . .	39
	Bibliography . . . . .	41

<b>3</b>	<b>Graphite oxidation chemistry is relevant for designing cleaning strategies for radiocarbon dating samples</b>	<b>45</b>
3.1	Introduction . . . . .	46
3.2	Experimental . . . . .	49
3.2.1	Oxidation of graphenic carbon materials . . . . .	49
3.2.2	Isolating GO and OD from oxidized graphenic carbon materials	50
3.2.3	Specimen characterization . . . . .	51
3.3	Results and discussion . . . . .	51
3.3.1	Separating mixtures with WSBA . . . . .	51
3.3.2	Interactions between GO and OD in water . . . . .	58
3.3.3	Comparing WSBA to radiocarbon sample cleaning protocols .	59
3.4	Conclusions . . . . .	63
3.5	Acknowledgements . . . . .	64
	Bibliography . . . . .	65
<b>4</b>	<b>Identifying and Extracting Oxidized Graphenic Materials from Environmentally Altered Sources of Graphite</b>	<b>73</b>
4.1	Introduction . . . . .	74
4.2	Experimental . . . . .	75
4.2.1	Materials . . . . .	75
4.2.2	Separation of oxidized materials using WSBA . . . . .	75
4.2.3	Characterization methods . . . . .	76
4.3	Results and discussion . . . . .	77
4.3.1	Uncleaned archaeological charcoal suspension . . . . .	77
4.3.2	Uncleaned archaeological charcoal (Raman analysis) . . . . .	79
4.3.3	Uncleaned archaeological charcoal (IR analysis) . . . . .	81
4.3.4	WSBA on archaeological charcoal . . . . .	84

4.4	Conclusions . . . . .	88
	Bibliography . . . . .	89
<b>5</b>	<b>Attempts to Differentiate Oxidized Graphenic Materials from Humic Acid in the Liquid Phase</b>	<b>91</b>
5.1	Introduction . . . . .	91
5.2	Experimental . . . . .	95
5.2.1	Materials . . . . .	95
5.2.2	Methods . . . . .	96
5.3	Results . . . . .	97
5.3.1	Effects of pH and solvent on bulk UV-Vis data . . . . .	97
5.3.2	aOG in acid and base . . . . .	99
5.3.3	Archaeological charcoal in acid and base . . . . .	101
5.3.4	SEC Blank analysis . . . . .	103
5.3.5	SEC-UV comparison . . . . .	105
5.3.6	SEC-UV on archaeological charcoal . . . . .	107
5.4	UV analysis of graphenic materials . . . . .	110
5.5	Conclusions . . . . .	116
5.6	Acknowledgments . . . . .	116
	Bibliography . . . . .	117
<b>6</b>	<b>Conclusions</b>	<b>120</b>
<b>A</b>	<b>Appendix</b>	<b>122</b>
A.1	Effects of pH and temperature on the Raman spectra of coal . . . . .	122
A.2	Homogenization of oxidized materials . . . . .	128
	Bibliography . . . . .	131

# List of Tables

3.1	A summary of the water/sonication-base-acid separation protocol. This produces three different solids: (1) as-prepared oxidized graphite (aOG), (2) graphite/graphene oxide (GO), and (3) oxidative debris (OD). . .	52
4.1	A summary of water/sonication-base-acid separation protocol on archaeological charcoal. This produces three different solids: (1) least oxidized, (2) moderately oxidized, and (3) highly oxidized materials. .	76
4.2	The pH variations of as-prepared oxidized graphite (aOG), humic acid (HA), and archaeological charcoal suspensions in nanopure water. The second row shows data from this project, while the third one shows data from the literature. . . . .	78

# List of Figures

1.1	A schematic representation of the graphite structure [11]. This figure is reused with the permission of The Royal Society of Chemistry. . . .	3
1.2	A schematic representation of one possible graphene oxide structure. .	5
1.3	A schematic representation of as-prepared oxidized graphite, including oxidative debris (OD) ovals [35]. This figure is reused with the permission of The Royal Society of Chemistry. . . . .	7
2.1	Representative Raman spectra of graphite flakes before and after oxidation: (black) graphite flakes, (orange) as-prepared oxidized graphite (aOG), (blue) graphene oxide (GO), (red) oxidative debris (OD). . .	32
2.2	Representative ATR-FTIR spectra of graphite flakes before and after oxidation: (black) graphite flakes, (orange) as-prepared oxidized graphite (aOG), (blue) graphene oxide (GO), (red) oxidative debris (OD). . . . .	34
2.3	Representative UV-Vis spectrum of as-prepared graphite (aOG). The peak near 230 nm is associated with the $\pi^* \leftarrow \pi$ electronic transitions of conjugated systems, while the one around 300 nm is assigned to $\pi^* \leftarrow n$ electronic transitions [22]. . . . .	36

2.4	Representative chromatogram of Suwannee River Humic Acid (SRHA) obtained at 300 nm. The unit of intensity on the Y-axis is mAu, which stands for milli-Absorbance unit. The peak around 9 min is associated with the elution of large molecules, whereas the one near 10 min represents elution of smaller molecules. . . . .	37
2.5	Representative optical microscope image of sonicated as-prepared oxidized graphite (aOG) taken with 20X magnification. . . . .	40
3.1	Schematic comparisons between (a) typical acid-base-acid (ABA) cleaning for radiocarbon samples and (b) steps to separate graphene oxide (GO) and oxidative debris (OD) from as-prepared oxidized graphite (aOG). All HCl and NaOH treatments are at 1M. . . . .	47
3.2	Water/sonication-base-acid (WSBA) protocol for separating GO (sediment 2) from graphite (sediment 1) and OD (sediment 3). . . . .	52
3.3	Representative ATR-FTIR spectra, before (blue) and after (red) sonication in water, of (a) graphite flakes, (b) aOG, (c) GO and (d) OD. Spectra are offset along the vertical axis for clarity. In each plot, the orange spectra correspond to the extracted component after the noted WSBA step. The plot legends indicate the precise preparation conditions for each sample, based on the procedure outlined in Table 1. In (c) and (d), the benchmark GO and OD samples were separated from unsonicated aOG using 1M NaOH (pH=13) followed by 1M HCl (pH=2). Note that the intensity scales for (a) and (d) are the same, and that they are expanded relative to (b) and (c). . . . .	53

3.4	(a) Representative ATR-FTIR spectra for solids extracted at different stages of the WSBA protocol: starting mixture (black), graphite from Step 3 (orange), GO from Step 6 (blue), and OD from Step 8 (red). (b) Representative ATR-FTIR spectra of GO before and after acid treatment.	57
3.5	Photographs of aOG (a,c) and aOG + extra OD (b,d) after one day (a,b) and seven days (c,d). Plot (e) compares representative UV-Vis spectra of fresh aOG suspension (black curve) with supernatants of aOG (blue curves) and OD-enriched aOG (red curves), after sitting for 1 day (solid curves) or 7 days (dashed curves).	60
3.6	Representative optical microscopy images of (a) graphite, (b) aOG, (c) sonicated graphite, and (d) sonicated aOG. The opaque graphite particles (a,c) show greater contrast than the optically transparent aOG (b,d). Scale bars represent 100 $\mu\text{m}$ in all images; in (d), the image is magnified to show particle outlines more clearly.	63
4.1	Images of (left) lab-synthesized aOG and (right) archaeological charcoal suspensions taken immediately after they were made.	78
4.2	(top) Representative Raman spectra of (black) graphite flakes, (orange) archaeological charcoal, (blue) lab-synthesized GO, and (red) lab-synthesized OD in region between 400-3000 $\text{cm}^{-1}$ . (bottom) Normalized spectra of the samples in the region from 1100 to 1800 $\text{cm}^{-1}$ . Black lines show D and G peaks for graphite at 1330 and 1570 $\text{cm}^{-1}$ , respectively.	80
4.3	The ATR-FTIR spectra of (red) lab-synthesized OD and (blue) GO, and (black) archaeological charcoal.	81

4.4	Representative attenuated total reflectance (ATR) infrared spectra of (top) archaeological charcoal and (bottom) graphite flakes after acid-base-acid (ABA) treatment: original (black), after first acid treatment (orange), after base-treatment (blue), and after last acid treatment (red). The relative intensity of peaks near 1700, 1600, and 1380 $\text{cm}^{-1}$ for archaeological charcoal, and near 1420 $\text{cm}^{-1}$ for graphite flakes, changes at different pH. . . . .	83
4.5	(a) Representative ATR-FTIR spectra for (black) graphite flakes and (red) least oxidized graphenic materials obtained from WSBA on archaeological charcoal. (b) Representative ATR-FTIR spectra for (black) lab-synthesized GO and (red) moderately oxidized graphenic materials obtained from WSBA on archaeological charcoal. (c) Representative ATR-FTIR spectra for (black) lab-synthesized OD and (red) highly oxidized graphenic materials extracted from archaeological charcoal. . . . .	85
4.6	Representative ATR data is in red for least (a), moderate (b), and highest (c) oxidized materials obtained from WSBA on archaeological charcoal. We compare these with transmission IR spectra of humic acids (black) from two different sources from the Infrared Spectra Library of the Kimmel Center for Archaeological Science Infrared Standards Library, Weizmann Institute of Science [11] (HA reference <b>1</b> is EAS5-AAA and HA reference <b>2</b> is Soil Masmiya). . . . .	87
5.1	UV-Vis spectra of (black) as-prepared oxidized graphite (aOG) and (red) Suwannee River Humic Acid (SRHA). . . . .	93
5.2	UV-Vis spectra of (red) concentrated (1M) HCl and (blue) concentrated (1M) NaOH. . . . .	97

5.3	UV spectra of Suwannee River Humic Acid (SRHA) dissolved in 1:1 volume ratio of (black) water/methanol, (blue) 25mM ammonium acetate/methanol, and (red) 25mM potassium phosphate/methanol. . .	98
5.4	(top) Representative images of (left) aOG, (middle) dilute base (pH=11) treated aOG, and (right) concentrated base (pH=13) treated aOG suspensions. (bottom) UV spectra of (black) aOG, (blue) dilute base (pH=11) treated aOG, and (red) clear colourless portion of a concentrated base (pH=13) treated aOG suspensions. . . . .	100
5.5	(top) Representative images of supernatants obtained from (left) acid treated, (middle) dilute base (pH=11) treated, and (right) concentrated base (pH=13) treated archaeological charcoal. (bottom) UV spectra of supernatants of archaeological charcoal treated in (black) 1M HCl, (blue) 0.1M NaOH, or (red) 1M NaOH. . . . .	102
5.6	The SEC-UV chromatograms of (top) ammonium acetate/methanol and (bottom) NaOH/methanol at three different wavelengths (black) 230, (blue) 250, and (red) 300 nm. . . . .	104
5.7	Representative (uncorrected) SEC-UV chromatograms of (top) Suwannee River Humic Acid (SRHA), (middle) as-prepared oxidized graphite, and (bottom) dilute base (pH=11) soluble portion of archaeological charcoal at three different wavelengths (black) 230, (blue) 250, and (red) 300 nm. The black vertical lines indicate the peak positions we assign to the elution of different groups of species (near 9 and 10 min, for SRHA, near 2 min, for aOG, and near 9.5 min for base treated charcoal.) . . . . .	106

5.8	Representative UV-Vis spectra of (black) as-prepared oxidized graphite (aOG), (blue) dilute base (pH=11) treated archaeological charcoal, and (red) Suwannee River Humic Acid (SRHA) dissolved in ammonium acetate and methanol. Normalized chromatograms of aOG, dilute base (pH=11) treated archaeological charcoal, and SRHA dissolved in acetate and methanol at 250 nm. . . . .	109
5.9	Representative UV-Vis spectra of (top) diluted and (bottom) non-diluted supernatants of acid treated graphite, modern charcoal, coal, and two different sources of archaeological charcoal. . . . .	111
5.10	Representative UV-Vis spectra of (top) diluted and (bottom) non-diluted supernatants of base (0.1M) treated graphite, modern charcoal, coal, and two different sources of archaeological charcoal. . . . .	113
5.11	Representative UV spectra of (top) diluted and (bottom) non-diluted supernatants of base (1M) treated graphite, modern charcoal, coal, and two different sources of archaeological charcoal. . . . .	115
A.1	The Raman spectra of coal before and after base (top), acid (middle), or water (bottom) treatments at different temperatures. The same original (before treatment) coal spectra are shown in black on all three plots. . . . .	124
A.2	Representative (a) raw and (b) analyzed Raman spectra of acidic coal at 23 °C. . . . .	125
A.3	Comparing D to G intensity <i>vs.</i> D peak widths before and after either a basic (top), acidic (middle), or water treatment. The same original (before treatment) coal values are shown in black on all three plots; coloured plots correspond to different treatment temperatures. . . . .	127

A.4 Raman spectra of (top) archaeological charcoal and (bottom) coal samples (blue) before and (red) after chemical oxidation. . . . .	129
----------------------------------------------------------------------------------------------------------------------------------------	-----

# List of Abbreviations and Symbols

ABA	Acid-Base-Acid
Abs	Absorption
aOC	as-prepared Oxidized Charcoal
aOG	as-prepared Oxidized Graphite
Arb	Arbitrary
ATR	Attenuated Total Reflectance
BA	Base-Acid
°C	Celsius
CMG	Chemically Modified Graphene
CVD	Chemical Vapor Deposition
Da	Dalton
DOM	Dissolved Organic Matter
<i>E</i>	Energy
FA	Fulvic Acid
FTIR	Fourier Transform Infrared
GO	Graphene Oxide
HA	Humic Acid
HN	Humin
HS	Humic Substances

mAu	milli-Absorbance unit
min	Minute
mL	Millilitre
MW	Molecular Weight
nm	Nanometre
OD	Oxidative Debris
rGO	Reduced Graphene Oxide
rpm	Rotation per Minute
SEC	Size Exclusion Chromatography
SRHA	Suwannee River Humic Acid
TRGO	Thermally Reduced Graphene Oxide
UV	Ultra Violet
Vis	Visible
WABA	Water-Acid-Base-Acid
WBA	Water-Base-Acid
WSBA	Water-Sonication-Base-Acid

# Chapter 1

## Introduction

Graphite, in charred organic materials, is broadly used for radiocarbon dating because graphite is a form of carbon that is widely believed to remain stable over time [1–3]. In fact, it is certainly more stable than other organic materials like cellulose and lignin. However, graphite can degrade in the environment. Earlier work proposes that graphite in archaeological charcoal may undergo oxidation [2]. Chemists prove that oxidized graphite degrades in water forming oxidized graphenic materials like graphene oxide (GO) and oxidative debris (OD) [4, 5].

Since these oxidized graphenic carbon materials would originate from graphitic carbon, it is essential to characterize and separate them for  $^{14}\text{C}$  dating. This is even more important for poorly preserved samples where sometimes no solid remains after radiocarbon cleaning procedures [2]. To date, no studies have investigated the presence and separation of oxidized graphenic materials in environmentally altered graphite-like archaeological charcoal.

I, as a chemist, take advantage of the well-established chemistry of these materials to characterize and salvage GO and OD from archaeological charcoal that can be used as valuable sources for radiocarbon dating measurement. However, I should note that

we do not do any  $^{14}\text{C}$  dating analyses in this work.

In this introductory chapter, I will discuss what is known about the structures and compositions of graphenic carbon materials, especially in their oxidized forms. I describe archaeological sources of graphite, their contaminants, and their common cleaning procedures. I also describe the synergy between the chemistry of graphite cleaning (used for radiocarbon dating) and GO synthesis strategies (used by material chemists). In this thesis, I will use these two bodies of knowledge to overcome existing challenges with well-known graphite cleaning protocols.

## 1.1 Graphenic carbon materials

In this thesis, I use word conventions that were introduced by an international editorial team for graphenic materials [6]. Graphite, graphene, graphene oxide (GO), and oxidative debris (OD) are the different types of graphenic carbon materials on which I will focus.

### 1.1.1 Graphite

Graphite is a well-known form of  $sp^2$  bonded carbon that contains hexagonal planes (Figure. 1.1) [7,8]. Since carbon has four valence electrons and each atom in graphite is bonded to three other atoms, it leaves one spare electron per carbon that is delocalized in conjugated  $\pi$  orbitals. Because of this, electrons can travel easily through the hexagonal plane, making graphite an electrically conductive material. On the other hand, graphite shows poor electrical conductivity in the out-of-plane direction because electrons cannot move easily between graphite layers. This is because the layers are held together by van der Waals forces.

Graphite is formed both in nature and in labs. Naturally occurring graphite

can be formed through graphitization of carbon materials like coal at temperatures near 2500 °C in the absence of oxygen [9]. Graphite can also be found in charcoal. Charcoal is produced by slow pyrolysis of wood. During this process, wood is heated in the absence of oxygen. Pyrolysis removes water, CO, and CO<sub>2</sub>, leaving graphite. Graphitization can also occur in nature when woods are buried in the ground over time under high pressure and temperature. The carbon content is then transformed into the crystalline structure under high temperature and pressure [10].

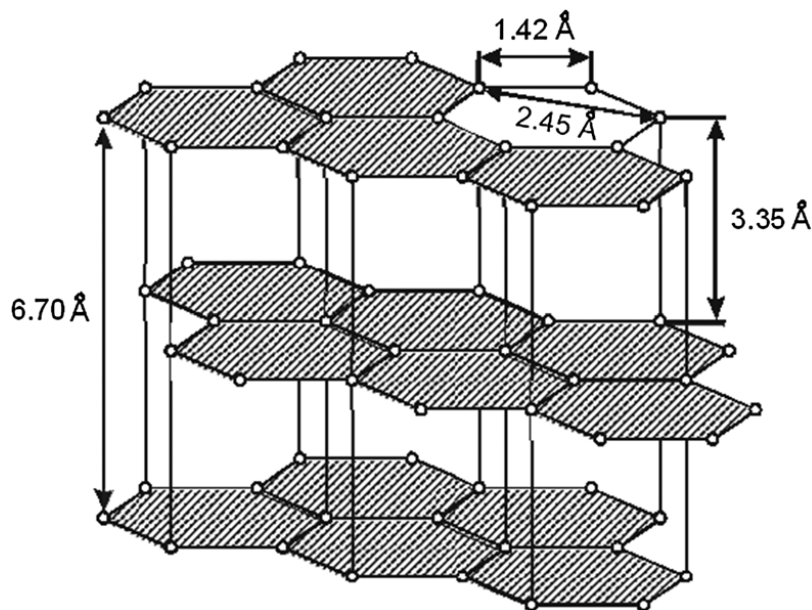


Figure 1.1: A schematic representation of the graphite structure [11]. This figure is reused with the permission of The Royal Society of Chemistry.

### 1.1.2 Graphene

A single layer within graphite is called graphene [12]. Graphene has drawn a great deal of attention because of its thermal, electronic, and optical properties [13, 14]. Graphene absorbs very little visible light due to its one-atom-thick structure. It contains conjugated  $\pi$  bonds that result in many physical properties [15]. Graphene has various potential applications in medicine (for targeted drug delivery) [16] and in

electronics (as transistors) [17].

Graphene is produced by different methods such as the mechanical exfoliation of highly oriented pyrolytic graphite (HOPG) [18], the epitaxial growth of graphene on a silicon carbide (SiC) [19], chemical vapor deposition (CVD) [20], and chemically-modified graphene (CMG) [5, 21], where the chemically-synthesized GO is reduced using different reducing agents, including  $\text{NaBH}_4$  and  $\text{N}_2\text{H}_4$ , to obtain graphene-like materials [22].

The first three methods produce highly ordered graphene with high thermal and electrical conductivity, but they are not appropriate for applications wherein a large amount of sample is required. The fourth procedure is helpful in producing graphene in bulk at a low cost.

### 1.1.3 Graphene Oxide (GO)

GO is graphene that is modified by different oxygen functional groups. It contains a mixture of  $sp^2$  and  $sp^3$  bonded carbon along with some oxygenated functional groups such as epoxides, carbonyls, alcohols, and carboxylic acids (Figure. 1.2). GO absorbs even less visible light than graphene due to the presence of oxygen functional groups in graphene structure. These groups disrupt the long-range  $\pi$  conjugation system and increase the energy gap between  $\pi^* \leftarrow \pi$  electronic states for GO. This leads to absorbing less visible light by GO.

A unique chemical structure for graphene oxide can never be defined. Two main factors that affect the chemical formula of GO are the density of pre-existing defects (initial source of graphite) and the quality of the subsequent degree of oxidation (influenced by the oxidation procedure). A typical range of C:O for GO is from 1.8 to 2.5 [23]. As an example, Brodie *et al.* reported a chemical formula of  $\text{C}_{2.19}\text{H}_{0.80}\text{O}_{1.00}$  for oxidized graphite [24]. Although oxygen functional groups create defects and make

GO electrically and thermally insulating, they also allow GO to be suspended in water or other aqueous solutions. This makes it useful for biological, energy storage, and water purification applications [25]. For example, GO is used to make supercapacitor devices [26], and it is used in glucose, protein, or DNA biosensor platforms [27, 28].

Different graphite oxidation methods have been introduced since 1855 to synthesize GO [29–32]. Here, I discuss several different protocols and their differences.

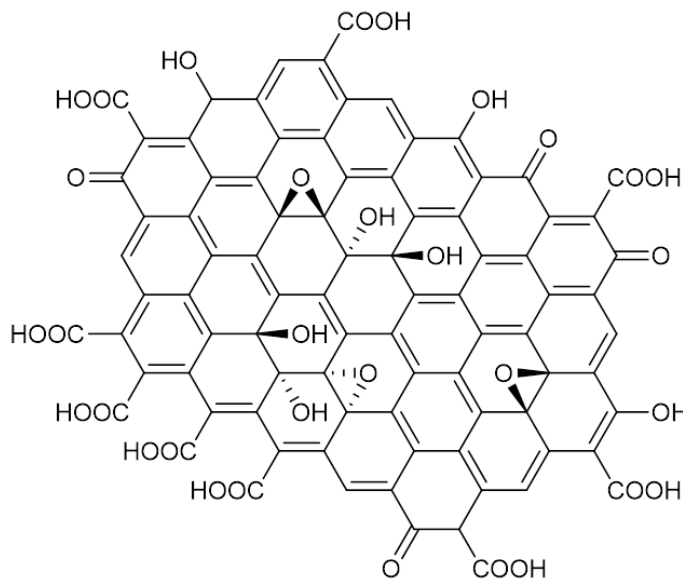


Figure 1.2: A schematic representation of one possible graphene oxide structure.

### Hummer's method

The most popular graphite oxidation protocol is Hummer's method [29], in which a mixture of concentrated  $\text{H}_2\text{SO}_4$ ,  $\text{NaNO}_3$ , and  $\text{KMnO}_4$  is held near  $0^\circ\text{C}$  for 1 hour to oxidize graphite flakes. Then, the oxidized graphite is exfoliated in water and hydrogen peroxide to yield GO. However, Hummer's method has some drawbacks, including a relatively low degree of graphene oxidation, and the generation of hazardous gases such as  $\text{NO}_2$  and  $\text{N}_2\text{O}_4$ .

## Modified Hummer's method

Kovtyukhova proposed a modified Hummer's method in 1999 [33]. The pretreatment process involves mixing graphite flakes with a concentrated mixture of  $\text{H}_2\text{SO}_4$ ,  $\text{K}_2\text{S}_2\text{O}_8$ , and  $\text{P}_2\text{O}_5$  at 80 °C for several hours to improve the oxidation degree of graphite [23, 30].

## Tour's method

Tour's method was introduced to maximize the oxidation degree of GO and to reduce the generation of toxic gases such as  $\text{NO}_2$  and  $\text{N}_2\text{O}_4$  [31]. In this method,  $\text{NaNO}_3$  was replaced with extra  $\text{KMnO}_4$ , and a combination of  $\text{H}_2\text{SO}_4$  and  $\text{H}_3\text{PO}_4$  (9:1 ratio) was used to improve the degree of oxidation. The final product yields a higher fraction of well-oxidized hydrophilic sites than the Hummer's method.

### 1.1.4 Oxidative debris (OD)

Recently, researchers found that the product of chemical-based graphite oxidation (as-prepared oxidized graphite (aOG)) is made of a mixture of poorly and highly oxidized graphene sheets (Figure 1.3) [5, 34, 35]. The poorly oxidized graphene is the one described in Section 1.1.3 as GO, and the more oxidized portion is called oxidative debris (OD) [5, 34, 35]. The latter constitutes almost one-third of aOG mass, and it is responsible for the water solubility and fluorescence properties of aOG. Rourke *et al.* show that the C:O ratio of aOG is 2:1, but this ratio changes to 4:1 for GO after removing the OD from aOG [35]. Researchers calculated formulas for OD (ranging from  $\text{C}_{12}\text{H}_{17}\text{O}_3$  to  $\text{C}_{20}\text{H}_{31}\text{O}_3$ ) based on mass spectroscopy information [35]. However, like GO, the exact size and chemical structure of OD is not fixed.

Studies suggest that OD is quite small in size and is made up of approximately ten

aromatic rings along with oxygen functional groups such as carboxyl and epoxide. Its molecular weight is between 200 and 800 Da, similar to that of fulvic acids [36–38].

In aOG, the OD adheres to GO by hydrogen bonding,  $\pi-\pi$  bonds, or van der Waals interactions [35,39]. Chemists found that OD can be separated from GO by base (1M NaOH), leaving a mixture of black residue (GO) and colourless suspension [5,35]. The colourless suspension can then be transformed into a white powder solid by adding 1M HCl, followed by drying. The black GO sediment is not capable of being re-suspended in water either using strong sonication or stirring [35]. This means that the more highly oxidized OD is what gives aOG the ability to remain suspended in water.

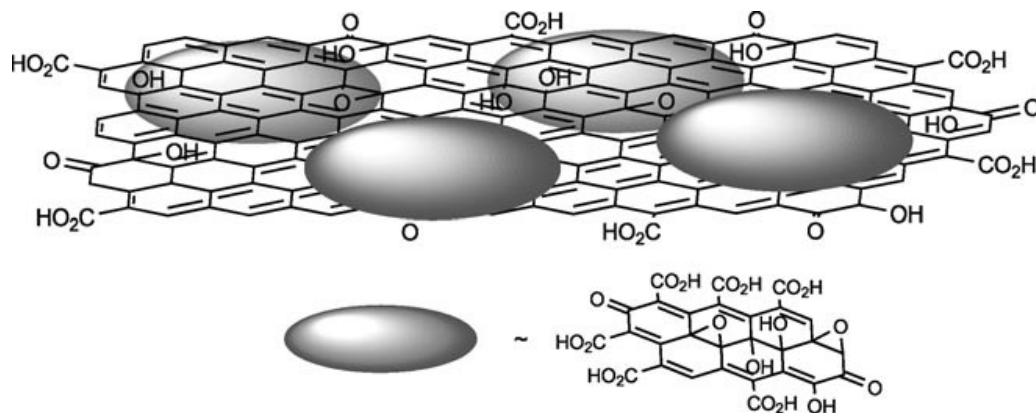


Figure 1.3: A schematic representation of as-prepared oxidized graphite, including oxidative debris (OD) ovals [35]. This figure is reused with the permission of The Royal Society of Chemistry.

## 1.2 Radiocarbon dating ( $^{14}\text{C}$ )

Carbon dating is a technique to analyze the age of organic materials through the determination of  $^{14}\text{C}$  and  $^{12}\text{C}$  contents ratio. Carbon has three isotopes  $^{12}\text{C}$ ,  $^{13}\text{C}$ , and

$^{14}\text{C}$  (relative proportions of 98.9 : 1.1 :  $1 \times 10^{-12}$ ). The first two isotopes are stable, and the last one is not.

### 1.2.1 $^{14}\text{C}$ production and decay

$^{14}\text{C}$  is formed naturally due to cosmic ray bombardment of atmospheric nitrogen [40,41]. Since  $^{14}\text{C}$  undergoes oxidation and forms radioactive carbon dioxide ( $^{14}\text{CO}_2$ ), it is then distributed on the Earth and consumed by living species. When a living species dies, it stops exchanging  $^{14}\text{CO}_2$  from the surrounding environment and loses the  $^{14}\text{C}$  as it decays back to  $^{14}\text{N}$  through negative beta decay. Since  $^{14}\text{C}$  is evenly distributed in the atmosphere, a global calibration method can be used to determine the age of an organic sample [42].

The age of a dead organic sample can be obtained by the determination of  $^{14}\text{C}$  concentration in the sample. The half-life of  $^{14}\text{C}$  isotope is 5,730 years. It means that the amount of  $^{14}\text{C}$  decreases to half of its initial amount after 5,730 years. Therefore, the older a sample, the less  $^{14}\text{C}$  is present. If we imagine 1 mg of a sample is from the present time, less than  $5 \times 10^7$  atoms are  $^{14}\text{C}$  compared with  $5 \times 10^{19}$   $^{12}\text{C}$ . In a 5,730 year old sample, however, the amount of  $^{14}\text{C}$  is halved due to its decay to  $^{14}\text{N}$ . This means that in a 45,000 year old sample, for instance, around 0.4 percent of the  $5 \times 10^7$  of  $^{14}\text{C}$  atoms remain. Therefore, it is crucial to properly prepare an old sample before radiocarbon dating; even a tiny amount of contaminants, either younger or older than the sample, makes the dating results unreliable.

### 1.2.2 $^{14}\text{C}$ measurement

Two methods are used to measure the concentration of  $^{14}\text{C}$  in a sample: radiometric dating and accelerator mass spectrometer (AMS) [43]. The AMS method is not only more precise than radiometric dating, but it also needs less sample than radiometric

dating [44].

In the radiometric method,  $^{14}\text{C}$  atoms are measured by the quantification of beta particles that are emitted from  $^{14}\text{C}$  radioactive decay. In AMS, the ratio of carbon isotopes ( $^{12}\text{C}$ ,  $^{13}\text{C}$ , and  $^{14}\text{C}$ ) in a sample is measured [43]. In this method, the carbon in the sample is converted to graphite through a catalytic process. The graphitic carbon is negatively ionized by a Cs ion beam, followed by a stripping process by which positively charged carbon ions are produced. The positively charged ions are accelerated using a magnetic field. Then, they are deflected to different angles based on their masses, and are then detected separately.

### 1.3 Radiocarbon samples

Samples rich in carbon content such as wood, charcoal, bone, and textile are good for radiocarbon dating. Charcoal and other sources of graphite-like charred seeds are especially valuable sources for  $^{14}\text{C}$  radiocarbon dating because the crystalline graphite is more stable in the environment over time.

Archaeological charcoal is composed of various carbonaceous materials, including graphite, humic substances (HS), carbonate minerals, and wood derivatives. Charcoal is generally made by pyrolysis of wood materials in an open-air fire. In this process, a pile of wood, covered with clay or soil, is combusted. The graphite part originates from charred cellulose and lignin, while HS comes from the surrounding soil and sediments. However, wood derivatives like lignin or cellulose can remain in poorly-charred wood.

Non-graphitic carbonaceous materials are considered to be contaminants and need to be removed. The contaminants may have carbon formed at a different time compared with the time the charcoal was produced. Contaminants could adhere to or penetrate into the charcoal.

### 1.3.1 Carbonaceous contaminants

#### Humic substances (HS)

Humic substances (HS) are naturally occurring carbonaceous materials that result from the breakdown of plant (lignin) and animal detritus [45]. HS reacts with other components in the environment, such as trace metals, thereby playing a critical role in the chemistry of soil [46]. HS are categorized based on their molecular weight, exchange acidity, solubility, and the content of carbon and oxygen. Humic substances like humic acid and fulvic acid are made of a mixture  $sp^2$  and  $sp^3$  carbon atoms along with different oxygen functional groups such as alcohol, carboxyl, epoxide, and carbonyl.

Humins (HN) are the largest molecules among HS with the highest content of aliphatic carbon that are not soluble in any pH [47]. The molecular weight of HN is higher than 300,000 Da. Humic acid (HA) is smaller than HN with a molecular weight of 2,000-200,000 Da. HA is not soluble in low or neutral pH. The smallest component of HS is fulvic acid (FA), which contains the highest content of aromatic carbon with MW of 600-1,000 Da. FA is soluble at any pH [45].

#### Carbonate minerals

Carbonate minerals are another source of carbonaceous contaminant that might exist in archaeological charcoal. Carbonate minerals like  $\text{CaCO}_3$  and  $\text{MgCO}_3$  can be formed due to the reaction of atmospheric  $\text{CO}_2$  with water in the presence of ions like  $\text{Ca}^{2+}$  and  $\text{Mg}^{2+}$ . These compounds are soluble in acidic solutions. Metal carbonates react with acid (HCl) and form metal chloride, water, and carbon dioxide.

### 1.3.2 Graphite sample cleaning for radiocarbon dating

Archaeological charcoal buried under the ground has been in contact with HS and other carbon-containing substances over a long period of time in changing environmental conditions. Therefore, contaminants must be removed before radiocarbon dating to obtain a reliable sample age.

#### Graphite cleaning procedures

Before radiocarbon dating graphitic carbon, one must separate contaminants from it. Acid-base-acid (ABA) cleaning is the most common method to clean and separate graphite from other carbonaceous contaminants [3, 48]. This method contains three consecutive steps: (1) acid wash (1M HCl), (2) base wash (1M NaOH), and (3) acid wash (1M HCl). Water is used between each step to rinse and wash the samples until they reach neutral pH. The second step is typically repeated until the supernatant obtained after this step is colourless.

Researchers use variations on the ABA aqueous cleaning strategies such as base-acid (BA), water-acid-base-acid (WABA), water-base-acid (WBA), and acid-base-oxidation (ABOx) [1, 3, 48, 49]. One step that is common to all aqueous cleaning methods is a base rinse. The concentrated base wash removes humic substances [1, 3, 48]. The  $\text{OH}^-$  ions, in strong alkaline conditions, cause C-C cleavage and form  $\text{CO}_2$  and smaller HS molecules with carboxyl groups; this occurs through nucleophilic attacks on carbonyl groups [4].

For ABA, previous studies have demonstrated that the first concentrated acid rinse removes carbonate and intercalated counter ions [3, 48, 50]. For example, when hydrochloric acid (HCl) reacts with calcium carbonate ( $\text{CaCO}_3$ ), calcium ( $\text{Ca}^{2+}$ ) and chloride ( $\text{Cl}^-$ ) ions form in solution and carbon dioxide ( $\text{CO}_2$ ) gas is released. The last concentrated acid wash removes surface-adsorbed  $\text{CO}_2$  [3, 48]. Dissolved car-

bon dioxide forms carbonic acid ( $\text{H}_2\text{CO}_3$ ), which dissociates to hydrogen carbonate ( $\text{HCO}_3^-$ ) and then carbonate ( $\text{CO}_3^{2-}$ ). This carbonate reacts with hydrochloric acid and produces  $\text{CO}_2$  gas and water, thereby removing it from the graphite surface.

### **Problems with cleaning procedures**

The ABA cleaning treatment works very well [3, 48, 51]. However, acid and base can cause significant damage to graphite, especially when some oxidized portion is present. Others have found that ABA can break down poorly preserved fossil charcoal, sometimes leaving no solid material for dating [3]. They showed this by obtaining statistically similar dates for the soluble portion of archaeological charcoal, and the solid remained after cleaning procedure (HCl and NaOH 1M) [52]. This suggests that the cleaning procedures can sometimes destroy graphenic carbon materials that are original to the specimen to be dated.

As a simple model for archaeological charcoal, three main carbon-based components might be present: graphite, GO, and HS. Here, I discuss the effects of acid and base with each of these separate components.

### **Problems with acid treatments**

Researchers have shown that both concentrated and diluted HCl form defects in graphene sheets [53, 54]. Reports by material scientists have shown that an acid treatment (1M HCl) enhances graphite intercalation and oxidation [50]. An acid wash (1M HCl) also damages crystalline graphite even in well preserved modern charcoal, resulting in sample loss [2, 3]. An acid wash protonates carboxylate ( $\text{RCOO}^-$ ) groups to form carboxylic acids ( $\text{RCOOH}$ ). This causes  $\text{RCOO}^-$  groups not to form complexes with counter-ions. These complexes make a salt-bridge between molecules that are assumed to help fossil charcoal structure stay more stable with respect to

time [3].

### **Problems with alkaline treatments**

Studies have also demonstrated the negative effects of alkaline treatment on graphenic carbon materials. One report demonstrates that sonication of graphite in alkaline conditions (pH=11) exfoliates a small portion of graphite layers [55]. Others proposed a model in which sodium and oxygen ions make a complex on the carbon lattice and weaken the C-C bonds, providing appropriate conditions for oxygen attack on the graphite lattice [56]. These observations are consistent with the loss of archaeological charcoal after a base treatment, where 80 weight percent of the sample is removed [2,3]. Chemists have also reported that deoxygenation and decarboxylation occur after mild and strong base treatment of GO, respectively. Both of these phenomena create defects in the GO structure by breaking C-C bonds [4]. A base treatment is also known to remove oxidative debris (OD) from less oxidized graphite [5, 34, 35].

### **Other cleaning treatments**

Due to the adverse effects of acid treatment on graphite, radiocarbon scientists tried to modify sample cleaning procedures by eliminating the first step in the ABA method or substituting it with a simple water wash [3]. Bird *et al.* developed another method called ABOx (acid-base-oxidation), which provides as reliable dates as the ABA method does for old samples [57, 58]. However, the last oxidation step is harsh and results in considerable sample loss. Researchers showed that typically more than 100 mg of well-preserved samples are required for ABOx cleaning procedures [59].

Hydropyrolysis (hypy) is another cleaning strategy in which neither acid nor base treatments are used to remove contaminants. In this method, pyrolysis is done in the presence of a molybdenum sulphide catalyst under high hydrogen pressure [60].

Ascough *et al.* isolated and dated charcoal from the Holocene age (the last 11,700 years of the Earth's history) using this method. The result obtained from hpy was similar to those obtained from the ABA and ABOx standard treatments [61]. However, hpy is not widely used by radiocarbon scientists. This might be due to its complicated pre-treatment method compared with the simpler ABA treatment. It is also likely that graphenic carbon materials are removed along with the chemically-similar carbon contaminants, thereby reducing the amount of datable materials.

## 1.4 Thesis objectives

I propose that GO could be used as a material for radiocarbon dating. Since it is possible that GO is formed as graphite degrades over time in charred carbon-rich materials, GO could contain carbon with a  $^{14}\text{C}$  signature that is identical to its graphite counterparts. To date, no studies have investigated whether GO exists in archaeological charcoal, or if it can be separated from other graphite materials and contaminants.

In this thesis, I describe how I met three important goals: (1) to develop a separation protocol to isolate GO from other graphitic materials; (2) to isolate GO from archaeological charcoal; and (3) to identify a strategy that could help distinguish between GO and chemically-similar contaminants such as HA.

In Chapter 2, I describe the different types of graphenic carbon materials that I used in my experiments. I also give detailed information regarding the different chemical treatments I performed using these materials. The reasons behind why we use each combination of material, experiment, and characterization technique is discussed. I explain what phases of graphenic materials, including solid, liquid, and suspension, are characterized with which techniques.

In Chapter 3, I address my first goal of developing a protocol to isolate GO from other graphitic materials. I show synergies between the chemistry involved in removing GO and OD from oxidized graphenic carbon materials, and the chemistry involved in a common cleaning procedure for radiocarbon dating. Then, I describe our separation protocol that draws on those synergies, using a simple test case of a lab-prepared mixture of graphite, GO, and OD.

In Chapter 4, I discuss my second goal of characterizing and separating oxidized graphenic materials, especially GO, in archaeological charcoal. We study the spectroscopic, chemical, and physical properties of an archaeological charcoal sample, without any pre-treatment, and then compare the results with a lab synthesized GO, which we prepared in our laboratory using a standard method. We also apply our developed separation protocol on archaeological charcoal to separate moderately oxidized (GO-like) and highly oxidized (OD-like) materials.

In Chapter 5, I address my third goal of distinguishing oxidized graphenic materials from contaminants like HA in the base soluble portion of archaeological charcoal. We treat archaeological charcoal with acid and base to simulate a common cleaning strategy (ABA) for radiocarbon dating. We analyze the supernatants obtained after each step using UV-Vis spectroscopy to monitor the removal of oxidized graphenic components. Since UV-Vis results do not allow us to distinguish among a complex mixture of carbonaceous materials, we also use size exclusion chromatography coupled with a UV detector to study UV absorption at specific wavelengths as a function of molecular size.

## 1.5 Copyright and authorship statement

This thesis contains a series of manuscript-style chapters, one of which has already been published in a peer-reviewed journal (Chapter 3). It is reprinted by permission of the Royal Society of Chemistry (Amir Joorab Doozha and Kristin M. Poduska, *Anal. Methods.* **11**, 2880-2887, 2019.). For the other chapters, I performed all experimental analysis and data collection and wrote them. My supervisor, Dr. Kristin Poduska, provided me with comments. For Chapter 5, I did the size exclusion chromatography measurements in collaboration with Dr. Cora Young.

Figures 1.1 and 1.3 were reused with the permission of the Royal Society of Chemistry and Wiley, respectively. All others are my own.

## Bibliography

- [1] Dani Alon, Genia Mintz, Illit Cohen, Steve Weiner, and Elisabetta Boaretto. The use of Raman spectroscopy to monitor the removal of humic substances from charcoal; quality control for  $^{14}\text{C}$  dating of charcoal. *Radiocarbon*, 44(1):1–11, 2002.
- [2] Ilit Cohen-Ofri, Lev Weiner, Elisabetta Boaretto, Genia Mintz, and Steve Weiner. Modern and fossil charcoal: aspects of structure and diagenesis. *J. Archaeol. Sci.*, 33(3):428 – 439, 2006.
- [3] N. R. Rebollo, I. Cohen-Ofri, R. Popovitz-Biro, O. Bar-Yosef, L. Meignen, P. Goldberg, S. Weiner, and E. Boaretto. Structural Characterization of Charcoal Exposed to High and Low pH: Implications for  $^{14}\text{C}$  Sample Preparation and Charcoal Preservation. *Radiocarbon*, 50(2):289–307, 2008.
- [4] Ayrat M. Dimiev, Lawrence B. Alemany, and James M. Tour. Graphene Oxide. Origin of Acidity, Its Instability in Water, and a New Dynamic Structural Model. *ACS Nano*, 7(1):576–588, 2013.
- [5] Helen R. Thomas, Stephen P. Day, William E. Woodruff, Cristina Valles, Robert J. Young, Ian A. Kinloch, Gavin W. Morley, John V. Hanna, Neil R. Wilson, and Jonathan P. Rourke. Deoxygenation of Graphene Oxide: Reduction or Cleaning? *Chem. Mater.*, 25(18):3580–3588, 2013.
- [6] Alberto Bianco, Hui-Ming Cheng, Toshiaki Enoki, Yuri Gogotsi, Robert H. Hunt, Nikhil Koratkar, Takashi Kyotani, Marc Monthieux, Chong Rae Park, Juan M. D. Tascon, and Jin Zhang. All in the graphene family - A recommended nomenclature for two-dimensional carbon materials. *Carbon*, 65:1–6, 2013.

- [7] Rajatendu Sengupta, Mithun Bhattacharya, S. Bandyopadhyay, and Anil K. Bhowmick. A review on the mechanical and electrical properties of graphite and modified graphite reinforced polymer composites. *Prog. Polym. Sci.*, 36(5):638–670, 2011.
- [8] A. Gupta, G. Chen, P. Joshi, S. Tadigadapa, and P. C. Eklund. Raman Scattering from High-Frequency Phonons in Supported n-Graphene Layer Films. *Nano Lett.*, 6(12):2667–2673, 2006.
- [9] J. S. Vogel. Rapid production of graphite without contamination for biomedical AMS. *Radiocarbon*, 34(3):344–350, 1992.
- [10] Adriano Ambrosi, Chun Kiang Chua, Bahareh Khezri, Zdenk Sofer, Richard D. Webster, and Martin Pumera. Chemically reduced graphene contains inherent metallic impurities present in parent natural and synthetic graphite. *Proc. Natl. Acad. Sci. U.S.A.*, 109(32):12899–12904, 2012.
- [11] Malgorzata Sliwinska-Bartkowiak, Henryk Drozdowski, Mateusz Kempinski, Monika Jazdzewska, Yun Long, Jeremy C. Palmer, and Keith E. Gubbins. Structural analysis of water and carbon tetrachloride adsorbed in activated carbon fibres. *Phys. Chem. Chem. Phys.*, 14:7145–7153, 2012.
- [12] A. C. Ferrari, J. C. Meyer, V. Scardaci, C. Casiraghi, Michele Lazzeri, Francesco Mauri, S. Piscanec, Da Jiang, K. S. Novoselov, S. Roth, and A. K. Geim. The Raman Fingerprint of Graphene. *Phys. Rev. Lett.*, 97:1–5, 2006.
- [13] Xiao Huang, Zongyou Yin, Shixin Wu, Xiaoying Qi, Qiyuan He, Qichun Zhang, Qingyu Yan, Freddy Boey, and Hua Zhang. Graphene-Based Materials: Synthesis, Characterization, Properties, and Applications. *Small*, 7(14):1876–1902, 2011.

- [14] Changgu Lee, Xiaoding Wei, Jeffrey W. Kysar, and James Hone. Measurement of the Elastic Properties and Intrinsic Strength of Monolayer Graphene. *Science*, 321(5887):385–388, 2008.
- [15] Matthew J. Allen, Vincent C. Tung, and Richard B. Kaner. Honeycomb carbon: a review of graphene. *Chem. Rev.*, 110(1):132, 2010.
- [16] Sumit Goenka, Vinayak Sant, and Shilpa Sant. Graphene-based nanomaterials for drug delivery and tissue engineering. *J. Control. Release*, 173(1):75–88, 2014.
- [17] Xuebei Yang, Guanxiong Liu, Alexander A Balandin, and Kartik Mohanram. Triple-mode single-transistor graphene amplifier and its applications. *ACS Nano*, 4(10):5532–5538, 2010.
- [18] K. S. Novoselov, V. I. Fal'ko, L. Colombo, P. R. Gellert, M. G. Schwab, and K. Kim. A roadmap for graphene. *Nature*, 490(7419):192–200, 2012.
- [19] Claire Berger, Zhimin Song, Xuebin Li, Xiaosong Wu, Nate Brown, Ccile Naud, Didier Mayou, Tianbo Li, Joanna Hass, Alexei N. Marchenkov, Edward H. Conrad, Phillip N. First, and Walt A. De Heer. Electronic Confinement and Coherence in Patterned Epitaxial Graphene. *Science*, 312(5777):1191–1196, 2006.
- [20] M. Eizenberg and J. M. Blakely. Carbon interaction with nickel surfaces: Monolayer formation and structural stability. *J. Chem. Phys.*, 71(8):3467–3477, 1979.
- [21] Sungjin Park and Rodney S. Ruoff. Chemical methods for the production of graphenes. *Nat. Nanotechnol.*, 4(4), 2009.
- [22] Chun Kiang Chua and Martin Pumera. Chemical reduction of graphene oxide: a synthetic chemistry viewpoint. *Chem. Soc. Rev.*, 43(1):291–312, 2013.

- [23] Ayrat Dimiev, Dmitry V. Kosynkin, Lawrence B. Alemany, Pavel Chaguine, and James M. Tour. Pristine Graphite Oxide. *J. Am. Chem. Soc.*, 134(5):2815–2822, 2012.
- [24] B. C. Brodie. On the Atomic Weight of Graphite. *Philos. Trans. Royal Soc.*, 149:249–259, 1859.
- [25] Charudatta Galande, Wei Gao, Akshay Mathkar, Andrew M. Dattelbaum, Tharangattu N. Narayanan, Aditya D. Mohite, and Pulikel M. Ajayan. Science and Engineering of Graphene Oxide. *Part. Part. Syst. Charact.*, 31(6):619–638, 2014.
- [26] Wei Gao, Neelam Singh, Li Song, Zheng Liu, Arava Leela Mohana Reddy, Lijie Ci, Robert Vajtai, Qing Zhang, Bingqing Wei, and Pulickel M. Ajayan. Direct laser writing of micro-supercapacitors on hydrated graphite oxide films. *Nat. Nanotechnol.*, 6(8), 2011.
- [27] Shijiang He, Bo Song, Di Li, Changfeng Zhu, Wenpeng Qi, Yanqin Wen, Lihua Wang, Shiping Song, Haiping Fang, and Chunhai Fan. A Graphene Nanoprobe for Rapid, Sensitive, and Multicolor Fluorescent DNA Analysis. *Adv. Funct. Mater.*, 20(3):453–459, 2010.
- [28] Jae Hwan Jung, Doo Sung Cheon, Fei Liu, Kang Bum Lee, and Tae Seok Seo. A Graphene Oxide Based Immuno-biosensor for Pathogen Detection. *Angew. Chem.*, 49(33):5708–5711, 2010.
- [29] William S. Hummers and Richard E. Offeman. Preparation of Graphitic Oxide. *J. Am. Chem. Soc.*, 80(6):1339–1339, 1958.
- [30] Scott Gilje, Song Han, Minsheng Wang, Kang L. Wang, and Richard B. Kaner. A Chemical Route to Graphene for Device Applications. *Nano Lett.*, 7(11):3394–3398, 2007.

- [31] Daniela C. Marcano, Dmitry V. Kosynkin, Jacob M. Berlin, Alexander Sinit-skii, Zhengzong Sun, Alexander Slesarev, Lawrence B. Alemany, Wei Lu, and James M. Tour. Improved Synthesis of Graphene Oxide. *ACS Nano*, 4(8):4806–4814, 2010.
- [32] Ji Chen, Bowen Yao, Chun Li, and Gaoquan Shi. An improved Hummers method for eco-friendly synthesis of graphene oxide. *Carbon*, 64:225–229, 2013.
- [33] Nina I. Kovtyukhova, Patricia J. Ollivier, Benjamin R. Martin, Thomas E. Mallouk, Sergey A. Chizhik, Eugenia V. Buzaneva, and Alexandr D. Gorchin-skiy. Layer-by-Layer Assembly of Ultrathin Composite Films from Micron-Sized Graphite Oxide Sheets and Polycations. *Chem. Mater.*, 11(3):771–778, 1999.
- [34] Helen R. Thomas, Cristina Valles, Robert J. Young, Ian A. Kinloch, Neil R. Wilson, and Jonathan P. Rourke. Identifying the fluorescence of graphene oxide. *J. Mater. Chem. C*, 1:338–342, 2013.
- [35] Jonathan P. Rourke, Priyanka A. Pandey, Joseph J. Moore, Matthew Bates, Ian A. Kinloch, Robert J. Young, and Neil R. Wilson. The Real Graphene Oxide Revealed: Stripping the Oxidative Debris from the Graphene-like Sheets. *Angew. Chem.*, 50(14):3173–3177, 2011.
- [36] Zhihong Wu, Charles U. Pittman, and Steven D. Gardner. Nitric acid oxidation of carbon fibers and the effects of subsequent treatment in refluxing aqueous NaOH. *Carbon*, 33(5):597–605, 1995.
- [37] Diego Stefani, Amauri J. Paula, Boniek G. Vaz, Rodrigo A. Silva, Nadia F. Andrade, Giselle Z. Justo, Carmen V. Ferreira, Antonio G. Souza Filho, Marcos N. Eberlin, and Oswaldo L. Alves. Structural and proactive safety aspects of oxida-

- tion debris from multiwalled carbon nanotubes. *J. Hazard. Mater.*, 189(1):391–396, 2011.
- [38] Zhaowei Wang, Mark D. Shirley, Steven T. Meikle, Raymond L. D. Whitby, and Sergey V. Mikhalovsky. The surface acidity of acid oxidised multi-walled carbon nanotubes and the influence of in-situ generated fulvic acids on their stability in aqueous dispersions. *Carbon*, 47(1):73–79, 2009.
- [39] Andréia F. Faria, Diego Stéfani T. Martinez, Ana C. M. Moraes, Marcelo E. H. Maia da Costa, Eduardo B. Barros, Antonio G. Souza Filho, Amauri J. Paula, and Oswaldo L. Alves. Unveiling the Role of Oxidation Debris on the Surface Chemistry of Graphene through the Anchoring of Ag Nanoparticles. *Chem. Mater.*, 24(21):4080–4087, 2012.
- [40] Ebbing and Gammon. *General Chemistry*. Houghton Mifflin, 10th edition, 2008.
- [41] R. E. (Royal Ervin) Taylor. *Radiocarbon dating : an archaeological perspective*. Routledge, second edition, 2014.
- [42] M. J. (Martin Jim) Aitken. *Science-based dating in archaeology*. Longman archaeology series. Longman, London ; New York, 1990.
- [43] A. P. McNichol, A. J. T. Juli, and G. S. Burr. Converting AMS data to radiocarbon values: Considerations and conventions. *Radiocarbon*, 43(2):313–320, 2001.
- [44] Ronny Friedrich, Bernd Kromer, Frank Sirocko, Jan Esper, Susanne Lindauer, Daniel Nievergelt, Karl Uwe Heussner, and Thorsten Westphal. Annual  $^{14}\text{C}$  tree-ring data around 400 AD: mid- and high-latitude records. *Radiocarbon*, page 1–12.

- [45] F. J. Stevenson. Humus chemistry, genesis, composition, reactions. *Humus chemistry, genesis, composition, reactions*, Wiley, 1982.
- [46] J. Buffle, F. L. Greter, and W. Haerdi. Measurement of complexation properties of humic and fulvic acids in natural waters with lead and copper ion-selective electrodes. *Anal. Chem.*, 49(2):216–222, 1977.
- [47] Manfred Schidlowski. Kerogen; insoluble organic matter from sedimentary rocks; book review. *Chem. Geol.*, 34(1):179–180, 1981.
- [48] Edwin A. Olson and W. S. Broecker. Section of Geology and Mineralogy: Sample Contamination and Reliability of Radiocarbon Dates. *Trans. N. Y. Acad. Sci.*, 20(7 Series II):593–604, 1958.
- [49] Michael I. Bird, Vladimir Levchenko, Philippa L. Ascough, Will Meredith, Christopher M. Wurster, Alan Williams, Emma L. Tilston, Colin E. Snape, and David C. Apperley. The efficiency of charcoal decontamination for radiocarbon dating by three pre-treatments – ABOx, ABA and hypy. *Quat. Geochronol.*, 22:25 – 32, 2014.
- [50] Feiyu Kang, Yang Leng, Tong-Yi Zhang, and Bensheng Li. Electrochemical synthesis and characterization of ferric chloride-graphite intercalation compounds in aqueous solution. *Carbon*, 36(4):383–390, 1998.
- [51] Elisabetta Boaretto, Xiaohong Wu, Jiarong Yuan, Ofer Bar-Yosef, Yan Pan, David Cohen, Tianlong Jiao, Shuicheng Li, Haibin Gu, Paul S. Goldberg, Steve Weiner, Vikki Chu, and Kexin Liu. Radiocarbon Dating of Charcoal and Bone Collagen Associated with Early Pottery at Yuchanyan Cave, Hunan Province, China. *Proc. Natl. Acad. Sci. U.S.A.*, 106(24), 2009.

- [52] E. M. Wild, P. Steier, P. Fischer, and F. Hofmayer.  $^{14}\text{C}$  Dating of Humic Acids from Bronze and Iron Age Plant Remains from the Eastern Mediterranean. *Radiocarbon*, 55(02):599–607, 2013.
- [53] Emir Bouleghlimat, Philip R. Davies, Robert J. Davies, Rebecca Howarth, Jiri Kulhavy, and David J. Morgan. The effect of acid treatment on the surface chemistry and topography of graphite. *Carbon*, 61:124–133, 2013.
- [54] V. A. Coleman, R. Knut, O. Karis, H. Grennberg, U. Jansson, R. Quinlan, B. C. Holloway, B. Sanyal, and O. Eriksson. Defect formation in graphene nanosheets by acid treatment: an x-ray absorption spectroscopy and density functional theory study. *J. Phys. D*, 41(6), 2008.
- [55] Karen B. Ricardo, Anne Sendeki, and Haitao Liu. Surfactant-free exfoliation of graphite in aqueous solutions. *ChemComm*, 50(21):2751–2754, 2014.
- [56] Jacob A. Moulijn and Freer Kapteijn. Towards a unified theory of reactions of carbon with oxygen-containing molecules. *Carbon*, 33(8):1155–1165, 1995.
- [57] Michael I. Bird and Darren R. Grocke. Determination of the abundance and carbon isotope composition of elemental carbon in sediments. *Geochim. Cosmochim. Acta*, 61(16):3413–3423, 1997.
- [58] M. I. Bird, L. K. Fifield, G. M. Santos, P. B. Beaumont, Y. Zhou, M. L. Di Tada, and P. A. Hausladen. Radiocarbon dating from 40 to 60 ka BP at Border Cave, South Africa. *Quat. Sci. Rev.*, 22(8):943–947, 2003.
- [59] Thomas Higham, Fiona Brock, Marco Peresani, Alberto Broglio, Rachel Wood, and Katerina Douka. Problems with radiocarbon dating the Middle to Upper Palaeolithic transition in Italy. *Quat. Sci. Rev.*, 28(13):1257–1267, 2009.

- [60] P. L. Ascough, M. I. Bird, F. Brock, T.F.G. Higham, W. Meredith, C.E. Snape, and C.H. Vane. Hydropyrolysis as a new tool for radiocarbon pre-treatment and the quantification of black carbon. *Quat. Geochronol.*, 4(2):140–147, 2009.
- [61] P. L. Ascough, M. I. Bird, W. Meredith, R. E. Wood, C. E. Snape, F. Brock, T. F. G. Higham, D. J. Large, and D. C. Apperley. Hydropyrolysis: Implications for Radiocarbon Pretreatment and Characterization of Black Carbon. *Radiocarbon*, 52(3):1336–1350, 2010.

# Chapter 2

## Materials and Methods

In this chapter, I describe graphenic carbon materials, including oxidized versions, that are relevant for my archaeological charcoal studies. I describe separation protocols that are widely used by chemists and radiocarbon scientists. Then, I provide information about sample preparations and characterization methods that I used to analyze carbon graphenic materials in solid, liquid, and suspension forms.

### 2.1 Materials

In this thesis, I use a combination of reference and environmentally-altered sources of graphite. Graphite flakes are not only used as a reference sample, but they also are used as a precursor to synthesize oxidized graphenic materials for reference: as-prepared oxidized graphite (aOG), graphene oxide (GO), and oxidative debris (OD). Carbonaceous Suwannee River Humic Acid (SRHA) is a helpful reference for liquid phase suspensions of humic acid (HA).

### **2.1.1 Graphite flakes**

Graphite flakes with 99.8% purity and 325 mesh size (44  $\mu\text{m}$ ) were purchased from Alfa Aesar. The flakes are used as a precursor to synthesize GO and OD.

### **2.1.2 As-prepared oxidized graphite (aOG)**

In this work, the improved Hummer's method is used to oxidize graphite flakes and modern charcoal [1]. Detailed information for the synthesis of aOG is provided in Chapter 3 (Section 3.2.1). In summary, graphite flakes and charcoal are oxidized using a mixture of  $\text{H}_2\text{SO}_4$  and  $\text{KMnO}_4$  under stirring and low-temperature (0-4  $^\circ\text{C}$ ) conditions. The thick mixture of graphite source and oxidizing agents are heated up to 90  $^\circ\text{C}$  within 2 hours, and then 200 mL of nanopure water and 6 mL of  $\text{H}_2\text{O}_2$  (30% w/w) are added under constant stirring conditions, respectively. The oxidized products are cooled down, centrifuged, and washed with nanopure water three times, followed by drying overnight at 50  $^\circ\text{C}$ .

### **2.1.3 Modern charcoal**

I use modern charcoal as a reference sample to compare with archaeological charcoal, following earlier studies [2]. We obtained the lab-synthesized modern charcoal from Dr. Robert J. Helleur (MUN Chemistry), who pyrolyzed a mixture of fir and pine wood, and heated it in a nitrogen atmosphere from 30  $^\circ\text{C}$  to 480  $^\circ\text{C}$  over 1 hour, then held at 480  $^\circ\text{C}$  for 20 min.

### **2.1.4 Archaeological charcoal**

Archaeological charcoal was obtained from Dr. Lisa Rankin (MUN Archaeology). The samples were excavated in Labrador, near Rigolet at the Double Mer Point site that

had been inhabited by 18<sup>th</sup> century Inuit (Sample reference: GbBO-2, H2, N1014, E971, NE 1/4, L2, S25, E60, D2:43, JB) on September 8, 2014. The archaeological sample was a mixture of charcoal, sand, soil, and dry leaf that was pulled out from a campfire. I physically separated the charcoal from the other parts and ground it with a mortar and pestle to make a fine powder.

### **2.1.5 Coal**

Coal is another type of environmentally altered source of graphite. A coal sample was sourced from Dr. Graham Layne (MUN Earth Science) with unknown origin. The lab-synthesized modern charcoal and coal samples were ground using mortar and pestle to obtain uniform powder before any chemical treatments.

### **2.1.6 Humic acid (HA)**

Suwannee River Humic Acid (SRHA), as a reference source of HA, was obtained from the International Humic Substances Society, Denver, CO. SRHA is commonly used for qualitative analysis of humic materials like humic acid in different samples like soil, compost, peat, and surface water [3–5].

## **2.2 Sample separation methods**

Chemical and physical separations are often necessary to remove contaminants from archaeological charcoal before radiocarbon dating to obtain a reliable age. The latter is essential because contaminants penetrate the sample and mix with graphenic materials under different environmental conditions over time. Chemical separation is also necessary to separate oxidized graphenic materials from aOG, so that helps to study the signature of these materials in archaeological charcoal.

### 2.2.1 Separation of GO and OD from aOG

I provided detailed information about the separation of GO and OD from aOG in Chapter 3 (Section 3.2.2). As a summary, a black precipitate of GO and clear colourless suspension of OD are obtained after the strong base (1M NaOH) treatment of aOG at a relatively high temperature. The OD suspension is then transformed into OD sediment after the addition of strong acid (1M HCl) followed by oven-drying at 60 °C overnight.

### 2.2.2 ABA treatment

Acid, base, acid (ABA) is the most common method used for removing contaminants from graphite present in archaeological charcoal samples before radiocarbon dating [6]. In the first step, 0.5 g of archaeological charcoal was added to 20 mL acid (1M HCl), and the solution stirred at 800 rpm for 1 hour. The suspension was then centrifuged, and the residue was neutralized using nanopure water until it reached a pH of around 6. The supernatant was collected and stored at room temperature in a dark place for further analysis, and the residue was dried overnight at 70 °C and used for the next steps. The residue obtained from the first acid treatment was treated with 20 mL of base (1M NaOH), and then with 20 mL of acid (1M HCl) under the same stirring condition for 1 hour. At the end of each step, the residual solid is separated from the supernatant and washed with nanopure water. The first supernatant obtained from the first acid treatment of archaeological charcoal contains carbonate ions from minerals like  $\text{CaCO}_3$  and  $\text{MgCO}_3$ , while the first residual solid contains charcoal and humic materials. After the base treatment, we end up with humic materials in the supernatant and graphite-like materials in the residual solid. After the last acid treatment, we obtain  $\text{CO}_2$  dissolved in the supernatant and graphite-like materials in

the residual solid. A small portion of the supernatants, obtained from each step, were filtered by syringe filter (0.2  $\mu\text{m}$ ), and subsequently stored in a dark and cool place (refrigerator).

### **2.2.3 Water-Sonication-Base-Acid (WSBA)**

We develop this protocol to separate a mixture of graphite and oxidized graphite taking advantage of the water treatment and sonication process near neutral pH, and the procedure of GO separation method [7]. The summary of this method is shown in Chapter 3 (Table 3.1).

0.02 g of graphite flakes and aOG were added and mixed into 10 mL nanopure water, followed by 60 min sonication. The mixture was centrifuged at 8500 rpm for 15 min and then filtered with 8  $\mu\text{m}$  filter paper (Whatman). The residual solid was dried in an oven for 8 to 12 hours at 50 °C. The filtrate was treated with 20 mL base (1M NaOH) at 100 °C under reflux condition for 1 hour. The mixture was centrifuged at 8500 rpm for 15 min and washed with nanopure water until a pH near 6 was obtained. The residue was dried in an oven at 50 °C for 8 to 12 hours. Then, 20 mL of 1M HCl was added to the supernatant and was then dried in an oven at 80 °C for 12 hours. The resultant white powder was ground using mortar and pestle to obtain a uniform powder. The same protocol was used to separate oxidized graphenic materials in archaeological charcoal.

## **2.3 Characterization methods**

The characterization of graphenic carbon materials in solid, liquid, and suspension helps us understand more about the structure, relative solubility, optical properties, and the sizes of these materials. In this thesis, I use indirect data to infer structure

changes after chemical reactions.

In this project, a combination of methods is used to characterize the presence of GO and OD in archaeological charcoal. This combination is essential because each of them alone is not effective. Raman spectroscopy, for example, helps us to monitor carbon-carbon vibrations and the geometry of graphenic carbon materials in the sample, while IR spectroscopy assists us in characterizing various oxygen functional groups.

### 2.3.1 Raman spectroscopy

Raman helps to characterize the geometry of graphenic structures, distinguishing between  $sp^2$  and  $sp^3$  bonded carbon atoms. Raman is a light scattering technique [8]. Raman peaks occur when monochromatic electromagnetic radiation of visible or near-infrared light irradiates a sample. Upon irradiation, samples can absorb or scatter light. There are three types of scattering processes: Stokes, anti-Stokes, and Rayleigh scattering. The last one, which is also called elastic scattering, involves no energy changes between the initial and scattered radiation. However, Stokes and anti-Stokes scattering are inelastic processes that have lower and higher energies compared to the incoming light, respectively. Raman scattering (anti-Stokes and Stokes) is much weaker than Rayleigh scattering, by a ratio of  $1:10^6$ . The peak intensity in Raman shows the number of scattered photons that reach the detector. Every Raman peak corresponds to a specific vibrational mode in a solid. In Raman spectroscopy, the polarizability of a chemical moiety has to change during the specific vibration modes to make a vibration Raman active.

We used a Renishaw spectrometer (632 nm excitation, 20X objective, 11 mW power, exposure time 30 s) to do the Raman measurements. Spectra were obtained in the range of  $100\text{-}3000\text{ cm}^{-1}$ . Each sample was transferred and pressed on a glass slide using a spatula.

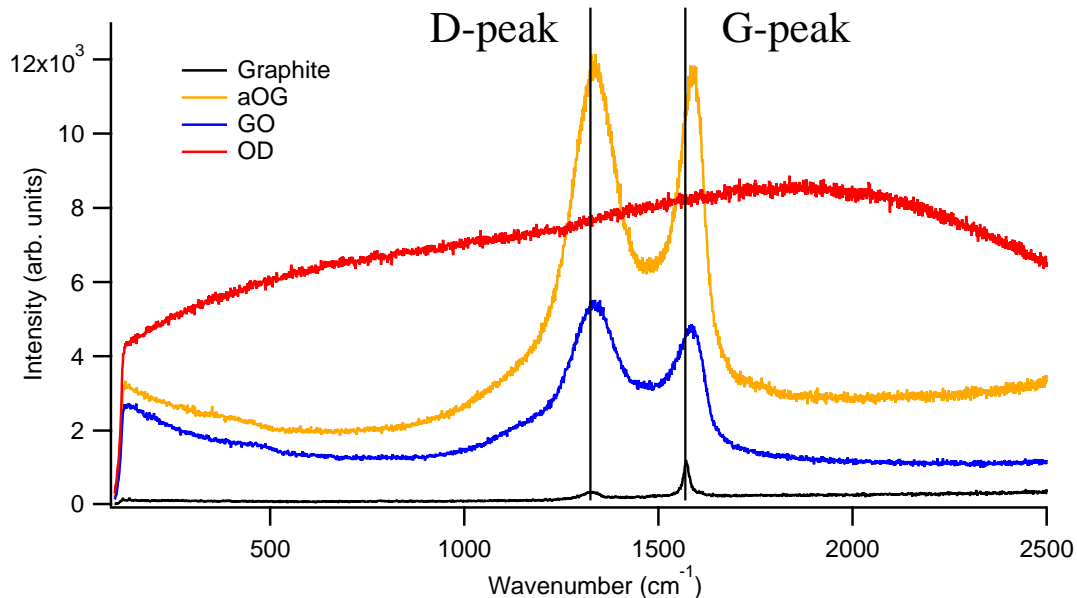


Figure 2.1: Representative Raman spectra of graphite flakes before and after oxidation: (black) graphite flakes, (orange) as-prepared oxidized graphite (aOG), (blue) graphene oxide (GO), (red) oxidative debris (OD).

### Characteristic peaks for graphenic carbon materials

Raman spectroscopy has been widely used to analyze graphite-related structures such as graphite, graphene oxide, and graphene [9]. In a typical Raman spectrum of graphenic carbon materials, two main peaks are observed [10]: G and D (Figure 2.1). The G peak, near  $1600\text{ cm}^{-1}$ , is assigned to the in-plane stretching vibration of  $sp^2$  C=C bonds in graphite materials. The D peak, near  $1300\text{ cm}^{-1}$ , is associated with the vibration of  $sp^3$  C-C bonds and breathing modes of benzene rings in the hexagonal geometry of graphenic structures [11].

The D peak appears when the polarizability is affected due to changes in the hexagonal geometry of the graphite structure. The G peak for as-prepared oxidized graphite (aOG) and GO shifts to higher energy and becomes broad, suggesting a disruption to the  $sp^2$  carbon arrangement of graphite. When the arrangement of C=C bonds is distorted due to oxygen functional groups, the conjugation of  $\pi$  bonds

is disrupted, thereby higher energy is required to change the polarizability of  $sp^2$  C=C in graphite lattice [12–15].

Others have shown that D to G intensity ratio increases after the chemical oxidation of graphite flakes due to the formation of defects and the addition of oxygen functional groups [12–14, 16, 17]. OD shows no G or D peaks compared with graphite, aOG, and GO. Since OD is highly fluorescent with small  $sp^2$  regions, we only observe a broad Raman spectrum with high background intensity [18].

### 2.3.2 IR spectroscopy

Infrared (IR) spectroscopy helps to characterize graphene oxide and its functional groups in both lab-prepared GO and archaeological charcoal [1, 19]. When a solid is irradiated with infrared light, bonds absorb energy if the frequency of the incident light is the same as the frequency of a specific vibrational mode. In IR spectroscopy, the dipole moment of a molecule has to change during the specific vibration modes to make a vibration IR active [20].

Attenuated total reflectance Fourier transform infrared (ATR-FTIR) spectra were recorded using a Bruker Alpha II spectrometer (diamond crystal, 36 scans, 4  $\text{cm}^{-1}$  resolution). The solid phase of our samples (less than 0.001 g) was transferred to the ATR crystal with a spatula. In the IR spectra of graphenic carbon materials like as-prepared oxidized graphite (aOG), we see vibration modes of many different functional groups. This includes C-O, C-OH, C-O-C,  $\text{COO}^-$  between 1400 and 1000  $\text{cm}^{-1}$ , stretching vibration modes of O-H from 2400 to 3800  $\text{cm}^{-1}$ , vibration of carbonyl groups near 1700  $\text{cm}^{-1}$ , and symmetric or asymmetric vibrations of  $\text{CH}_2$  at 2800 and 2900  $\text{cm}^{-1}$  (Figure 2.2) [1, 10, 21, 22]. Peaks near 1700  $\text{cm}^{-1}$  (carbonyl groups vibration) and 1619  $\text{cm}^{-1}$  (O-H bending vibration) are the important vibration bands to study GO. Other peaks in the fingerprint region, between 1000 and 1400  $\text{cm}^{-1}$ , are

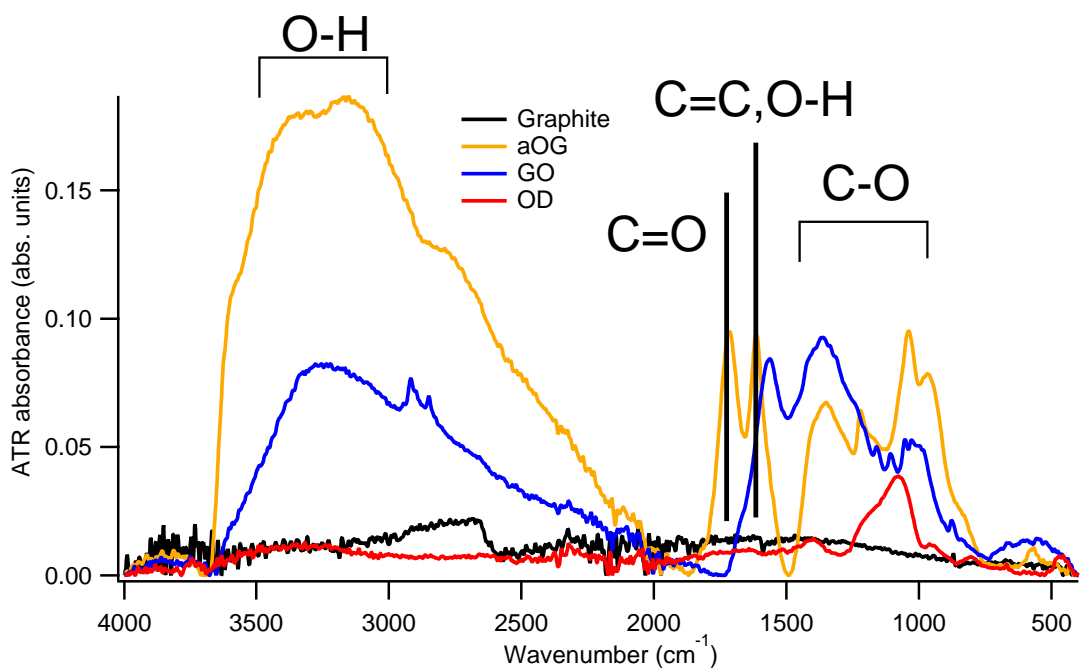


Figure 2.2: Representative ATR-FTIR spectra of graphite flakes before and after oxidation: (black) graphite flakes, (orange) as-prepared oxidized graphite (aOG), (blue) graphene oxide (GO), (red) oxidative debris (OD).

challenging to interpret due to many overlapping peaks from different oxygen-based functional groups.

### 2.3.3 pH measurements

A pH measurement determines the activity of  $H^+$  ions showing the acidity or alkalinity of solutions. GO decreases the pH of water due to the generation of hydrogen ions in the solution through an acidification process [23]. In this process, protons are generated through the ionization of alcohol, followed by the cleavage of C-C bonds and the formation of vinylogous carboxylic acids. We take advantage of this characteristic property to monitor GO in environmentally altered sources of graphite-like archaeological charcoal.

0.001 g of aOG, obtained from graphite flakes, and archaeological charcoal were transferred to separate vials, and 20 mL of nanopure water was added to each one. Both suspensions were stirred for 30 min at 800 rpm. Then, the pH of the solutions was measured using a calibrated pH meter. The calibration was done using three different buffers that came with the pH meter. The pH of the buffers was 4, 7, and 10. The buffer with a pH of 4 was made of  $C_8H_5O_4K$ . The one with the pH of 7 was composed of a combination of  $Na_2HPO_4$ ,  $KH_2PO_4$ , and  $C_4H_6BrNO_4$ . The one with a pH of 10 was made of a combination of  $Na_2CO_3$  and  $NaHCO_3$ .

### 2.3.4 UV-Vis spectroscopy

A UV-Vis spectrum measures the intensity of transmitted light as a function of wavelength. The peak intensity indicates the concentration ( $c$ ) of absorbing species, which is calculated by Beer's law:  $A = -\log(I/I_0) = \epsilon bc$ .  $A$  is absorbance,  $I$  and  $I_0$  are the intensity of passed and incident light,  $\epsilon$  is a constant known as the molar absorptivity, and  $b$  is the path length over which absorption occurs. I should note that we do not

calculate concentration in my work.

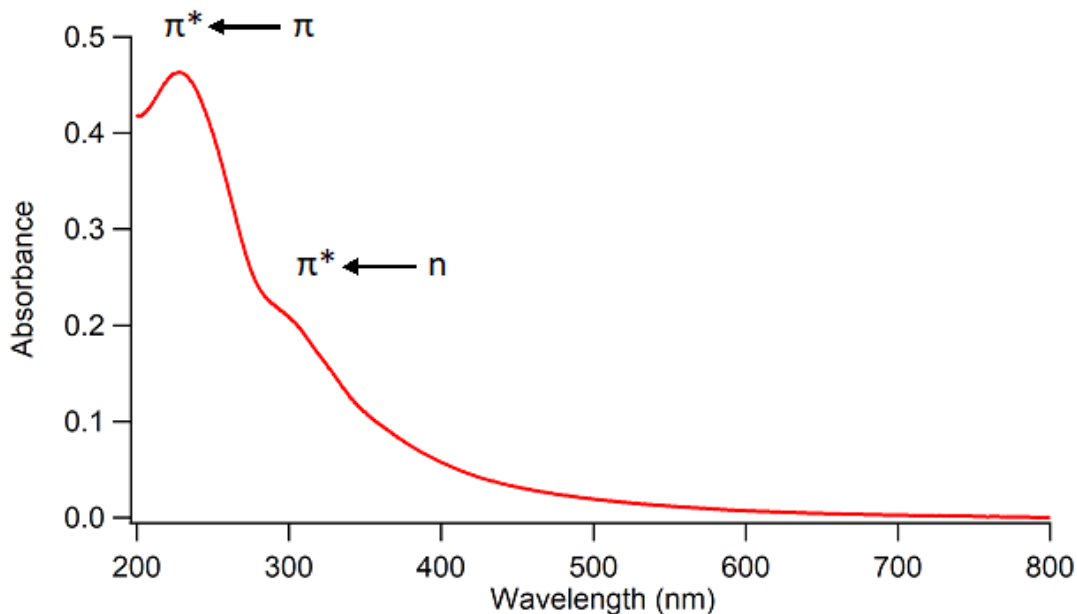


Figure 2.3: Representative UV-Vis spectrum of as-prepared graphite (aOG). The peak near 230 nm is associated with the  $\pi^* \leftarrow \pi$  electronic transitions of conjugated systems, while the one around 300 nm is assigned to  $\pi^* \leftarrow n$  electronic transitions [22].

UV-Vis spectroscopy is helpful in analyzing both humic substances and graphene oxide. In a typical spectrum of graphene oxide, there are two main absorption peaks at around 230 and 300 nm, which are related to  $\pi^* \leftarrow \pi$  and  $\pi^* \leftarrow n$  electron transitions of  $sp^2$  and  $sp^3$  domains, respectively [22] (Figure 2.3). The more oxygenated functional groups in highly oxidized graphene lead to more lone pair electrons in the molecule, which eventually lead to higher absorption intensity near 300 nm.

The bulk UV-Vis spectra were acquired with a Varian Cary 6000 spectrometer with 0.1 second average time, 1 nm resolution, and 600 nm/min scan rate. As an example to show how a sample was prepared for UV-Vis analysis, we added 0.5 g of graphenic carbon sample to 20 mL of liquid and stirred the suspension at 800 rpm for 1 hour. The suspension was centrifuged to obtain the supernatant for the UV-Vis measurement.

### 2.3.5 Size exclusion chromatography (SEC)

Size exclusion chromatography is one type of liquid chromatography in which a mixture of chemical compounds is separated based on their molecular sizes [24]. In this technique, larger molecules pass through the stationary phase quicker than the smaller ones. The small pores of the stationary phase exclude large molecules but not small ones. Large molecules elute without entering the pores, while small ones penetrate the pores and spend more time on the column.

Size Exclusion Chromatography coupled with UV (SEC-UV) measurements is used to study the UV absorption of chemical compounds at a specific wavelength as a function of size.

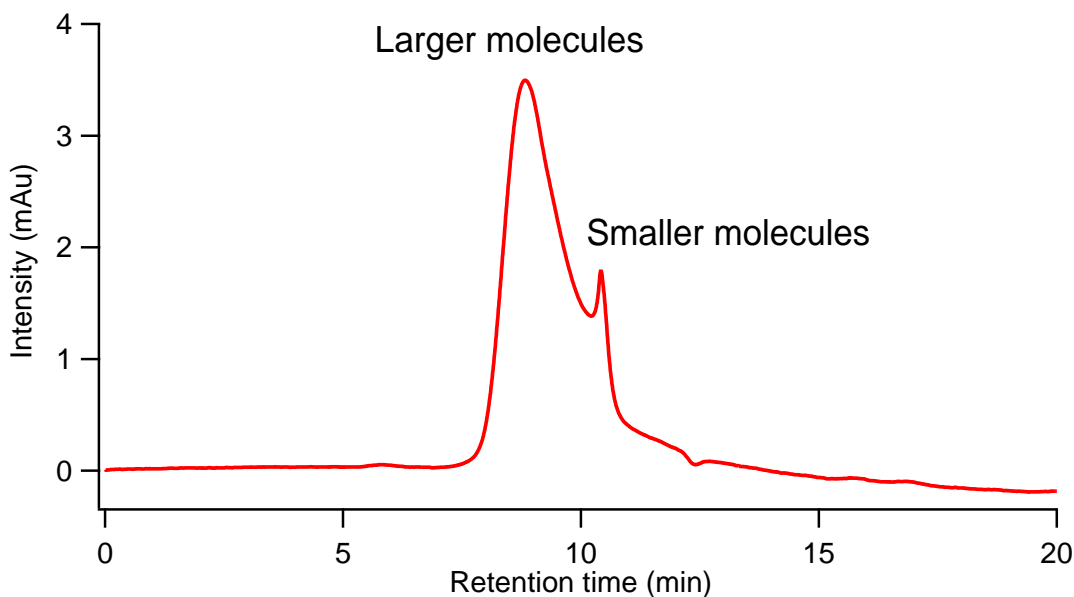


Figure 2.4: Representative chromatogram of Suwannee River Humic Acid (SRHA) obtained at 300 nm. The unit of intensity on the Y-axis is mAu, which stands for milli-Absorbance unit. The peak around 9 min is associated with the elution of large molecules, whereas the one near 10 min represents elution of smaller molecules.

The SEC-UV measurements are conducted with a High Performance Liquid Chromatograph (HPLC) (1260 Infinity, Agilent Technologies, Santa Clara, CA, USA) cou-

pled to a diode array detector (1260, Agilent Technologies, Santa Clara, CA, USA). An aqueous gel filtration column (molecular weight range: 250 – 75,000 Da, Polysep GFC P-3000, Phenomenex, Torrance, CA, USA) was used in this project.

The chromatography conditions are detailed below. The mobile phase composition contained 50:50 methanol and ammonium acetate with a concentration of 25 mM. Measurements were performed under an isocratic condition at a flow rate of 1 mL/min with an injection volume of 100  $\mu$ L. The UV wavelengths were 230, 250, and 300 nm. The SEC-UV measurements were performed using the same chromatography conditions as Di Lorenzo and Young [5].

Around 0.2 g of acid-treated archaeological charcoal was added into 20 mL of 0.1M NaOH, followed by stirring at 800 rpm at 40 °C for 1 hour. The suspension was then centrifuged at 8,500 rpm for 15 min to separate the supernatant from the residual solid. The supernatant was then filtered by a syringe filter (0.2  $\mu$ m) and stored in a dark place.

Figure 2.4 shows a representative chromatogram of Suwannee River Humic Acid (SRHA) obtained at 300 nm using the chromatography conditions explained above. The chromatogram depicts two main peaks around 9 and 10 min [5]. The main peak at 9 min corresponds to larger molecules that were eluted first from the column. A typical SEC-UV chromatogram depicts absorption intensity at a specific wavelength as a function of retention time, which is related to molecular size.

To analyze the liquid phase of oxidized graphite, humic acid, and base treated archaeological charcoal, we use a combination of bulk UV-Vis spectroscopy and SEC-UV. Bulk UV-Vis analysis helps to study an analyte across the full UV-Vis region, whereas SEC-UV can measure a mixture of analyte at a few user-specified wavelength as a function of retention time/molecular size, separately.

### 2.3.6 Optical microscopy

In Chapter 3, we show that sonication can break down aOG particles more easily than graphite. To prove that, representative particle sizes for graphite and as-prepared oxidized graphite before and after sonication were extracted from optical microscopy images (Leica, 5X and 20X NPLAN objectives). The images were analyzed using Fiji particle analysis routines [25].

Particles must be uniformly dispersed on a glass slide to obtain well-separated particles that do not overlap. To do this, I used 0.001 g of graphite and aOG that were separately transferred into two 20 mL vials, and 10 mL ethanol was added to each batch. For non-sonicated samples, one droplet of each suspension was drawn by a disposable pipette and transferred on a glass slide. Ethanol evaporated after a few seconds and left the samples behind. For sonicated samples, the suspensions were sonicated in a water bath for one hour and then the same method was applied to prepare the samples for imaging. Figure 2.5 shows an image of aOG, dispersed in ethanol and obtained using 20X magnification.

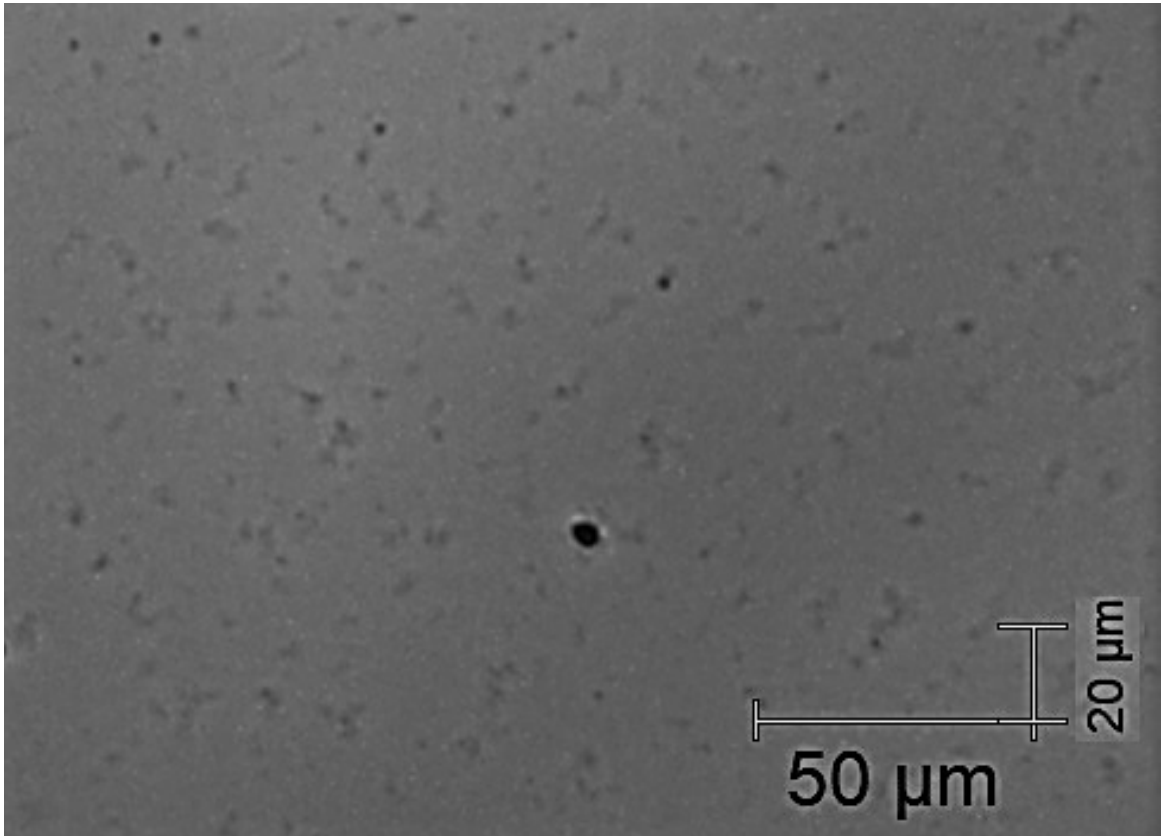


Figure 2.5: Representative optical microscope image of sonicated as-prepared oxidized graphite (aOG) taken with 20X magnification.

## Bibliography

- [1] Ji Chen, Bowen Yao, Chun Li, and Gaoquan Shi. An improved Hummers method for eco-friendly synthesis of graphene oxide. *Carbon*, 64:225–229, 2013.
- [2] Ilit Cohen-Ofri, Lev Weiner, Elisabetta Boaretto, Genia Mintz, and Steve Weiner. Modern and fossil charcoal: aspects of structure and diagenesis. *J. Archaeol. Sci.*, 33(3):428 – 439, 2006.
- [3] Uwe Klaus, Thomas Pfeifer, and Michael Spiteller. APCI-MS/MS:A Powerful Tool for the Analysis of Bound Residues Resulting from the Interaction of Pesticides with DOM and Humic Substances. *Environ. Sci. Technol.*, 34(16):3514–3520, 2000.
- [4] Namguk Her, Gary Amy, David Foss, Jaeweon Cho, Yeomin Yoon, and Paul Kosenka. Optimization of Method for Detecting and Characterizing NOM by HPLC–Size Exclusion Chromatography with UV and On-Line DOC Detection. *Environ. Sci. Technol.*, 36(5):1069–1076, 2002.
- [5] Robert A. Di Lorenzo and Cora J. Young. Size separation method for absorption characterization in brown carbon: Application to an aged biomass burning sample. *Geophys. Res. Lett*, 43(1):458–465, 2016.
- [6] Edwin A. Olson and W. S. Broecker. Section of Geology and Mineralogy: Sample Contamination and Reliability of Radiocarbon Dates. *Trans. N. Y. Acad. Sci.*, 20(7 Series II):593–604, 1958.
- [7] Amir Joorab Doozha and Kristin M. Poduska. Graphite oxidation chemistry is relevant for designing cleaning strategies for radiocarbon dating samples. *Anal. Methods*, 11:2880–2887, 2019.

- [8] C. Banwell. Fundamentals of molecular spectroscopy. *Fundamentals of molecular spectroscopy*, McGraw-Hill, 2nd edition, 1972.
- [9] A. Gupta, G. Chen, P. Joshi, S. Tadigadapa, and P. C. Eklund. Raman Scattering from High-Frequency Phonons in Supported n-Graphene Layer Films. *Nano Lett.*, 6(12):2667–2673, 2006.
- [10] Martin Rosillo-Lopez and Christoph G. Salzmann. A simple and mild chemical oxidation route to high-purity nano-graphene oxide. *Carbon*, 106:56–63, 2016.
- [11] A. C. Ferrari and J. Robertson. Interpretation of Raman spectra of disordered and amorphous carbon. *Phys. Rev. B*, 61(20):14095–14107, 2000.
- [12] Konstantin N. Kudin, Bulent Ozbas, Hannes C. Schniepp, Robert K. Prudhomme, Ilhan A. Aksay, and Roberto Car. Raman spectra of graphite oxide and functionalized graphene sheets. *Nano Lett.*, 8(1):36–41, 2008.
- [13] Jianchang Li, Xiangqiong Zeng, Tianhui Ren, and Emile van Der Heide. The Preparation of Graphene Oxide and Its Derivatives and Their Application in Bio-Tribological Systems. *Lubricants*, 2(3):137–161, 2014.
- [14] Rempeng Gu, William Z. Xu, and Paul A. Charpentier. Synthesis of polydopamine coated graphene polymer nanocomposites via RAFT polymerization. *J. Polym. Sci. A*, 51(18):3941–3949, 2013.
- [15] Siegfried Eigler, Michael Enzelberger-Heim, Stefan Grimm, Philipp Hofmann, Wolfgang Kroener, Andreas Geworski, Christoph Dotzer, Michael Rockert, Jie Xiao, Christian Papp, Ole Lytken, Hans-Peter Steinruck, Paul Muller, and Andreas Hirsch. Wet Chemical Synthesis of Graphene. *Adv. Mater.*, 25(26):3583–3587, 2013.

- [16] Tuinstra F. and Koenig J. L. Raman spectrum of graphite. *J. Chem. Phys.*, 53(3):1126–1130, 1970.
- [17] M. A. Pimenta, G. Dresselhaus, M. S. Dresselhaus, L. G. Canado, A. Jorio, and R. Saito. Studying disorder in graphite-based systems by Raman spectroscopy. *Phys. Chem. Chem. Phys.*, 9(11):1276–1290, 2007.
- [18] Helen R. Thomas, Cristina Valles, Robert J. Young, Ian A. Kinloch, Neil R. Wilson, and Jonathan P. Rourke. Identifying the fluorescence of graphene oxide. *J. Mater. Chem. C*, 1:338–342, 2013.
- [19] N. R. Rebollo, I. Cohen-Ofri, R. Popovitz-Biro, O. Bar-Yosef, L. Meignen, P. Goldberg, S. Weiner, and E. Boaretto. Structural Characterization of Charcoal Exposed to High and Low pH: Implications for  $^{14}\text{C}$  Sample Preparation and Charcoal Preservation. *Radiocarbon*, 50(2):289–307, 2008.
- [20] Donald L. Pavia. *Introduction to spectroscopy*. Brooks/Cole, Cengage Learning, Australia ; Belmont, CA, 4th edition, 2009.
- [21] Helen R. Thomas, Stephen P. Day, William E. Woodruff, Cristina Valles, Robert J. Young, Ian A. Kinloch, Gavin W. Morley, John V. Hanna, Neil R. Wilson, and Jonathan P. Rourke. Deoxygenation of Graphene Oxide: Reduction or Cleaning? *Chem. Mater.*, 25(18):3580–3588, 2013.
- [22] Ayrat Dimiev, Dmitry V. Kosynkin, Lawrence B. Alemany, Pavel Chaguine, and James M. Tour. Pristine Graphite Oxide. *J. Am. Chem. Soc.*, 134(5):2815–2822, 2012.
- [23] Ayrat M. Dimiev, Lawrence B. Alemany, and James M. Tour. Graphene Oxide. Origin of Acidity, Its Instability in Water, and a New Dynamic Structural Model. *ACS Nano*, 7(1):576–588, 2013.

- [24] Daniel C. Harris. *Quantitative chemical analysis*. W.H. Freeman ; Palgrave Macmillan, 6th edition, 2002.
- [25] J. Schindelin, I. Arganda-Carreras, and E. Frise. Fiji: an open-source platform for biological-image analysis. *Nature Meth.*, 9(7):676–682, 2012.

## Chapter 3

# Graphite oxidation chemistry is relevant for designing cleaning strategies for radiocarbon dating samples\*

We demonstrate that mixtures of graphite and lab-oxidized graphenic carbon materials can be separated into three individual components (graphite, graphene/graphite oxide (GO) and oxidative debris (OD)) by a series of aqueous treatments. Our results show that a key part of this separation procedure involves water treatment and sonication near neutral pH in order to separate GO from OD. We show that the relative proportions of OD and GO – independent of any humic substances – can affect the ability of oxidized graphite to be suspended in water, which can influence the efficiency of the separation procedures we describe. We compare and contrast our protocol with others that are widely used for cleaning archaeological charcoal prior

---

\*This chapter is used with the permission of the Royal Society of Chemistry (Amir Joorab Doozha and Kristin M. Poduska, *Anal. Methods*. **11**, 2880-2887, 2019.).

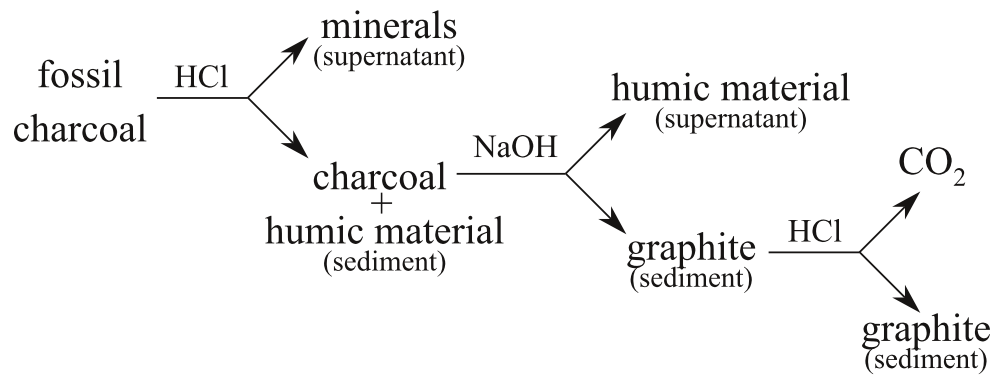
to radiocarbon dating. Our protocol has potential applications for tailored cleaning procedures for graphenic carbon materials, including the possibility of separating GO from both OD and graphite, for radiocarbon dating purposes.

### 3.1 Introduction

Graphenic carbon material from archaeological samples is widely used for radiocarbon ( $^{14}\text{C}$ ) dating. [1–3] However, datable material must be cleaned to remove carbonaceous contaminants that contribute to specimen radiocarbon levels. Because different forms of carbon-containing materials have very different chemistry, there are specialized decontamination procedures for minerals (such as bone), organic materials (such as collagen), and graphenic materials (such as charcoal). An extremely effective cleaning method – that applies uniquely to graphenic carbon materials – involves a successive acid-base-acid (ABA) treatment, [4], as shown schematically in Figure 3.1a. Previous studies have concluded that the first concentrated acid rinse expands the spacing between graphitic layers to remove intercalated counterions [5, 6] and mineralized carbonates, [2] washing with concentrated base remove humic substances, [1, 2, 4], and the last concentrated acid wash removes surface-adsorbed  $\text{CO}_2$ . [2] Samples are exposed to water between each step to rinse and neutralize pH. Although the ABA cleaning method is used routinely in radiocarbon laboratories throughout the world, poorly preserved specimens can be completely broken down during the water and base rinses, thereby leaving no solid material for dating. To address this problem, it is an ongoing area of research to investigate modifications and alternatives to the ABA cleaning treatment that can be tailored for poorly preserved specimens. [2, 3, 7, 8]

The radiocarbon ABA treatment steps resemble the series of base and acid treatments that are typically involved in producing graphene oxide from graphite. Graphite

**(a) Acid-Base-Acid radiocarbon cleaning treatment**



**(b) Separation of graphene oxide from oxidative debris**

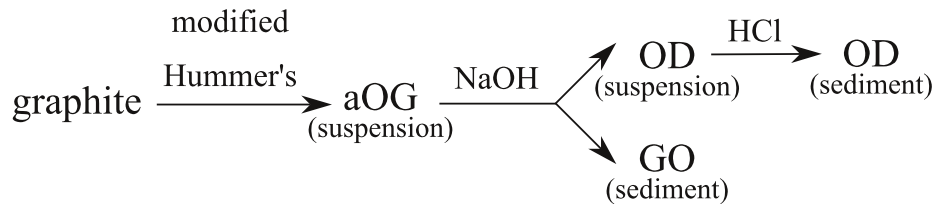


Figure 3.1: Schematic comparisons between (a) typical acid-base-acid (ABA) cleaning for radiocarbon samples and (b) steps to separate graphene oxide (GO) and oxidative debris (OD) from as-prepared oxidized graphite (aOG). All HCl and NaOH treatments are at 1M.

oxidation has drawn a great deal of attention from chemists since it improves the ability to suspend graphenic carbon materials in water. [9,10] However, the oxidation processes tend to yield graphenic particles with a range of different lateral dimensions, thicknesses, oxidation levels, and surface terminations. [11,12] For clarity, in this work, we adopt nomenclature for different kinds of graphenic carbon particles that was put forward by others. [13]

One of the most efficient ways to oxidize graphite is by chemical methods, [14, 15] as shown schematically in Figure 3.1b. As-prepared oxidized graphite (aOG) is readily suspended in water, and it has been shown to consist of a combination of graphene oxide (GO) along with highly oxidized, low molecular weight oxidative debris (OD). [16,17] In order to separate GO from OD, the as-prepared product can be treated with concentrated base causing the GO to sediment while the OD remains in the supernatant. [10,17] OD can then be precipitated from the supernatant using concentrated acid. [10,17]

Despite the similarities between the radiocarbon ABA cleaning procedure and the GO isolation procedure, there is virtually no overlap between these two fields in the literature. It is well documented that the ABA protocol separates humic substances, which are highly oxidized carbonaceous species, from graphite. [1, 2, 4] Previous radiocarbon-related literature shows evidence that oxidized graphite exists in archaeological charcoal. [18] GO-related literature is more recent, and some reports equate OD with humic substances. [10,19] However, no studies have investigated how graphenic carbon material that is intentionally oxidized is affected during different steps of the ABA cleaning procedure.

In this work, we show that there are synergies between (1) the chemistry involved in removing OD and GO from aOG and (2) the chemistry involved in the ABA cleaning of graphenic carbon materials used for radiocarbon dating. First, we show that a

different cleaning sequence of water/sonication-base-acid (WSBA) helps to separate oxidized graphite from graphite and oxidative debris. Next, we use existing knowledge of OD chemistry to explain why water and base rinses could diminish the quantity of graphenic carbon material that can be recovered after a standard ABA treatment. Finally, we demonstrate that the relative proportions of OD and aOG – independent of any humic substances – can affect the ability of oxidized graphite to be suspended in water, which can affect the efficiency of such separation procedures.

## 3.2 Experimental

### 3.2.1 Oxidation of graphenic carbon materials

Starting materials were graphite flakes (Alfa Aesar, 99.8% purity, 325 mesh) or pyrolyzed charcoal (mixture of fir and pine, heated in a nitrogen atmosphere from 30 °C to 480 °C over 1 hour, then held at 480 °C for 20 min). All purchased chemicals were ACS reagent grade:  $\text{KMnO}_4$  (99%),  $\text{NaOH}$  (97%), and  $\text{H}_2\text{O}_2$  (30%) from ACP, with  $\text{HCl}$  (38%) from Caledon, and  $\text{H}_2\text{SO}_4$  (98%) from Merck. All reactions used ultrapure water (Barnstead Nanopure Diamond, 18.2  $\text{M}\Omega\cdot\text{cm}$ ).

Our graphite oxidization protocol followed an improved Hummer’s method. [20,21] Powdered graphite or charcoal (1 g) was stirred in 50 mL  $\text{H}_2\text{SO}_4$  for 1 hour while immersed in an ice bath to hold the temperature at 0 °C. Then, 3 g of  $\text{KMnO}_4$  was added very slowly over 1 hour while keeping the temperature between 0 and 5 °C. The mixtures were then removed from the ice bath and warmed to room temperature during continuous stirring. After an hour, the mixtures became very thick and difficult to stir. They were then heated to 40 °C and left for 1 hour under automatic stirring (800 rpm). 80 mL of nanopure water was then added to the mixtures over a span of 5 min, after which the temperature was increased to 90 °C, followed by stirring

for another hour. Afterwards, 6 mL  $\text{H}_2\text{O}_2$  was added to the mixtures along with 200 mL water, followed by 1 hour of stirring. At this point, the product from graphite flakes transformed into a golden suspension, while the product from charcoal became an opaque dark brown suspension. The mixtures were centrifuged at 8500 rpm for 10 min to separate the sediment from the supernatant. The sediments were washed three times with nanopure water, yielding either a brown jelly (when derived from graphite flakes) or a dark brown sludge (when derived from charcoal). Sediments were dried in an oven overnight at 50 °C. In the remainder of this work, we refer to these dried sediments as either as-prepared oxidized flake graphite (aOG) or as-prepared oxidized charcoal (aOC).

### **3.2.2 Isolating GO and OD from oxidized graphenic carbon materials**

Sequential base and acid treatments facilitated separation of graphite/graphene oxide (GO) and oxidative debris (OD) from aOG and aOC. [10, 17]

0.05 g of brown aOG solid (or black aOC solid) was dispersed in 250 mL of 1M NaOH and stirred for 1 hour under reflux conditions at 90 °C. Immediately after adding the base, the aOG mixture became dark and opaque; the aOC became transparent light brown. After the coagulants cooled to room temperature, centrifugation separated the black solid residuals from the supernatants. The supernatant from aOG was clear and colourless, while the aOC supernatant was transparent light brown. The solid residuals were dispersed in water and centrifuged; after five such rinses, the supernatant had neutral pH. The resulting sediment was GO, and the supernatant contained OD in suspension.

250 mL of 1M HCl was added to the OD-containing supernatants obtained after both base washing and neutralization, followed by 30 min of stirring and oven-drying

at 60 °C overnight. The powder that remained was OD (white from the aOG precursor, and pale yellow from the aOC precursor).

### **3.2.3 Specimen characterization**

Attenuated total reflectance Fourier transform infrared (ATR-FTIR) spectra were recorded using a Bruker Alpha II spectrometer (diamond crystal, 36 scans, 4 cm<sup>-1</sup> resolution). UV-VIS spectra were acquired with a Varian Cary 6000 spectrometer with 0.1 second average time, 1 nm resolution, and 600 nm/min scan rate. Representative particle sizes were assessed from optical microscopy images (Leica, 5X and 20X NPLAN objectives) that were analyzed using Fiji particle analysis routines. [22]

## **3.3 Results and discussion**

### **3.3.1 Separating mixtures with WSBA**

In an archaeological charcoal sample, one might expect to find a mixture of graphite, GO, and OD, along with other foreign material. As a simpler test case, we outline a protocol to separate a mixture of graphite, aOG, and OD. This water/sonication-base-acid (WSBA) procedure is shown schematically in Figure 3.2, and summarized in Table 3.1.

Infrared spectroscopy allowed us to track structural changes in individual components, and also provided a qualitative way to monitor the efficacy and range of product variability at each separation step. Figure 3.3 compares ATR-FTIR spectra for each component at different stages of the WSBA procedure, displaying representative spectra from three different separation experiments using the same starting materials. These spectra are discussed below in the context of each stage of the separation protocol.

Action	Description
0. Starting mixture	graphite (0.02 g) + aOG (0.02 g) + nanopure water (10 mL)
1. Sonication	60 min
2. Filtration	8 $\mu$ m pore size paper (Whatman)
3. Dry solid (1), retain	8-12 hours at 50 $^{\circ}$ C
4. Base treat the filtrate	1M NaOH (pH=13, 20 mL) for 1 hour at 100 $^{\circ}$ C
5. Filtration	8 $\mu$ m filter paper (Whatman)
6. Dry solid (2), retain	8-12 hours at 40 $^{\circ}$ C
7. Acidify the filtrate	1M HCl (pH=2, 20 mL)
8. Dry solid (3), retain	12 hours at 80 $^{\circ}$ C

Table 3.1: A summary of the water/sonication-base-acid separation protocol. This produces three different solids: (1) as-prepared oxidized graphite (aOG), (2) graphite/graphene oxide (GO), and (3) oxidative debris (OD).

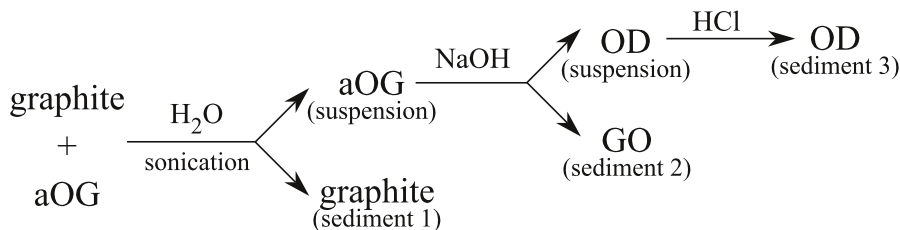


Figure 3.2: Water/sonication-base-acid (WSBA) protocol for separating GO (sediment 2) from graphite (sediment 1) and OD (sediment 3).

The first step in our WSBA protocol is sonication in water. Others report that, during sonication, aOG breaks into smaller pieces more easily than graphite breaks. [23,24] There is a strong precedent in the literature for using sonication to alter the size of oxidized graphenic carbon. [25–27] We exploit this to separate the larger graphite pieces from the smaller aOG pieces by filtration (Step 2 in Table 3.1).

Our IR data suggest that this combination of sonication and filtration works very well to extract graphite. Reports by others [28,29] show that graphite flakes do not exhibit many distinguishable IR peaks, and our data (Figure 3.3a) is consistent with this. Weak absorption bands at 3400 and 1600  $\text{cm}^{-1}$  are due to O-H stretches and

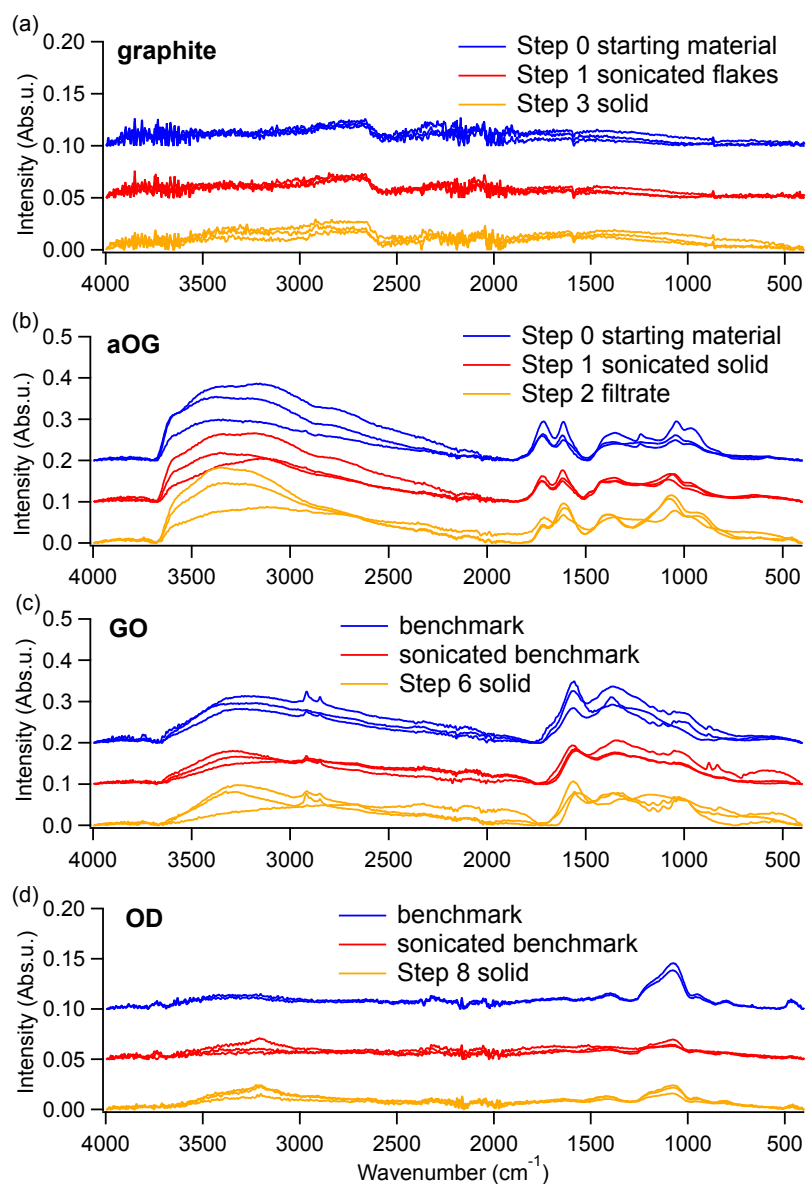


Figure 3.3: Representative ATR-FTIR spectra, before (blue) and after (red) sonication in water, of (a) graphite flakes, (b) aOG, (c) GO and (d) OD. Spectra are offset along the vertical axis for clarity. In each plot, the orange spectra correspond to the extracted component after the noted WSBA step. The plot legends indicate the precise preparation conditions for each sample, based on the procedure outlined in Table 1. In (c) and (d), the benchmark GO and OD samples were separated from unsonicated aOG using 1M NaOH (pH=13) followed by 1M HCl (pH=2). Note that the intensity scales for (a) and (d) are the same, and that they are expanded relative to (b) and (c).

C=C vibrations, respectively. [29] Figure 3.3a shows that there is no change in the IR peak positions between the starting graphite flakes (blue spectra) and the graphite after sonication (red spectra). Furthermore, the sonicated, large-size-filtered solid (orange spectra) does not show any additional peaks in the IR spectrum.

Unlike graphite, the aOG that exists in the filtrate (Step 2 in Table 3.1) shows very distinctive IR peaks (Figure 3.3b) due to the formation of oxygen-related functional groups such as carboxyl, alcohol, epoxide, and carbonyl. The peak positions for our aOG specimens are consistent with results from others. [17, 20, 21, 30] The peaks at 2800 and 2900  $\text{cm}^{-1}$  are due to  $\text{CH}_2$  symmetric and asymmetric stretching modes, respectively. The peak at 1600  $\text{cm}^{-1}$  is associated with water bending, while the 1300  $\text{cm}^{-1}$  peak results from C-O stretches. The broad band from 2400 to 3800  $\text{cm}^{-1}$  is related to O-H stretching modes, the sharp peak near 1700  $\text{cm}^{-1}$  is associated with carbonyl groups, and the peak near 1030  $\text{cm}^{-1}$  is related to C-O bonds in ester and carboxylic acid. Others have shown that size of GO flakes, and thus changes to the edge-to-area ratio, will affect the relative proportion of edge-groups (COOH) and in-sheet defects (C-O), which contributes to variations in relative FTIR peak intensities. [26, 27] Indeed, we observed changes in FTIR relative peak intensities before and after sonication. We note that we cannot rule out the possibility that some smaller graphite pieces exist and remain mixed with the aOG in the Step 2 filtrate. Similarly, it is possible that a small amount of aOG remains attached to the filter paper.

Once the graphite solid is removed, the filtrate is then treated with a strong base (Step 4 in Table 3.1) to dissociate GO (which is larger and less hydrophilic) from OD (which is smaller and tends to remain in suspension). [10, 17, 31] We note that these experimental conditions (NaOH at pH 11 and 25 °C) are not strong enough to trigger any reduction processes, and merely serves to decouple aOG into its two

components: GO and OD. Figure 3.3c shows that GO obtained after base treatment, filtration, and drying (Steps 4, 5, 6 in Table 3.1) has similar IR peak positions and relative intensities whether with or without exposure to sonication. The peak intensity variations that occur in the fingerprint region between 1000 and 1300  $\text{cm}^{-1}$  vary from work to work and from sample to sample, regardless of exposure to sonication. [12,16,17,20] The vibrational modes that contribute to peaks in this region are difficult to identify definitively because different oxygen-based functional groups contribute to many overlapping peaks. However, a typical FTIR spectrum for GO shows a broad peak near 3400-3700  $\text{cm}^{-1}$  for O-H stretching, a peak near 1720  $\text{cm}^{-1}$  due to carbonyl vibrations, another peak near 1600  $\text{cm}^{-1}$  for water bending modes, and a peak near 1040  $\text{cm}^{-1}$  for C-O. We note that peaks at 2800 and 2900  $\text{cm}^{-1}$  are associated with symmetric and asymmetric stretching modes [32] of  $\text{CH}_2$  and have been reported in GO samples, [33–35] but could be influenced by sonication. [36]

To extract the remaining solid component (OD), the filtrate is acidified and dried (Steps 7, 8 in Table 3.1) by using chemistry that is well documented in the literature. [10, 17, 31] Figure 3.3d shows that the IR spectra of OD are similar with or without exposure to sonication. Oxidized functional groups (C-OH and O-H) can cause the sharp peaks at 1100 and 3200  $\text{cm}^{-1}$  for OD. [10, 37]

We note that filter paper alone is not sufficient to separate GO from OD; both will pass through filter paper. OD (like GO) has a variable chemical composition and size. It is well documented in the literature that the main difference between them is that OD is smaller and more highly oxidized than GO. It is also well established that in neutral and alkaline solutions, OD complexes with GO. When aOG is added to a highly alkaline solution, it dissociates into its two constituents: the GO sediments, while the OD remains suspended.

As an overall comparison of the WSBA protocol, Figure 3.4a compares IR spectra

for the starting mixture (Step 0) with spectra for the three extracted solids: graphite, GO, and OD (from Steps 3, 6, and 8, respectively). It is noteworthy that the sum of the three spectra for the extracted solids would not be identical to spectra for the starting mixture. One of the most obvious discrepancies occurs in the range of 1500-1700  $\text{cm}^{-1}$  (Figure 3.4a), where a definitive GO peak does not align with any spectral features from the starting mixture. There are several contributing factors to these discrepancies.

First, the pH history of GO affects its IR spectrum. Figure 3.4b shows that there are many changes to peak positions and relative intensities after GO is exposed to different pH conditions (while in aqueous suspension) and then dried. After exposure to 1M NaOH, GO peaks near 1600 and 1400  $\text{cm}^{-1}$  increase, while spectral features near 1700  $\text{cm}^{-1}$  decrease. The relative peak intensities reverse after exposure to 1M HCl. Such pH-dependent changes have been noted by others who monitored the IR spectra of charcoal after ABA treatments, [2] and also by others investigating water-GO interactions. [12] Interpreting these pH-dependent peak intensity changes is surprisingly complex. For graphenic carbon materials, IR peaks have been attributed to carbonyl vibrations [12] (near 1700  $\text{cm}^{-1}$ ), C=C vibrations [29, 38, 39] (near 1600  $\text{cm}^{-1}$ ), and stretching modes of  $\text{COO}^-$  or C-OH (near 1400 and 1200  $\text{cm}^{-1}$ ). [2, 39] However, a bending mode of water also occurs in this region [11, 12, 40] (1609  $\text{cm}^{-1}$ ), as do S=O stretching modes. [30] In our case, it is possible that sulfates were introduced at epoxide groups [30] while in the presence of  $\text{H}_2\text{SO}_4$  during the initial preparation of the oxidized graphite starting material.

If one naively assumes that changes in relative IR peak intensities near 1600  $\text{cm}^{-1}$  are affected solely by the relative number of these different chemical moieties, then one might conclude from Figure 3.4b that a pH increase removes carbonyl groups and increases water,  $\text{COO}^-$ , C-OH, or S=O groups. However, detailed studies by others [12]

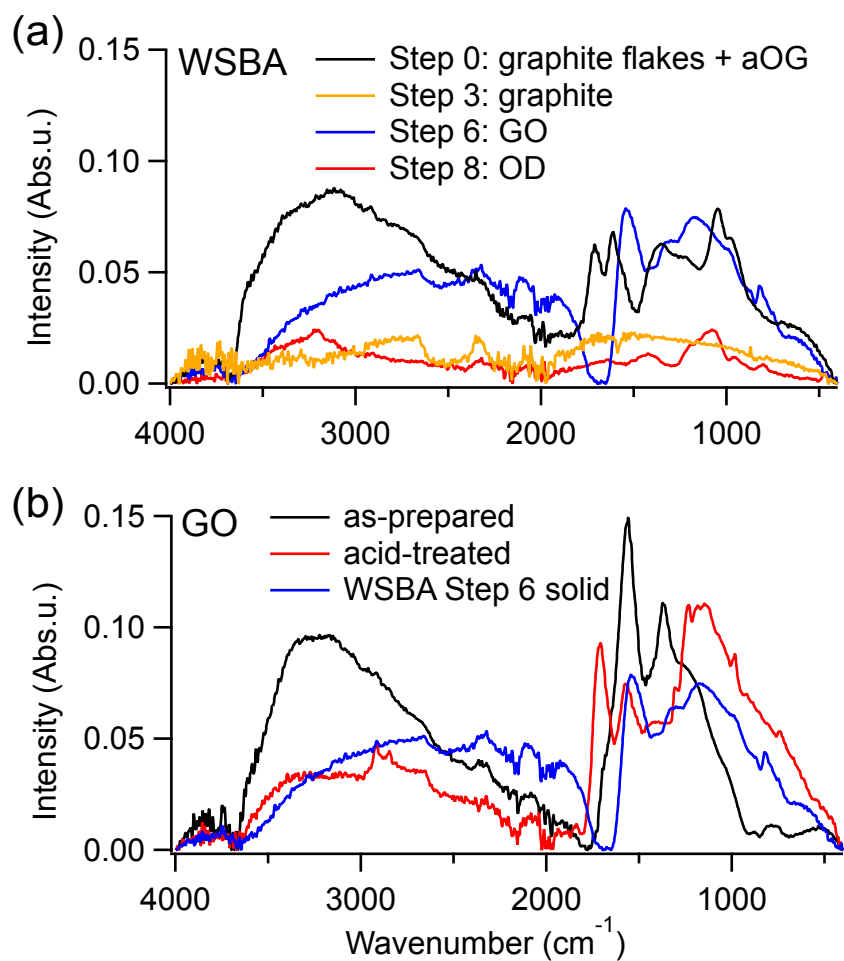


Figure 3.4: (a) Representative ATR-FTIR spectra for solids extracted at different stages of the WSBA protocol: starting mixture (black), graphite from Step 3 (orange), GO from Step 6 (blue), and OD from Step 8 (red). (b) Representative ATR-FTIR spectra of GO before and after acid treatment.

that correlated IR spectra with NMR in isotopically-altered samples suggest that such changes are likely caused by IR absorbance differences of water due to a reorientation in the presence of  $\text{Na}^+$ . Thus, even though the changes in relative IR peak intensities are consistent across different specimens and are clearly correlated with the sample's pH history, it is not appropriate to infer detailed structural information from IR peak intensity changes alone.

### 3.3.2 Interactions between GO and OD in water

Since the WSBA separation procedure relies on separating components by sedimentation, there is the potential to fine tune the separation procedure if one can change the amount or stability of the material in suspension. We show that the relative quantity of OD plays an important role in the ability of aOG to remain suspended in water over time.

For context, previous studies have shown that chemical oxidization produces GO and OD in 2:1 ratio, and that OD adheres to GO by hydrogen bonding to making the as-prepared complex easy to suspend in water. [10] Because both OD and GO react readily with water and can exist in a range of sizes, there is no fixed chemical structure or composition for either OD or GO. [16]

In our experiments with enriched OD levels, 0.03 g of aOG was dispersed in 50 mL of nanopure water, then divided into 15 mL aliquots, with 0.5 g of OD added (extracted from either aOG or aOC). These mixtures, along with a control sample containing only aOG, were stirred at 400 rpm for 15 min and then left standing for one day.

Figure 3.5 shows different time-dependent sedimentation behavior with and without enriched OD levels. After one day, an aOG suspension (Figure 3.5a) shows a dark opaque sediment that is clearly separated from a translucent brown supernatant.

Under the same conditions, the presence of additional OD (Figure 3.5b) causes a uniformly coloured translucent suspension with no visible sediment. Based on these results, it is tempting to assume that additional OD makes aOG more soluble in water. However, lengthening the sedimentation time to 7 days (Figure 3.5c,d) demonstrates that OD does not dissolve aOG, but instead helps it to aggregate and precipitate out over time. To help support this conclusion, representative UV-Vis spectra for these different supernatants are compared in Figure 3.5e. The aOG (solid black curve) has a distinctive peak near 220 nm and a shoulder near 300 nm, which others have attributed to different electronic transitions within graphenic carbon materials. [15,20] These characteristic spectral features appear in supernatants from unenriched aOG after 1 day (solid blue curve) and 7 days (dashed blue curve), as well as in OD-enriched mixtures after 1 day (solid red curve). However, supernatant from OD-enriched mixtures after 7 days (dashed red curve) have no distinctive UV-Vis features, which is consistent with the absence of aOG in the supernatant. [31]

This simple enrichment experiment is important for several reasons. First, our results demonstrate that the relative proportions of OD and aOG – independent of any humic substances – can affect how readily oxidized graphite stays in suspension over time. This means that time and OD enrichment protocols could – in principle – be developed to help separate graphite from OD and GO.

### **3.3.3 Comparing WSBA to radiocarbon sample cleaning protocols**

In this work, we apply a water/sonication-base-acid (WSBA) treatment, which includes sonication during the water treatment, in order to separate a mixture of graphite, GO, and OD. This mixture is a simplistic model system that mimics the types of graphenic carbon materials that could be present in fossilized charcoal. This

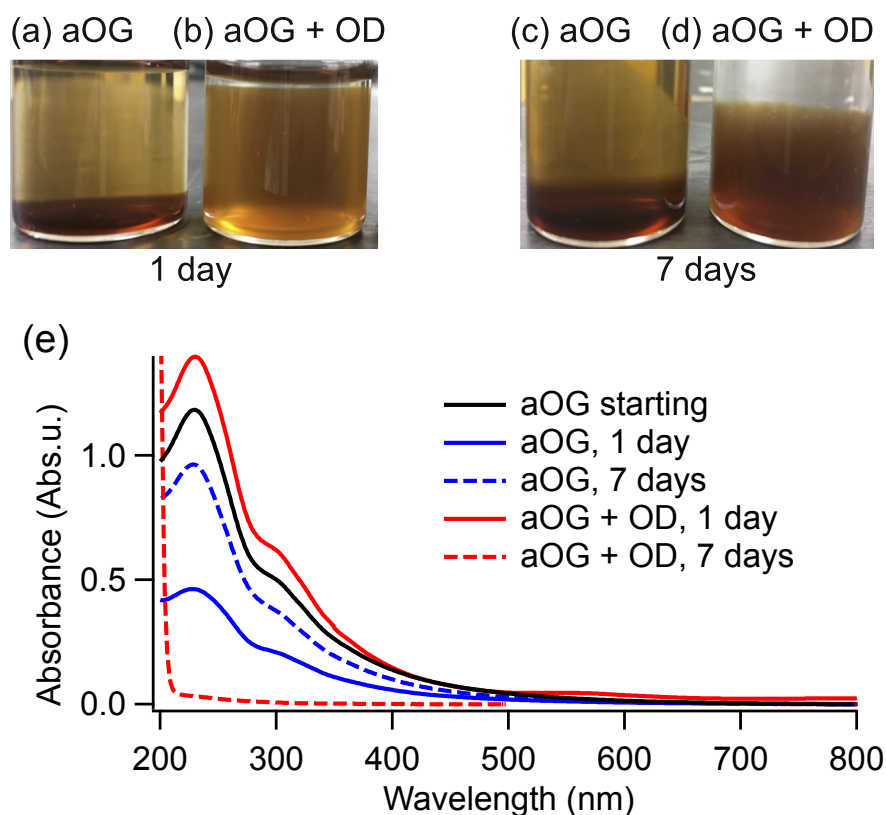


Figure 3.5: Photographs of aOG (a,c) and aOG + extra OD (b,d) after one day (a,b) and seven days (c,d). Plot (e) compares representative UV-Vis spectra of fresh aOG suspension (black curve) with supernatants of aOG (blue curves) and OD-enriched aOG (red curves), after sitting for 1 day (solid curves) or 7 days (dashed curves).

is the first time that graphenic carbon chemistry [10, 17] been applied rationally to the separation of graphite-based materials related to radiocarbon dating applications.

We are not the first to use water treatments to separate charcoal from other carbonaceous material. In an earlier study, others found that significant weight loss can occur after water treatment of fossil charcoal. [2] They attributed the weight loss to the removal of poorly preserved (oxidized) graphite, citing earlier work that suggested that fossil charcoal can be oxidized during weathering to produce carboxyl groups. [1, 18] These earlier studies also suggested the possibility of OD formation in archaeological samples, proposed in terms of "self-humification." [18] These studies

from the radiocarbon literature [1,2,18] pre-date much of the GO and OD separation literature that informs our WSBA protocol. [10,12,17]

In a broader context, the reason that our experiments, and an explicit link between GO/OD literature and ABA literature, are important, is that they introduce informed strategies to capture and separate GO and OD from graphite. We are the first to propose this. This is significant because it opens the door for new experiments that could test the viability of using GO or OD as a material for radiocarbon dating. In principle, the oxidation processes that produce GO and OD from graphitic materials would not alter a specimen's original (datable) carbon. However, this idea has not been broached in the radiocarbon dating literature. The current norm is that oxidized graphite should be removed before dating. For example, one modification of the ABA procedure is ABOx, wherein an oxidation process (based on  $K_2Cr_2O_7$  and  $H_2SO_4$ ) replaces the last acid (HCl) treatment in the usual ABA protocol, in order to remove oxidizable carbon before dating. [3,7]

Although it is logical that graphite would remain the preferred material for radiocarbon dating, some samples disintegrate dramatically after base (NaOH) washes during the standard ABA treatment. [2] For such poorly preserved samples wherein severe graphite oxidation is suspected, our WSBA protocol could be helpful for capturing additional graphenic carbon material, in the form of GO and/or OD. A substantial number of future experiments would be necessary to explore the conditions under which our WSBA treatment could help extract graphite-based materials that produce reliable radiocarbon dates.

One of the main operational differences between our WSBA separation procedure and other ABA-based cleaning procedures for datable radiocarbon materials is our use of sonication (Step 1 in Table 1). We explored a range of different experimental conditions to determine that filtration of suspensions (pH 5-8) and/or centrifugation

(2000-8500 rpm, 1-15 min) on their own are not effective for separating graphite flakes from aOG. We found that the most effective method was to centrifuge (8500 rpm for 10 min) when the aqueous solution was strongly alkaline (pH= 11), followed by filtering (8  $\mu\text{m}$  pore size).

As described above, sonication is known to break aOG into smaller pieces more easily than graphite. [23–27] Optical microscopy images of our samples before and after sonication confirm that this holds true in our experiments (Figure 3.6). We note that these representative images do not give truly comprehensive information about the distribution of sizes within the full sample, but they do provide evidence that sonication reduces the particle sizes of aOG well below the pore size of our filter paper (8  $\mu\text{m}$  diameter,  $\sim 60 \mu\text{m}^2$  cross-sectional area). For example, statistical analyses of particle sizes shown in Figure 3.6 indicate that sonication reduces the median particle area of graphite from  $\sim 110 \mu\text{m}^2$  to  $\sim 80 \mu\text{m}^2$ , and reduces the median particle area of aOG from  $\sim 110 \mu\text{m}^2$  to  $\sim 10 \mu\text{m}^2$ . This illustrates why it is feasible to separate the larger graphite pieces from the smaller aOG pieces using filtration. Based on our FTIR data (Figure 3.2), filtration-based size separation is very effective on our simplistic test mixture.

However, applying this method successfully to archaeological samples would likely be much more challenging. Factors such as oxidation method, reaction time, oxidants, pH, and sonication are known to affect the sizes of aOG particles [41–45], ranging from less than 1  $\mu\text{m}$  to greater than 200  $\mu\text{m}$ . [26, 38, 46, 47] The stability and dispersibility of aOG in water are strongly associated with the lateral size of aOG and C-O content, and some studies have correlated zeta potential (effective surface charge) data with the suspension behaviours of aOG. [27] Thus, since any oxidation within an archaeological charcoal sample will undoubtedly occur in a very different manner from the harsh chemical oxidation that we used in our simplistic test model, the sonication step

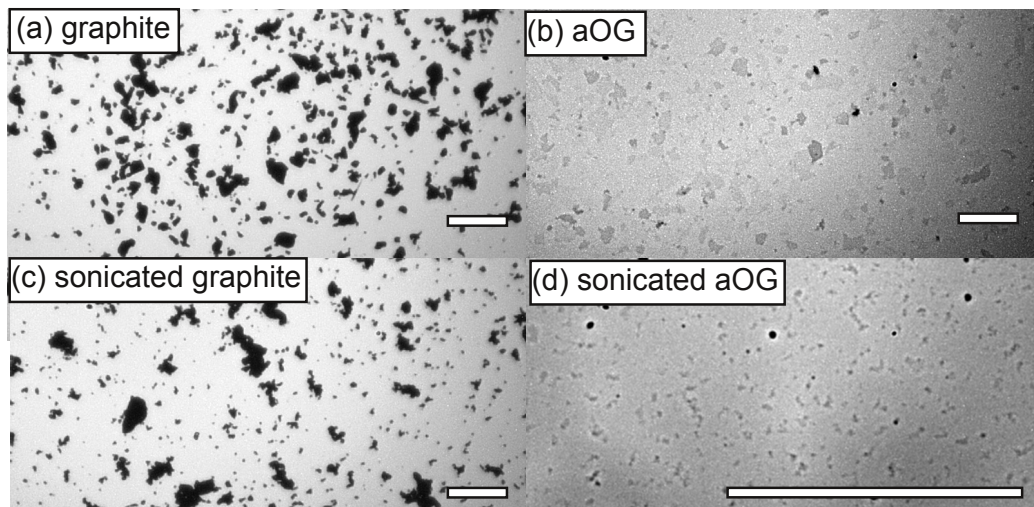


Figure 3.6: Representative optical microscopy images of (a) graphite, (b) aOG, (c) sonicated graphite, and (d) sonicated aOG. The opaque graphite particles (a,c) show greater contrast than the optically transparent aOG (b,d). Scale bars represent 100  $\mu\text{m}$  in all images; in (d), the image is magnified to show particle outlines more clearly.

would likely have different effects on any given archaeological sample.

It is also worth noting that cleaning procedures for radiocarbon dating samples must be designed to avoid introducing different sources of carbon into the specimen. For example, samples are never handled with bare hands, and all stages of the cleaning involve aqueous treatments (to avoid contact with organic solvents). In the case of the WSBA procedure outlined here, we use carbon-based filter paper at two different stages (Steps 2 and 5 in Table 3.1). If future studies indicate a need to avoid contact with filter paper, we note that others have used a range of methods to isolate aOG particles based on size differences, including centrifugation, magnetic stirring, density gradient ultracentrifugation, and electrophoresis. [47–49]

### 3.4 Conclusions

In this work, we show synergies between (1) the chemistry involved in removing graphenic oxide (GO) and oxidative debris (OD) from oxidized graphenic carbon

materials, and (2) the chemistry involved in ABA cleaning of graphenic carbon materials used for radiocarbon dating. Drawing on literature from the subfields of GO chemistry and radiocarbon dating, we introduce a different cleaning sequence of water/sonication-base-acid (WSBA) that is designed to separate graphite from GO and OD. Furthermore, we demonstrate that the relative proportions of OD and aOG – independent of any humic substances – can affect the ability of oxidized graphite to be suspended in water, which can effect the efficiency of the separation procedures we describe. In principle, this could be used to fine tune separation procedures during sample cleaning for radiocarbon sample preparation. Finally, we use the chemistry of OD to explain why WSBA could be more advantageous than traditional ABA cleaning procedures in some situations, such as the case when water and base treatments diminish the quantity of poorly preserved (oxidized) graphite that could be recovered after a standard ABA cleaning treatment. Looking forward, it is interesting to speculate whether GO and OD could be viable materials for radiocarbon dating, if extracted from archaeological charcoal samples.

### **3.5 Acknowledgements**

Thanks to Dr. Bob Helleur for charcoal samples. KMP thanks the NSERC (Canada) Discovery Grant program for funding.

## Bibliography

- [1] Dani Alon, Genia Mintz, Illit Cohen, Steve Weiner, and Elisabetta Boaretto. The use of Raman spectroscopy to monitor the removal of humic substances from charcoal; quality control for  $^{14}\text{C}$  dating of charcoal. *Radiocarbon*, 44(1):1–11, 2002.
- [2] N. R. Rebollo, I. Cohen-Ofri, R. Popovitz-Biro, O. Bar-Yosef, L. Meignen, P. Goldberg, S. Weiner, and E. Boaretto. Structural Characterization of Charcoal Exposed to High and Low pH: Implications for  $^{14}\text{C}$  Sample Preparation and Charcoal Preservation. *Radiocarbon*, 50(2):289–307, 2008.
- [3] Michael I. Bird, Vladimir Levchenko, Philippa L. Ascough, Will Meredith, Christopher M. Wurster, Alan Williams, Emma L. Tilston, Colin E. Snape, and David C. Apperley. The efficiency of charcoal decontamination for radiocarbon dating by three pre-treatments – ABOx, ABA and hypy. *Quat. Geochronol.*, 22:25 – 32, 2014.
- [4] Edwin A. Olson and W. S. Broecker. Section of Geology and Mineralogy: Sample Contamination and Reliability of Radiocarbon Dates. *Trans. N. Y. Acad. Sci.*, 20(7 Series II):593–604, 1958.
- [5] Emir Bouleghimat, Philip R. Davies, Robert J. Davies, Rebecca Howarth, Jiri Kulhavy, and David J. Morgan. The effect of acid treatment on the surface chemistry and topography of graphite. *Carbon*, 61:124–133, 2013.
- [6] Feiyu Kang, Yang Leng, Tong-Yi Zhang, and Bensheng Li. Electrochemical synthesis and characterization of ferric chloride-graphite intercalation compounds in aqueous solution. *Carbon*, 36(4):383–390, 1998.

- [7] M. I. Bird, L. K. Ayliffe, L. K. Fifield, C. S. M. Turney, R. G. Cresswell, T. T. Barrows, and B. David. Radiocarbon Dating of “Old” Charcoal Using a Wet Oxidation, Stepped-Combustion Procedure. *Radiocarbon*, 41(2):127–140, 1999.
- [8] P. L. Ascough, M. I. Bird, W. Meredith, R. E. Wood, C. E. Snape, F. Brock, T. F. G. Higham, D. J. Large, and D. C. Apperley. Hydropyrolysis: Implications for Radiocarbon Pretreatment and Characterization of Black Carbon. *Radiocarbon*, 52(3):1336–1350, 2010.
- [9] Siegfried Eigler, Michael Enzelberger-Heim, Stefan Grimm, Philipp Hofmann, Wolfgang Kroener, Andreas Geworski, Christoph Dotzer, Michael Rockert, Jie Xiao, Christian Papp, Ole Lytken, Hans-Peter Steinruck, Paul Muller, and Andreas Hirsch. Wet Chemical Synthesis of Graphene. *Adv. Mater.*, 25(26):3583–3587, 2013.
- [10] Jonathan P. Rourke, Priyanka A. Pandey, Joseph J. Moore, Matthew Bates, Ian A. Kinloch, Robert J. Young, and Neil R. Wilson. The Real Graphene Oxide Revealed: Stripping the Oxidative Debris from the Graphene-like Sheets. *Angew. Chem.*, 50(14):3173–3177, 2011.
- [11] Tamas Szabo, Etelka Tombacz, Erzsebet Illes, and Imre Dekany. Enhanced acidity and pH-dependent surface charge characterization of successively oxidized graphite oxides. *Carbon*, 44(3):537–545, 2006.
- [12] Ayrat M. Dimiev, Lawrence B. Alemany, and James M. Tour. Graphene Oxide. Origin of Acidity, Its Instability in Water, and a New Dynamic Structural Model. *ACS Nano*, 7(1):576–588, 2013.
- [13] Alberto Bianco, Hui-Ming Cheng, Toshiaki Enoki, Yuri Gogotsi, Robert H. Hunt, Nikhil Koratkar, Takashi Kyotani, Marc Monthieux, Chong Rae Park, Juan

- M. D. Tascon, and Jin Zhang. All in the graphene family - A recommended nomenclature for two-dimensional carbon materials. *Carbon*, 65:1–6, 2013.
- [14] William S. Hummers and Richard E. Offeman. Preparation of Graphitic Oxide. *J. Am. Chem. Soc.*, 80(6):1339–1339, 1958.
- [15] Daniela C. Marcano, Dmitry V. Kosynkin, Jacob M. Berlin, Alexander Sinit-skii, Zhengzong Sun, Alexander Slesarev, Lawrence B. Alemany, Wei Lu, and James M. Tour. Improved Synthesis of Graphene Oxide. *ACS Nano*, 4(8):4806–4814, 2010.
- [16] Ayrat M. Dimiev and James M. Tour. Mechanism of Graphene Oxide Formation. *ACS Nano*, 8(3):3060–3068, 2014.
- [17] Helen R. Thomas, Stephen P. Day, William E. Woodruff, Cristina Valles, Robert J. Young, Ian A. Kinloch, Gavin W. Morley, John V. Hanna, Neil R. Wilson, and Jonathan P. Rourke. Deoxygenation of Graphene Oxide: Reduction or Cleaning? *Chem. Mater.*, 25(18):3580–3588, 2013.
- [18] Ilit Cohen-Ofri, Lev Weiner, Elisabetta Boaretto, Genia Mintz, and Steve Weiner. Modern and fossil charcoal: aspects of structure and diagenesis. *J. Archaeol. Sci.*, 33(3):428 – 439, 2006.
- [19] Zhaowei Wang, Mark D. Shirley, Steven T. Meikle, Raymond L. D. Whitby, and Sergey V. Mikhalovsky. The surface acidity of acid oxidised multi-walled carbon nanotubes and the influence of in-situ generated fulvic acids on their stability in aqueous dispersions. *Carbon*, 47(1):73–79, 2009.
- [20] Ji Chen, Bowen Yao, Chun Li, and Gaoquan Shi. An improved Hummers method for eco-friendly synthesis of graphene oxide. *Carbon*, 64:225–229, 2013.

- [21] Martin Rosillo-Lopez and Christoph G. Salzmänn. A simple and mild chemical oxidation route to high-purity nano-graphene oxide. *Carbon*, 106:56–63, 2016.
- [22] J. Schindelin, I. Arganda-Carreras, and E. Frise. Fiji: an open-source platform for biological-image analysis. *Nature Meth.*, 9(7):676–682, 2012.
- [23] Artur Ciesielski and Paolo Samori. Graphene via sonication assisted liquid-phase exfoliation. *Chem. Soc. Rev.*, 43:381–398, 2014.
- [24] Shibing Ye and Jiachun Feng. The effect of sonication treatment of graphene oxide on the mechanical properties of the assembled films. *RSC Advances*, 6(46):39681–39687, 2016.
- [25] Zhong-Shuai Wu, Wencai Ren, Libo Gao, Bilu Liu, Jinping Zhao, and Hui-Ming Cheng. Efficient synthesis of graphene nanoribbons sonochemically cut from graphene sheets. *Nano Research*, 3(1):16–22, 2010.
- [26] Akshaya Kumar Swain, Dan Li, and Dharendra Bahadur. UV-assisted production of ferromagnetic graphitic quantum dots from graphite. *Carbon*, 57:346–356, 2013.
- [27] Jaemyung Kim, Laura J. Cote, Franklin Kim, Wa Yuan, Kenneth R. Shull, and Jiaying Huang. Graphene Oxide Sheets at Interfaces. *J. Am. Chem. Soc.*, 132(23):8180–8186, 2010.
- [28] Rengeng Gu, William Z. Xu, and Paul A. Charpentier. Synthesis of polydopamine coated graphene polymer nanocomposites via RAFT polymerization. *J. Polym. Sci. A*, 51(18):3941–3949, 2013.

- [29] Shuge Peng, Xinjie Fan, Shuang Li, and Jun Zhang. Green Synthesis and Characterization of Graphite Oxide by Orthogonal Experiment. *J. Chil. Chem. Soc.*, 58:2213 – 2217, 2013.
- [30] Ayrat Dimiev, Dmitry V. Kosynkin, Lawrence B. Alemany, Pavel Chaguine, and James M. Tour. Pristine Graphite Oxide. *J. Am. Chem. Soc.*, 134(5):2815–2822, 2012.
- [31] Helen R. Thomas, Cristina Valles, Robert J. Young, Ian A. Kinloch, Neil R. Wilson, and Jonathan P. Rourke. Identifying the fluorescence of graphene oxide. *J. Mater. Chem. C*, 1:338–342, 2013.
- [32] Robert A. Meyers and John Coates. *Interpretation of Infrared Spectra, A Practical Approach*. New York, NY (USA) Wiley, 2000.
- [33] Andréia F. Faria, Diego Stéfani T. Martinez, Ana C. M. Moraes, Marcelo E. H. Maia da Costa, Eduardo B. Barros, Antonio G. Souza Filho, Amauri J. Paula, and Oswaldo L. Alves. Unveiling the Role of Oxidation Debris on the Surface Chemistry of Graphene through the Anchoring of Ag Nanoparticles. *Chem. Mater.*, 24(21):4080–4087, 2012.
- [34] C. Montaserin, M. Blanco, E. Aranzabe, A. Aranzabe, J.M. Laza, A. Larranaga-Varga, and J.L. Vilas. Effects of graphene oxide and chemically-reduced graphene oxide on the dynamic mechanical properties of epoxy amine composites. *Polymers*, 9(9):1–16, 2017.
- [35] Yan Li, Hui Liu, Xin-qian Liu, Sen Li, Lifeng Wang, Ning Ma, and Dengli Qiu. Free-Radical-Assisted Rapid Synthesis of Graphene Quantum Dots and Their Oxidizability Studies. *Langmuir*, 32(34):8641–8649, 2016.

- [36] Alessandra Bonanni, Adriano Ambrosi, Chun Kiang Chua, and Martin Pumera. Oxidation Debris in Graphene Oxide Is Responsible for Its Inherent Electroactivity. *ACS Nano*, 8(5):4197–4204, 2014.
- [37] Raquel Verdejo, Steven Lamoriniere, Ben Cottam, Alexander Bismarck, and Milo Shaffer. Removal of oxidation debris from multi-walled carbon nanotubes. *ChemComm*, (5):513–515, 2007.
- [38] Ji Chen, Yingru Li, Liang Huang, Naer Jia, Chun Li, and Gaoquan Shi. Size Fractionation of Graphene Oxide Sheets via Filtration through Track-Etched Membranes. *Adv. Mater.*, 27(24):3654–3660, 2015.
- [39] Wenjun Zhang, Xuefeng Zou, Huanrong Li, Jingju Hou, Jinfeng Zhao, Jianwen Lan, Baolong Feng, and Shuting Liu. Size fractionation of graphene oxide sheets by the polar solvent-selective natural deposition method. *RSC Adv.*, 5:146–152, 2015.
- [40] Tamas Szabo, Otto Berkesi, Péter Forgo, Katalin Josepovits, Yiannis Sanakis, Dimitris Petridis, and Imre Dekany. Evolution of Surface Functional Groups in a Series of Progressively Oxidized Graphite Oxides. *Chem. Mater.*, 18(11):2740–2749, 2006.
- [41] Jinping Zhao, Songfeng Pei, Wencai Ren, Libo Gao, and Hui-Ming Cheng. Efficient Preparation of Large-Area Graphene Oxide Sheets for Transparent Conductive Films. *ACS Nano*, 4(9):5245–5252, 2010.
- [42] Xufeng Zhou and Zhaoping Liu. A scalable, solution-phase processing route to graphene oxide and graphene ultralarge sheets. *ChemComm*, 46(15):2611–2613, 2010.

- [43] Xiluan Wang, Hua Bai, and Gaoquan Shi. Size Fractionation of Graphene Oxide Sheets by pH-Assisted Selective Sedimentation. *J. Am. Chem. Soc.*, 133(16):6338–6342, 2011.
- [44] Ching Yuan Su, Yanping Xu, Wenjing Zhang, Jianwen Zhao, Xiaohong Tang, Chuen Horng Tsai, and Lain Jong Li. Electrical and Spectroscopic Characterizations of Ultra-Large Reduced Graphene Oxide Monolayers. *Chem. Mater.*, 21(23):5674–5680, 2009.
- [45] Shuyang Pan and Ilhan A. Aksay. Factors Controlling the Size of Graphene Oxide Sheets Produced via the Graphite Oxide Route. *ACS Nano*, 5(5):4073–4083, 2011.
- [46] Kyung Eun Lee, Ji Eun Kim, Uday Narayan Maiti, Joonwon Lim, Jin Ok Hwang, Jongwon Shim, Jung Jae Oh, Taeyeong Yun, and Sang Ouk Kim. Liquid Crystal Size Selection of Large-Size Graphene Oxide for Size-Dependent N-Doping and Oxygen Reduction Catalysis. *ACS Nano*, 8(9):9073–9080, 2014.
- [47] Hongya Geng, Bowen Yao, Jiajia Zhou, Kai Liu, Guoying Bai, Wenbo Li, Yanlin Song, Gaoquan Shi, Masao Doi, and Jianjun Wang. Size Fractionation of Graphene Oxide Nanosheets via Controlled Directional Freezing. *J. Am. Chem. Soc.*, 139(36):12517–12523, 2017.
- [48] Yong Liu, Dong Zhang, Shiwu Pang, Yanyun Liu, and Yu Shang. Size separation of graphene oxide using preparative free-flow electrophoresis. *J. Sep. Sci.*, 38(1):157–163, 2015.
- [49] Sha Li, Fengsen Zhu, Fanjun Meng, Haibo Li, Lei Wang, Jingjing Zhao, Qiaoli Yue, Jifeng Liu, and Jianbo Jia. Separation of graphene oxide by density gra-

dient centrifugation and study on their morphology-dependent electrochemical properties. *J. Electroanal. Chem.*, 703:135–145, 2013.

## Chapter 4

# Identifying and Extracting Oxidized Graphenic Materials from Environmentally Altered Sources of Graphite

Oxidized graphenic materials like graphene oxide (GO) and oxidative debris (OD) in archaeological charcoal, if formed as graphite oxidizes over time, could be valuable sources for radiocarbon dating because their  $^{14}\text{C}$  levels would be the same as the parent graphite. However, no studies have investigated whether GO and OD exist in archaeological charcoal. Here, we try to identify and separate oxidized graphenic materials from archaeological charcoal. This result is important because it is the first step toward a method to extract oxidized graphenic materials from archaeological charcoal for radiocarbon dating analyses.

## 4.1 Introduction

Earlier studies found that graphite, humic acid (HA), and minerals are present in archaeological charcoal, but only the graphite portion is cleaned and used for radiocarbon dating [1–3]. However, we propose that oxidized graphenic carbon could also be used because the  $^{14}\text{C}$  levels in these materials would be the same as the graphite from which it was derived. To date, no studies have explicitly investigated the presence of GO and OD in archaeological charcoal. We do so in this chapter.

In Chapter 3, we used chemistry from the literature to show that moderately oxidized (GO) and highly oxidized (OD) graphenic carbon materials can be separated using a sequential base and acid treatments. We also developed a method to separate different graphenic carbon materials from a standard mixture of graphite and as-prepared oxidized graphite (aOG). Our results confirm an acceptable separation for this test mixture. However, we want to see whether this method works for a naturally occurring mixture of carbon-based materials in archaeological charcoal. An important challenge regarding the preparation of uncleaned archaeological charcoal is removing contaminants like soil, sand, and roots from the sample. Sand and tree roots can be physically removed from the sample, while minerals and humic materials, which can penetrate between graphite layers, need chemical treatments. Others have used aqueous solutions at different pH values to eliminate minerals and humic materials [1, 2, 4]. The chemical separation, however, is harder and more challenging than the physical one since acidic and alkaline treatments affect the charcoal adversely [2].

In this part of the research, we use Raman and IR spectroscopy along with pH data to look for the presence of oxidized graphenic materials in archaeological charcoal. We use our water-sonication-base-acid (WSBA) method (described in Chapter 3) to extract oxidized graphenic materials from the archaeological charcoal. Since the composition of oxidized graphenic carbon is unclear in archaeological charcoal, we will

classify the WSBA products as follows: (1) least oxidized, (2) moderately oxidized, and (3) highly oxidized.

## 4.2 Experimental

### 4.2.1 Materials

In this chapter, we study two different sources of graphenic carbon materials: (1) reference and (2) environmentally-altered sources. Graphite and GO are the representatives of the first group, while archaeological charcoal and coal are examples of the second one. Graphite flakes came from Alfa Aesar, 99.8 percent purity, 325 mesh. GO was prepared from graphite flakes using a modified Hummer's method [5, 6] as I described in Chapter 2. The SRHA was obtained from the International Humic Substances Society, Denver, CO (USA) and Sigma Aldrich HA was from St. Louis, MO (USA). Archaeological charcoal was obtained from Dr. Lisa Rankin (MUN Archaeology), Labrador, Canada (as described in Chapter 2). The archaeological sample was a mixture of charcoal, sand, soil, and dry leaf, which was pulled out from a campfire. The black part, which we identified as charcoal, was physically separated from the other parts and was ground by mortar and pestle to obtain a fine powder.

### 4.2.2 Separation of oxidized materials using WSBA

We used our water, sonication, base, acid (WSBA) protocol, which was described in Chapter 3, to isolate highly oxidized materials from less oxidized ones in our archaeological sample. This procedure is summarized in Table 4.1. 0.20 g of charcoal was crushed using a mortar and pestle and added to 20 mL of nanopure water followed by sonication for 60 min. The black-dark brown suspension was filtered by 8  $\mu\text{m}$  pore size Whatman filter paper, leaving solid **1** and a light brown filtrate. The filtered

Action	Description
0. Starting mixture	Archaeological charcoal (0.2 g) + nanopure water (20 mL)
1. Sonication	60 min
2. Filtration	8 $\mu\text{m}$ pore size paper
3. Dry solid <b>1</b> , retain	8-12 hours at 40 °C
4. Base treatment of the filtrate	1M NaOH (pH=13, 100 mL) for 1 hour at 100 °C
5. Filtration	8 $\mu\text{m}$ pore size paper
6. Dry solid <b>2</b> , retain	8-12 hours at 40 °C
7. Acidify the filtrate	1M HCl (pH=2, 100 mL)
8. Dry solid <b>3</b> , retain	12 hours at 80 °C

Table 4.1: A summary of water/sonication-base-acid separation protocol on archaeological charcoal. This produces three different solids: (1) least oxidized, (2) moderately oxidized, and (3) highly oxidized materials.

residual was dried in an oven overnight at 40 °C. The light brown filtrate was treated with 100 mL of 1M NaOH at 100 °C for one hour. After the base treatment, the mixture was filtered using the filter paper, and solid **2** was dried overnight at 40 °C. Then, the filtrate was acidified with 100 mL of 1M HCl followed by stirring at 800 rpm for 30 min. The solution was dried at 80 °C for 12 hours to yield solid **3**. Data presented here are based on two different WSBA separations on the same archaeological charcoal sample.

### 4.2.3 Characterization methods

Raman measurements used a Renishaw spectrometer (632 nm excitation, 20X objective, 11 mW power, exposure time 30 s). Spectra were collected in the range of 100-3000  $\text{cm}^{-1}$ . Attenuated total reflectance Fourier transform infrared (ATR-FTIR) spectra were recorded using a Bruker Alpha II spectrometer with a diamond crystal, 36 scans, and 4  $\text{cm}^{-1}$  resolution in the range of 4000-400  $\text{cm}^{-1}$ . The pH measurements were done using Schott Instruments Lab 860 pH meter calibrated by three buffers at

pH 4, 7, and 11.

## 4.3 Results and discussion

In this section, we first look for the presence of oxidized graphenic materials in uncleaned archaeological charcoal. In principle, carbonaceous contaminants like HA should also exist in archaeological charcoal. Archaeologists have used base treatment to remove HA from graphenic materials in different archaeological charcoal samples before radiocarbon measurement [2, 4]. We analyze the uncleaned sample because the aqueous cleaning treatments at different pH also remove the oxidized graphenic carbon that we want to characterize. Then, we try to separate graphenic materials, with different levels of oxidation, from the archaeological charcoal.

### 4.3.1 Uncleaned archaeological charcoal suspension

Oxidized graphite suspensions have properties that can be easily identified by visual observation and pH analysis. We use them to check if oxidized graphite exists in archaeological charcoal.

Figure 4.1 compares suspensions of aOG, as a reference for oxidized graphite, with an archaeological charcoal sample. A typical suspension of aOG is brown and translucent. The aOG suspensions settle out after one day, forming darker opaque sediment and translucent brown supernatant. The suspensions of graphite flakes are black and opaque, and they settle out quickly in one hour, resulting in a clear, colourless supernatant.

Visual observations suggest that archaeological charcoal in water behaves more like graphite than aOG because the suspension of archaeological charcoal is black and opaque, and settles out quickly like graphite suspension.



Figure 4.1: Images of (left) lab-synthesized aOG and (right) archaeological charcoal suspensions taken immediately after they were made.

Table 4.2: The pH variations of as-prepared oxidized graphite (aOG), humic acid (HA), and archaeological charcoal suspensions in nanopure water. The second row shows data from this project, while the third one shows data from the literature.

Samples	water	water+aOG	water+HA	water+charcoal
pH (my data)	$6.5 \pm 0.3$	$3.3 \pm 0.1$	$7.2 \pm 0.2$	$4.6 \pm 0.1$
pH (literature)	$6.6 \pm 0.1$ [7]	$3.7 \pm 0.2$ [8]	$6.8 \pm 0.2$ [9]	$4.5 \pm 0.5$ [4]

pH measurements on these suspensions indicate that oxidized graphite might be present because the uncleaned archaeological charcoal suspension decreases the pH of water. Table 4.2 shows that the pH of nanopure water (6.5) decreases to 3.3 and 4.6 after adding aOG and archaeological charcoal, respectively. Since humic acid (HA) could also be present in archaeological charcoal, we decided to measure the pH of two different references of HA (Suwannee River and Sigma Aldrich) to see how it affects the pH of nanopure water. Unlike aOG, HA references increase the pH of nanopure water to 7.2 and 7.3. pH measurements were repeated twice with the same samples.

Our assessments of the pH analyses on these suspensions suggest that oxidized graphite might be present in the uncleaned archaeological charcoal since it reduced the pH of water like the aOG even though the magnitude of the decrease is smaller

than aOG. aOG degrades in water generating  $H^+$  ions, resulting in the reduction of pH [8]. We speculate this could be due to a mixture of HA with oxidized graphite in our sample.

### 4.3.2 Uncleaned archaeological charcoal (Raman analysis)

Next, we compared the Raman spectra of archaeological charcoal with the spectra of reference graphenic carbon materials to look for signatures of oxidized graphenic materials. Figure 4.2 (top) compares Raman spectra of graphite flakes, lab-synthesized GO, and the archaeological sample. If we zoom in the region between 1100 and 1800  $cm^{-1}$ , very broad D and G peaks are observed for the archaeological charcoal sample, which encompass both graphite flakes and GO peaks (Figure 4.2 (bottom)). The origins of these peaks for graphenic carbon materials and information about their positions and relative intensity are provided in Chapter 2 (Section 2.3.2).

The high background intensity in the archaeological charcoal spectrum indicates the presence of fluorescent material in the sample [1]. Figure 4.2 (top) depicts a Raman spectrum of OD, obtained from aOG, that only shows a high background intensity with no graphite related peaks (*i.e.* D and G peaks). Since the Raman spectrum of HA also shows high background intensity [1], we are unsure if we have HA or OD, or a mixture of both, in the uncleaned archaeological charcoal.

Our assessments of these solid phase analyses by Raman suggest that a mixture of graphenic materials (with different levels of oxidation) along with fluorescent materials are present in the uncleaned archaeological charcoal. This result is consistent with pH analysis, where we suggested a mixture of HA and oxidized graphenic carbon might exist in the sample.

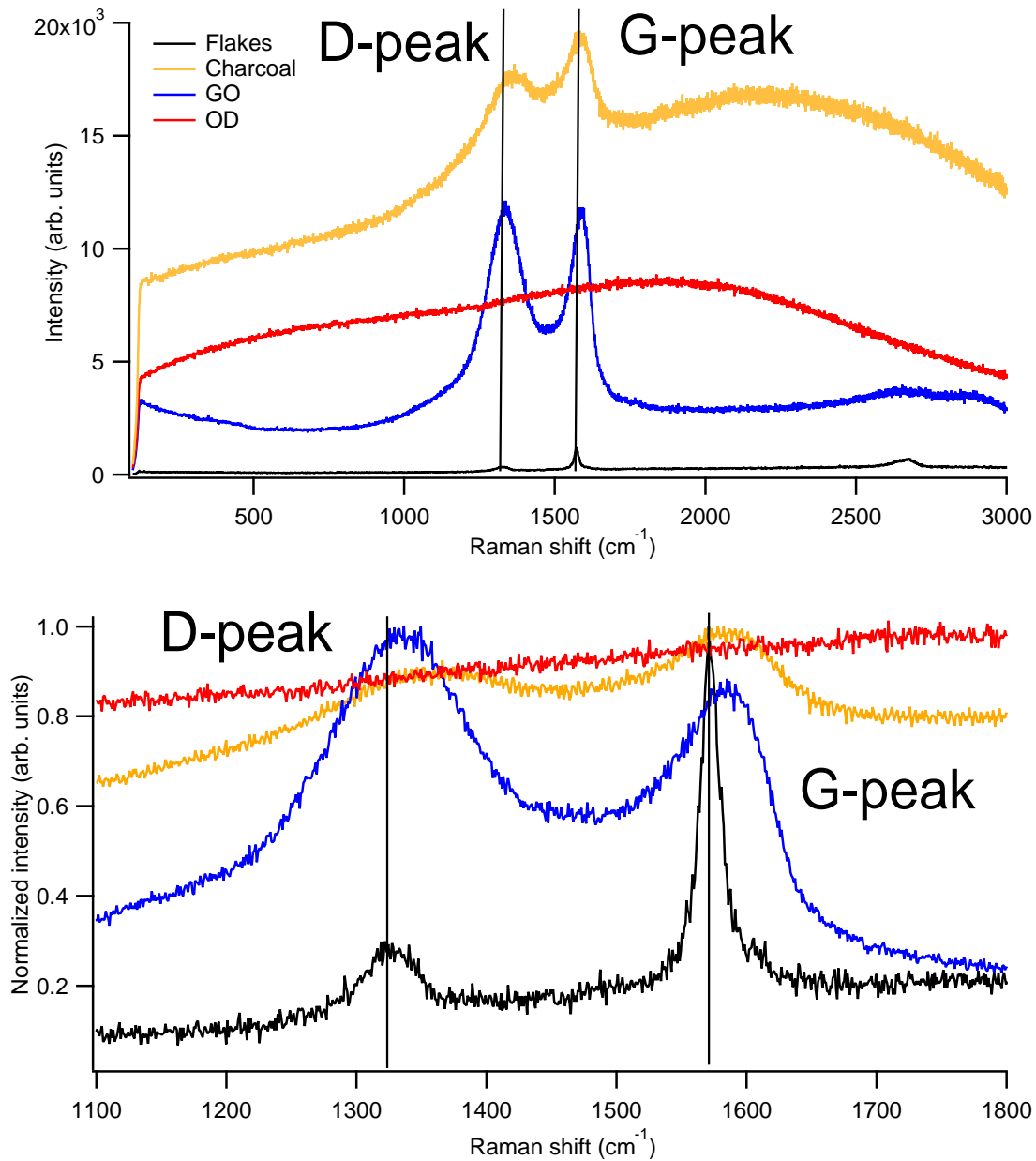


Figure 4.2: (top) Representative Raman spectra of (black) graphite flakes, (orange) archaeological charcoal, (blue) lab-synthesized GO, and (red) lab-synthesized OD in region between  $400\text{-}3000 \text{ cm}^{-1}$ . (bottom) Normalized spectra of the samples in the region from  $1100\text{ to }1800 \text{ cm}^{-1}$ . Black lines show D and G peaks for graphite at  $1330$  and  $1570 \text{ cm}^{-1}$ , respectively.

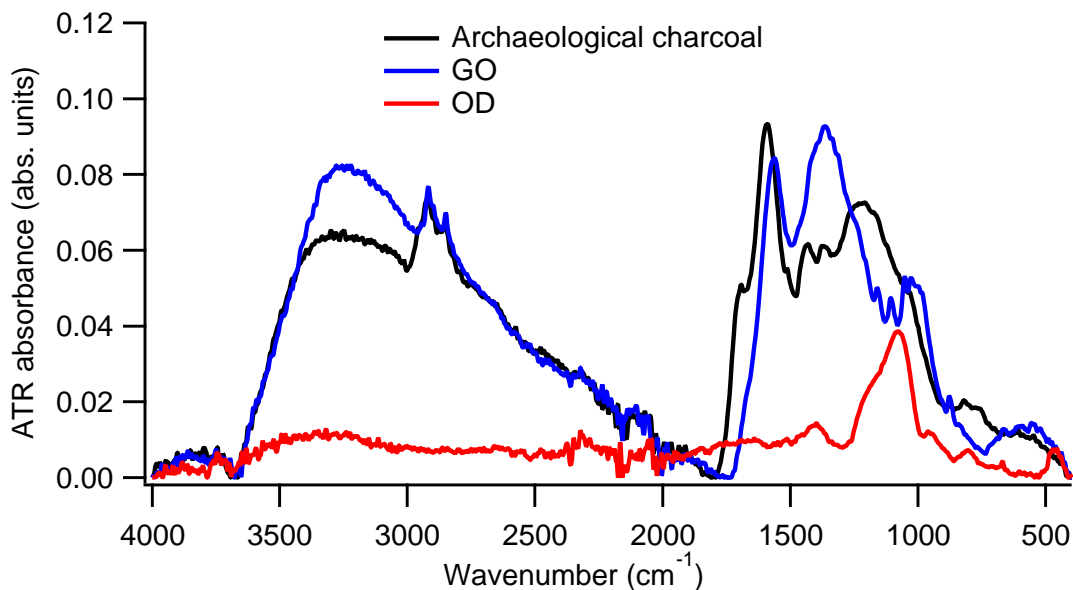


Figure 4.3: The ATR-FTIR spectra of (red) lab-synthesized OD and (blue) GO, and (black) archaeological charcoal.

### 4.3.3 Uncleaned archaeological charcoal (IR analysis)

In this section, we compare the ATR-FTIR spectra of reference oxidized graphenic materials with archaeological charcoal to monitor the presence of GO and OD in archaeological charcoal (Figure 4.3). Detailed information about IR peak positions for graphenic carbon materials is provided in Chapter 2 (Section 2.3.3).

ATR-FTIR spectra of archaeological charcoal show peaks at 3400 (O-H vibration), 2800 and 2900 (C-H vibration), and 1619 (C=C vibration)  $\text{cm}^{-1}$  similar to lab-synthesized GO. The vibrational modes that contribute to the peaks in the fingerprint region between 1000 and 1400  $\text{cm}^{-1}$  for archaeological charcoal and lab-synthesized GO do not match very well. It is also surprising that our most oxidized material shows virtually no evidence of O-H related IR peaks. In Chapter 3, however, we showed that the relative peak intensity and peak position in this region are difficult to interpret, and they are different from sample to sample because there are a series of overlapping bands and oxygen functional groups. Here, we discuss another important challenge

to interpret IR data of graphenic carbon materials after acid and base treatments. Acid and base are used to separate GO and OD from oxidized graphite in our reference samples. High and low pH also causes reversible changes to the IR signatures of oxidized graphenic carbon materials.

Figure 4.4 (top) shows the ATR spectra of archaeological charcoal after sequential acid-base-acid (ABA) treatments. Our results demonstrate that the peak positions and intensities did not change after the first acid (1M HCl) treatment, while the peaks near 1600 and 1400  $\text{cm}^{-1}$  increase after exposure to 1M NaOH, and the one near 1700  $\text{cm}^{-1}$  decreases. However, when the sample is treated with 1M HCl after the base treatment, spectral features near 1600 and 1400  $\text{cm}^{-1}$  decrease and the peak at 1700  $\text{cm}^{-1}$  increases. The relative peak intensity fluctuations near 1400, 1600, and 1700  $\text{cm}^{-1}$  are more obvious than in other regions of spectrum.

We also observe a pH dependency on the IR spectral features of graphite. Figure 4.4 (bottom) depicts IR spectra of graphite after ABA treatment. Our results demonstrate that a peak near 1400  $\text{cm}^{-1}$  appears after the base treatment and then disappears after the subsequent acid wash. This peak is assigned to the vibration of  $\text{COO}^-$  groups, but the reason why this peak appears reversibly is unclear. We assume that the  $\text{COO}^-$  peak is dominant due to stronger molecular dipole moment of  $\text{NaCOO}$  compared with  $\text{HCOOH}$ .

Both archaeologists and chemists demonstrate that IR peaks for reference and environmentally-altered sources of graphenic carbon materials change at different pH, and this behaviour occurs indefinitely if the sample is treated with acid and base sequentially [2, 8, 10]. It might be first assumed that changes in relative IR peak intensities near 1700, 1600, and 1400  $\text{cm}^{-1}$  are due to changes in the structure of graphenic materials. However, earlier studies by Dimiev *et al.* suggested that such changes are likely caused by different IR absorbance of water due to a reorientation in

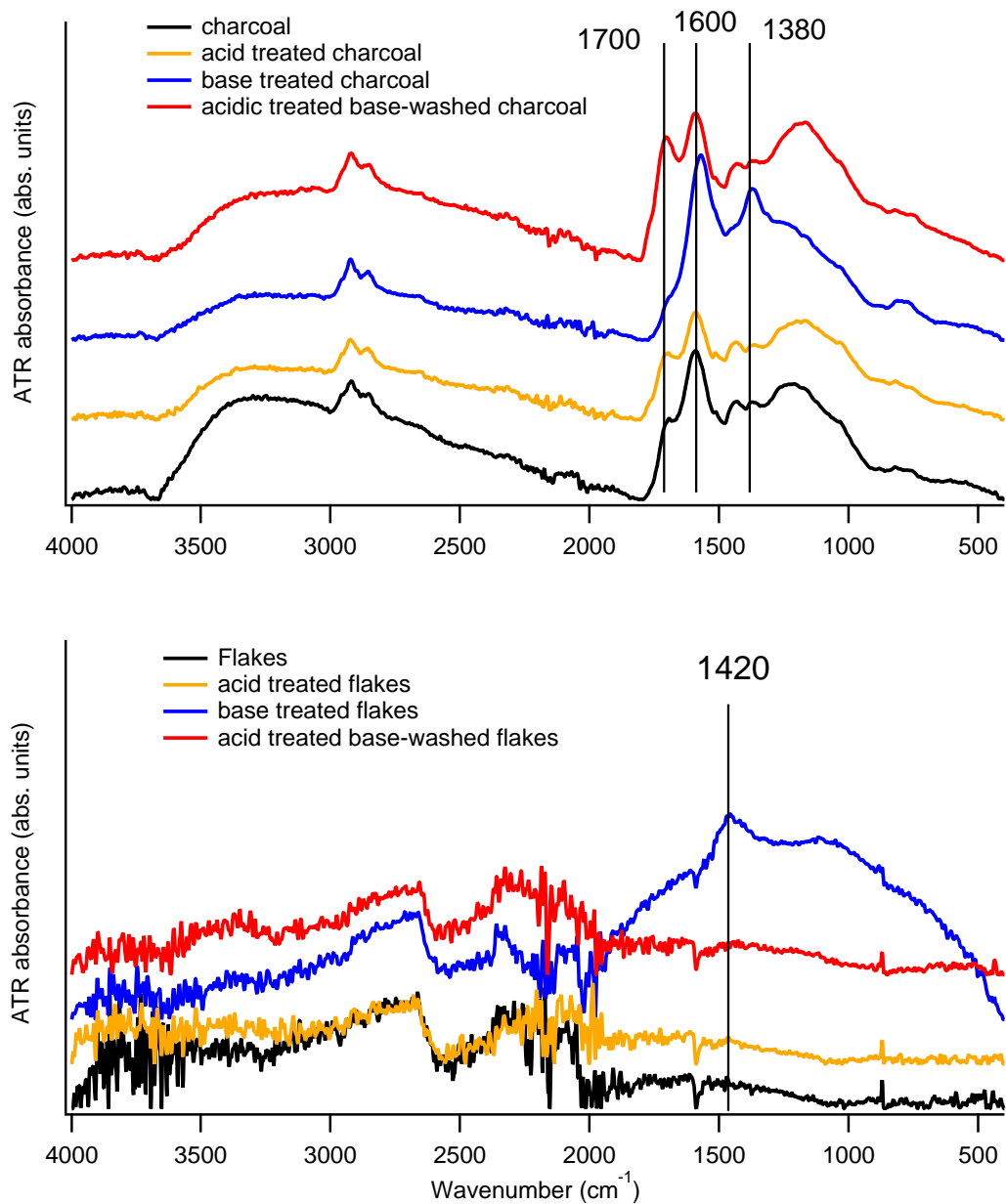


Figure 4.4: Representative attenuated total reflectance (ATR) infrared spectra of (top) archaeological charcoal and (bottom) graphite flakes after acid-base-acid (ABA) treatment: original (black), after first acid treatment (orange), after base-treatment (blue), and after last acid treatment (red). The relative intensity of peaks near 1700, 1600, and 1380  $\text{cm}^{-1}$  for archaeological charcoal, and near 1420  $\text{cm}^{-1}$  for graphite flakes, changes at different pH.

the presence of  $\text{Na}^+$  [8]. Therefore, the interpretation of IR data would be unreliable if there is no information about the pH history of the sample.

Despite challenges in the interpretation of IR relative peak intensities for graphenic materials, our assessments of these solid phase analyses suggest that oxidized carbon materials exist in the uncleaned archaeological charcoal. Our pH and Raman analyses suggest that at least a portion of the oxidized carbon is oxidized graphenic material. However, we cannot rule out the possibility that carbonaceous contaminants like HA are also present.

#### 4.3.4 WSBA on archaeological charcoal

In Chapter 3, we demonstrated that the WSBA treatment can separate a mixture of graphite and lab-prepared oxidized graphite into three individual components (graphite, GO, and OD). Here, we show that three groups of oxidized graphenic components are also obtained using WSBA on archaeological charcoal. Figure 4.5 compares the ATR spectra of reference graphite, GO, and OD with the least, moderately, and highly oxidized graphenic materials isolated from archaeological charcoal using our WSBA technique.

Solid **1** (Table 4.1) is the least oxidized graphenic materials, the most like graphite (Figure 4.5a). The least oxidized graphenic materials show peaks near 2800 and 2900  $\text{cm}^{-1}$  (symmetric and asymmetric vibrations), 1619  $\text{cm}^{-1}$  (O-H bending vibration), and a broad peak between 1000 and 1300  $\text{cm}^{-1}$  (C-O, C-OH, C-O-C vibrations). The least oxidized graphenic materials stayed in the filter paper. The moderately oxidized graphenic materials obtained from archaeological charcoal (Figure 4.5b) shows peaks at 3400 (O-H vibration), 2800 and 2900 (C-H vibration), 1619 (C=C vibration), and 1400 ( $\text{COO}^-$  vibration)  $\text{cm}^{-1}$  similar to lab-synthesized GO. Highly oxidized graphenic materials extracted from archaeological charcoal are similar to lab-

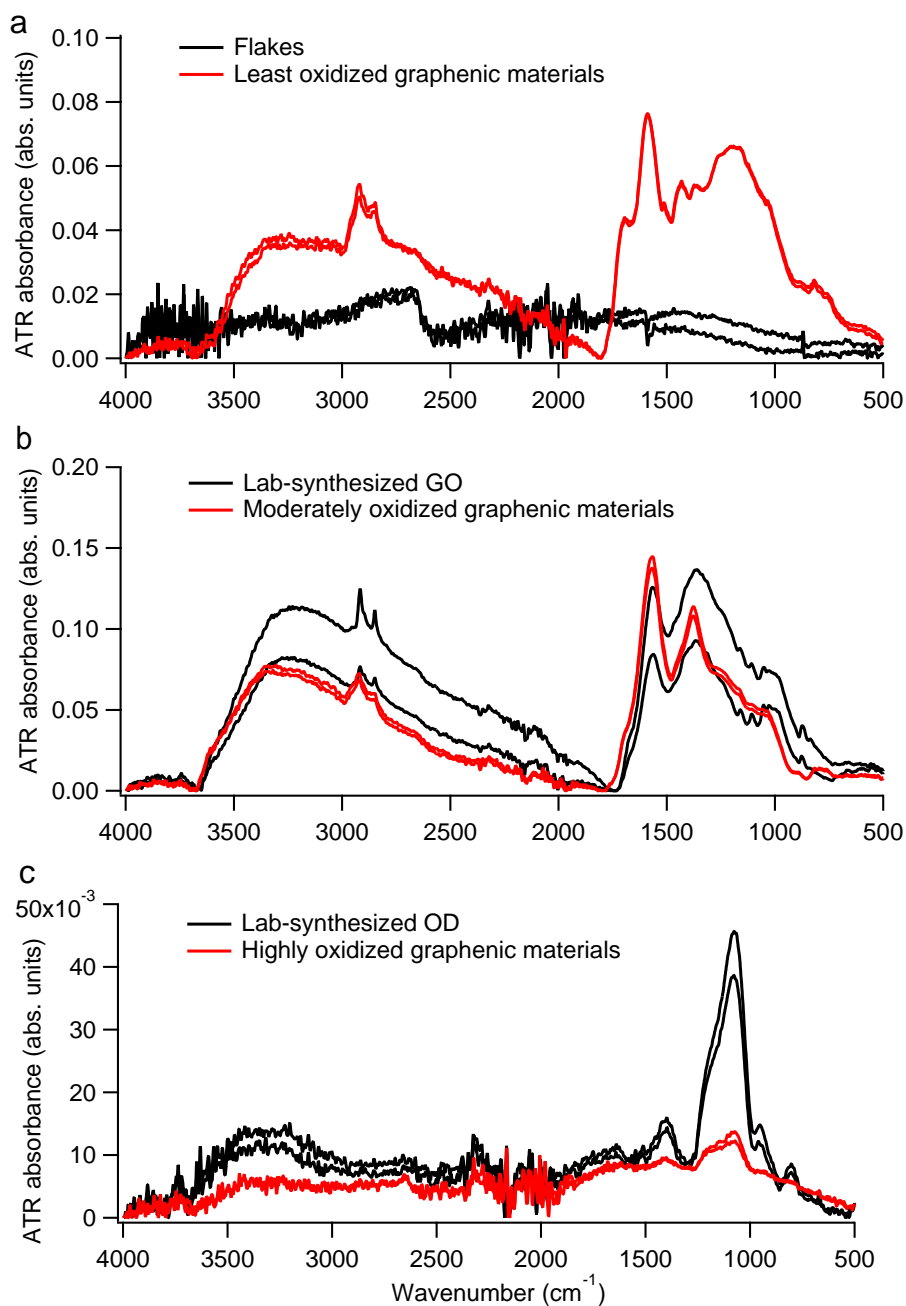


Figure 4.5: (a) Representative ATR-FTIR spectra for (black) graphite flakes and (red) least oxidized graphenic materials obtained from WSBA on archaeological charcoal. (b) Representative ATR-FTIR spectra for (black) lab-synthesized GO and (red) moderately oxidized graphenic materials obtained from WSBA on archaeological charcoal. (c) Representative ATR-FTIR spectra for (black) lab-synthesized OD and (red) highly oxidized graphenic materials extracted from archaeological charcoal.

synthesized OD (Figure 4.5c). Peaks appear at 3400, 1400, and 1100  $\text{cm}^{-1}$  for highly oxidized graphenic materials. Again, it is puzzling that O-H related IR peaks are diminished in the most oxidized samples. Our results confirm that oxidized graphenic materials with three different levels of oxidation can be extracted from our archaeological charcoal using our WSBA protocol.

As I mentioned earlier, we also suspect that HA is in archaeological charcoal. In the first step of the WSBA protocol, archaeological charcoal is mixed with nanopure water (pH=6.5) and sonicated. HA is not soluble in neutral or low pH [4]. Thus, we suggest that HA could remain in solid **1** (Figure 4.51) obtained from WSBA on archaeological charcoal, along with least oxidized graphenic materials. If we assume that some portions of HA are dissolved in water after the sonication process, the subsequent strong base and acid treatments will keep the HA in the liquid phase. Then HA would end up in the OD suspension.

Figure 4.6 shows the IR spectra of two different reference HAs (EAS5-AAA and Soil Masmiya) [11], and our oxidized materials obtained from WSBA on archaeological charcoal. Despite similarity in the peaks that appear at 2900 and 2800  $\text{cm}^{-1}$  ( $\text{CH}_2$  symmetric and asymmetric vibrations), there are extremely different features near 3400 (O-H vibration), 1700 (carbonyl groups vibration), and 1619  $\text{cm}^{-1}$  (O-H bending vibration) between oxidized graphenic materials and HA (Figure 4.6a, b, and c). It is important to note that the HA standards are measured via transmission IR spectroscopy, while our data are collected in ATR geometry. These different geometries cause small peak shifts along with changes in peak widths and shapes. These differences originate from the different indices of refraction between the diamond ATR crystal and the sample. Nevertheless, our IR results demonstrate that either HA is not present in our archaeological sample, or there is not enough HA in the mixture to be detected by IR spectroscopy.

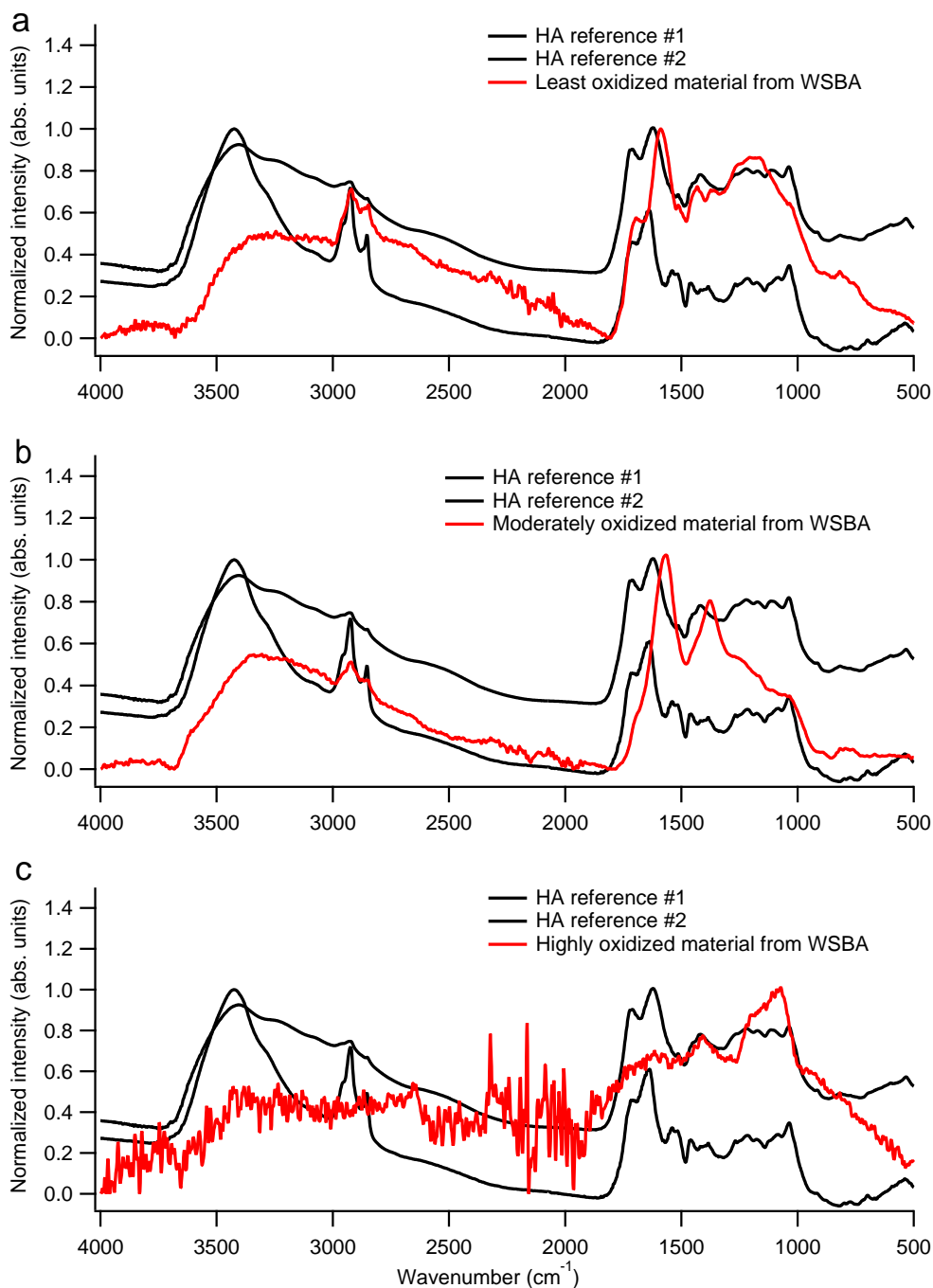


Figure 4.6: Representative ATR data is in red for least (a), moderate (b), and highest (c) oxidized materials obtained from WSBA on archaeological charcoal. We compare these with transmission IR spectra of humic acids (black) from two different sources from the Infrared Spectra Library of the Kimmel Center for Archaeological Science Infrared Standards Library, Weizmann Institute of Science [11] (HA reference **1** is EAS5-AAA and HA reference **2** is Soil Masmiya).

## 4.4 Conclusions

In this chapter, we used vibrational spectroscopy on solids and pH analysis on suspensions to see what kinds of oxidized carbon materials, if any, exist in an archaeological charcoal sample. pH analyses suggest that oxidized graphenic material is present in our archaeological charcoal. Although infrared and Raman spectra suggest that a mixture of oxidized carbon materials are present in archaeological charcoal, they do not provide enough information to confirm if HA also exists in the sample. From our archaeological charcoal sample, we separated materials with three different oxidation levels: the least, moderate, and the highest. IR analyses suggest that the separated materials are primarily composed of oxidized graphenic materials, but they cannot rule out the possibility that a small amount of HA is also present.

## Bibliography

- [1] Dani Alon, Genia Mintz, Illit Cohen, Steve Weiner, and Elisabetta Boaretto. The use of Raman spectroscopy to monitor the removal of humic substances from charcoal; quality control for  $^{14}\text{C}$  dating of charcoal. *Radiocarbon*, 44(1):1–11, 2002.
- [2] N. R. Rebollo, I. Cohen-Ofri, R. Popovitz-Biro, O. Bar-Yosef, L. Meignen, P. Goldberg, S. Weiner, and E. Boaretto. Structural Characterization of Charcoal Exposed to High and Low pH: Implications for  $^{14}\text{C}$  Sample Preparation and Charcoal Preservation. *Radiocarbon*, 50(2):289–307, 2008.
- [3] Michael I. Bird, Vladimir Levchenko, Philippa L. Ascough, Will Meredith, Christopher M. Wurster, Alan Williams, Emma L. Tilston, Colin E. Snape, and David C. Apperley. The efficiency of charcoal decontamination for radiocarbon dating by three pre-treatments – ABOx, ABA and hypy. *Quat. Geochronol.*, 22:25 – 32, 2014.
- [4] Edwin A. Olson and W. S. Broecker. Section of Geology and Mineralogy: Sample Contamination and Reliability of Radiocarbon Dates. *Trans. N. Y. Acad. Sci.*, 20(7 Series II):593–604, 1958.
- [5] Scott Gilje, Song Han, Minsheng Wang, Kang L. Wang, and Richard B. Kaner. A Chemical Route to Graphene for Device Applications. *Nano Lett.*, 7(11):3394–3398, 2007.
- [6] Martin Rosillo-Lopez and Christoph G. Salzmann. A simple and mild chemical oxidation route to high-purity nano-graphene oxide. *Carbon*, 106:56 – 63, 2016.

- [7] Jae-Hun Lee and Jae-Hwan Choi. The production of ultrapure water by membrane capacitive deionization (MCDI) technology. *J Membrane Sci*, 409-410:251–256, 2012.
- [8] Ayrat M. Dimiev, Lawrence B. Alemany, and James M. Tour. Graphene Oxide. Origin of Acidity, Its Instability in Water, and a New Dynamic Structural Model. *ACS Nano*, 7(1):576–588, 2013.
- [9] Christi Young and Ray von Wandruszka. A comparison of aggregation behavior in aqueous humic acids. *Geochem T*, 2(1):1–5, 2001.
- [10] Ilit Cohen-Ofri, Lev Weiner, Elisabetta Boaretto, Genia Mintz, and Steve Weiner. Modern and fossil charcoal: aspects of structure and diagenesis. *J. Archaeol. Sci.*, 33(3):428 – 439, 2006.
- [11] Infrared Spectra Library of Kimmel Center for Archaeological Science Infrared Standards Library, Weizmann Institute of Science. <https://www.weizmann.ac.il/kimmel-arch/infrared-spectra-library>. Accessed: 2019-09-26.

# Chapter 5

## Attempts to Differentiate Oxidized Graphenic Materials from Humic Acid in the Liquid Phase

In this chapter, we focus on the analysis of humic acid (HA) and oxidized graphenic carbon in the liquid phase. Oxidized graphenic materials and HA can both be suspended in 0.1M NaOH (pH=11). Here, we use UV-Vis spectroscopy and size exclusion chromatography (SEC) to see if there are distinguishing characteristics between HA and as-prepared oxidized graphite (aOG), which is made of graphene oxide (GO) and oxidative debris (OD).

### 5.1 Introduction

In Chapter 4, we confirmed that three groups of oxidized graphenic materials can be separated from archaeological charcoal through a series of aqueous treatments under different pH conditions. Both oxidized graphenic materials and HA are composed of

$sp^2$  and  $sp^3$  carbon bonds along with many oxygen functional groups. These structural similarities make their chemistry similar. Researchers have confirmed that HA is dissolved in alkaline solutions [1]. Similarly, chemists confirmed that concentrated base (pH=13) treatment (1M NaOH) removes highly oxidized graphenic materials called oxidative debris (OD) from oxidized graphite [2,3]. Since HA and OD can be suspended in aqueous solution in the same alkaline pH range, we are likely to remove both from archaeological charcoal during radiocarbon cleaning protocols. Hence, if one wants to isolate oxidized graphenic materials for radiocarbon dating applications, then it is important to separate them from HA in the liquid base wash. We take the first step toward this and try to find a method to distinguish HA from oxidized graphenic carbon.

UV-vis spectroscopy is commonly used to identify conjugated systems like oxidized graphenic materials and HA [4, 5]. Figure 5.1 shows UV-Vis spectra of aOG and Suwannee River Humic Acid (SRHA). Both samples absorb visible light at wavelengths below 600 nm. The aOG spectrum indicates a peak at 230 nm and a shoulder around 300 nm, while SRHA only shows a shoulder near 280 nm. Since the spectral features of these two samples are not very different, UV-Vis data alone will not be informative enough to differentiate a mixture of oxidized graphite and HA.

Oxidized graphenic materials and HA vary in molecular weight. Therefore, size exclusion chromatography coupled with a UV detector (SEC-UV) could be an appropriate technique to distinguish between them.

In general, liquid chromatography is a powerful method in analytical chemistry to separate chemical compounds in a mixture due to their differential retention on the stationary phase by a mobile phase [6]. The mobile phase that contains liquid solvent and analyte passes through the stationary phase, using high pressure, which is packed in a column. Liquid chromatography is classified based on the stationary phase or

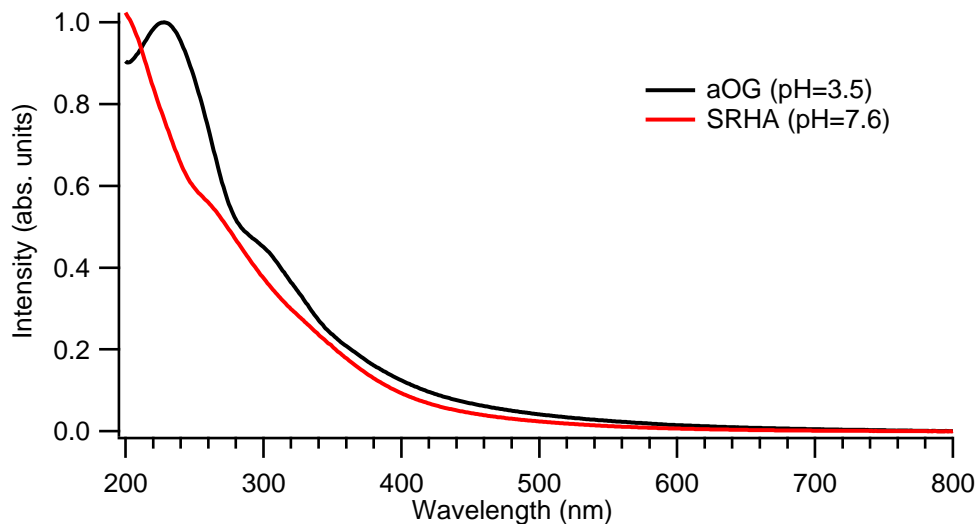


Figure 5.1: UV-Vis spectra of (black) as-prepared oxidized graphite (aOG) and (red) Suwannee River Humic Acid (SRHA).

separation mechanism. Liquid-liquid chromatography, liquid-solid chromatography, ion chromatography, and size exclusion chromatography are different kinds of liquid chromatography.

Common liquid chromatography is an effective method to isolate low molecular weight compounds, but this is an inappropriate technique for the separation of a mixture with large molecular weight components since they are quickly eluted from the column and provide indiscernible resolution. Size exclusion chromatography is one type of liquid chromatography in which a mixture of chemical compounds is separated based on their molecular size [7]. SEC with larger column pore sizes ranging from 50 to 100,000 angstroms can be used to separate large molecular components such as HA and aOG because it gives them more interaction with stationary phase.

The SEC column contains uniform porous silica or polymer particles into which liquid solvent and solute can penetrate. As the mobile phase passes through the pores in the column, chemical components are trapped and released. The retention time of components depends on their size. Small molecules are retained longer than large

ones because small molecules penetrate the pores and can be trapped for longer times. Large molecules do not penetrate the pores and elute the column at a longer retention time. Size exclusion chromatography coupled to a UV detector is a powerful technique not only for the separation of large and small particles but also for comparing the optical properties of separated compounds [6].

Researchers did SEC-UV measurements on SRHA and compared them with Brown Carbon (BrC) in aerosol samples [8]. BrC is made of carbonaceous particles that contain a large fraction of organic species with the ability to absorb visible light. These carbon particles can be dissolved in nanopure water, and they are called BrC because they are brown when in suspension. They found similar absorption intensity between BrC and SRHA as a function of wavelength and molecular weight, but with different composition/average size. The molecular weight of chemical compounds can be estimated from a negative log-linear relationship between molecular weight and retention time in SEC columns.

In our experiment, aOG and HA are similar in structure and appear brown. Therefore, we expect that these earlier BrC studies are an appropriate comparison to aOG and HA. Here, we analyze SRHA using the same experimental setup, used in studies by others [8]. Once we find similar SEC-UV pattern for SRHA, we measure the dilute base (pH=11) soluble portion of archaeological charcoal to compare the terrestrial BrC (aOG and HA) in our sample with the atmospheric BrC described by Ref [8].

In this chapter, we try to link the bulk UV-Vis data with the SEC-UV to characterize and distinguish the optical absorbance properties of oxidized graphenic materials and HA in an archaeological charcoal sample. UV-Vis spectra show the intensity of light for the entire sample as a function of wavelength. However, SEC-UV chromatograms depict absorbance as a function of retention time (molecular size) at a specific wavelength.

Data obtained from these two techniques can be correlated. We can take integrals of different chromatograms, for one sample, at different wavelengths to obtain the overall intensity absorbed by an analyte, then compare the results with the bulk UV-Vis data. Data from the bulk UV-Vis analysis can help to select reasonable wavelengths for further SEC-UV measurements. However, linking these two sets of data might be challenging. An important challenge with the bulk UV-Vis spectroscopy is the effect of solvent choice on the spectra of suspended particles. For instance, aOG is best suspended for bulk UV-Vis spectroscopy near pH 3.5, but it is analyzed around pH 7 with SEC-UV due to the requirement of using buffer during the separation.

## 5.2 Experimental

### 5.2.1 Materials

Suwannee River Humic Acid (SRHA), as reference material, was obtained from Alfa Aesar. A reference sample of aOG was synthesized in our lab using the improved Hummer's method [9]. I provided detailed information about the preparation of aOG in Chapter 3 (Section 3.2.1).

Archaeological charcoal analyzed here is the same described in Chapter 4 (Section 4.2.1). Before measurements, contaminants like sand and roots were removed from the sample. Then, it was crushed using a mortar and pestle to make a fine powder. 0.5 g was added into 20 mL of 1M HCl, followed by stirring at 800 rpm at 40 °C for one hour. The suspension was centrifuged at 8500 rpm to separate the supernatant from the residual. The residual was divided equally into two portions. One portion was treated in 20 mL of 0.1M NaOH, and the other half was treated with 1M NaOH. The supernatants obtained after each treatment were filtered by a 0.2  $\mu\text{m}$  syringe filter. Then, they were stored in a dark and cool place. These supernatants were the

materials used for subsequent UV-Vis and SEC-UV measurements.

### 5.2.2 Methods

The bulk UV-VIS spectra were acquired from both original and diluted supernatants, with a Varian Cary 6000 spectrometer with 0.1 second average time, 1 nm resolution, and a 600 nm/min scan rate. To dilute the supernatants, I transferred two droplets of an original sample, using a disposable pipette, into a vial, and then added 10 mL of nanopure water.

Size Exclusion Chromatography coupled with a UV detector (SEC-UV) was executed exactly like those repeated by Lorenzo *et al.* [8], and were done with direct guidance from Dr. Cora Young (MUN Chemistry). The HPLC system (1260 Infinity, Agilent Technologies, Santa Clara, CA, USA) was coupled to a diode array detector (1260, Agilent Technologies, Santa Clara, CA, USA). An aqueous gel filtration column (molecular weight range = 250 – 75,000 Da, Polysep GFC P-3000, Phenomenex, Torrance, CA, USA) was used.

For SEC experiments, 1 mL of dilute base (pH=11) supernatant of archaeological charcoal was mixed with 1 mL of methanol. Then, 100  $\mu$ L of this mixture was injected into the column with the mobile phase flow rate of 1 mL/min for 20 min. The mobile phase composition contained 50:50 methanol and ammonium acetate with a concentration of 25 mM. Isocratic elutions were performed at a flow rate of 1 mL/min with an injection volume of 100  $\mu$ M. The wavelengths of UV detection were selected to be 230, 250, and 300 nm. Each sample was run only one time.

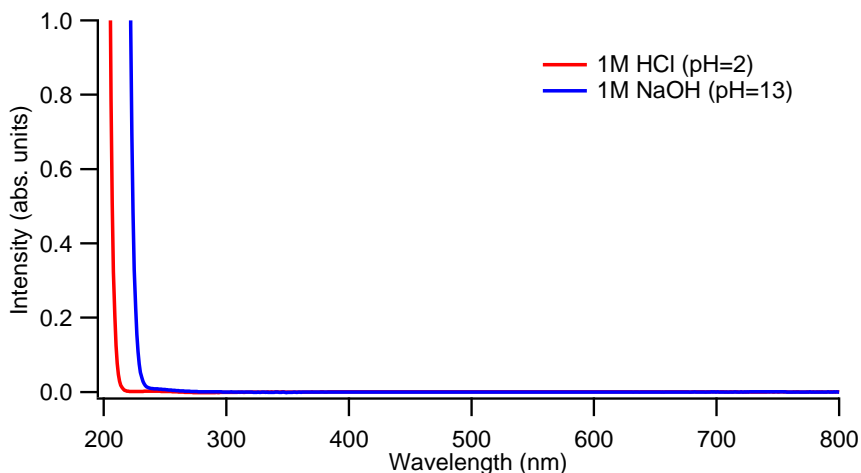


Figure 5.2: UV-Vis spectra of (red) concentrated (1M) HCl and (blue) concentrated (1M) NaOH.

## 5.3 Results

### 5.3.1 Effects of pH and solvent on bulk UV-Vis data

In this chapter, we study graphenic carbon materials that are soluble in acid or base. We find that different pH and solvents can change UV-Vis spectra considerably.

#### Blanks

First, we see how acid and base blanks affect UV-Vis spectra. Figure 5.2 shows UV-Vis spectra of 1M HCl and 1M NaOH. Clear colourless concentrated acid and base solutions depict no absorption in the visible region. However, the base (1M NaOH) starts absorbing light at 230 nm, while the threshold for acid (1M HCl) is around 210 nm. This difference was consistent each time we analyzed these blanks. The reason for this behaviour has not been reported.

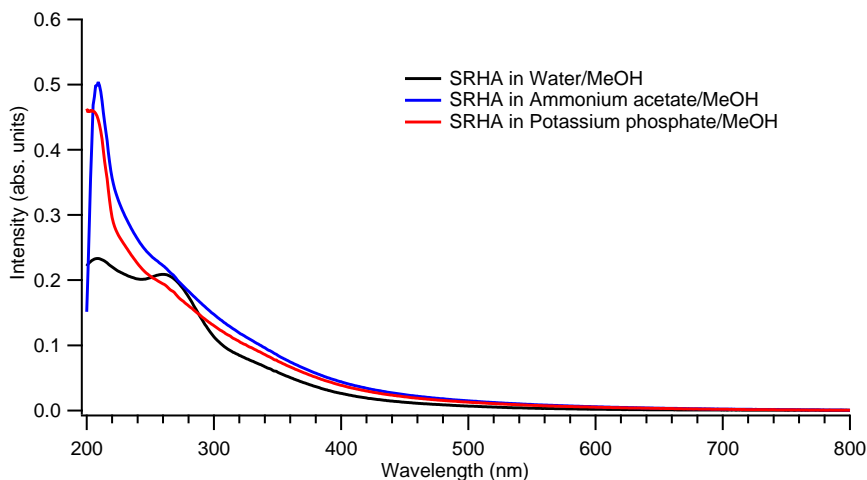


Figure 5.3: UV spectra of Suwannee River Humic Acid (SRHA) dissolved in 1:1 volume ratio of (black) water/methanol, (blue) 25mM ammonium acetate/methanol, and (red) 25mM potassium phosphate/methanol.

### Effects of solvent on SRHA spectra

The chemical composition of the mobile phase and solvent is an important factor to consider before SEC-UV measurements because it affects both the UV-Vis spectrum and separation results. It is known that 100 percent water damages the packing materials in the chromatography column. On the other hand, 100 percent organic solvents cannot be used since a buffer is required to stabilize the conditions of separation throughout the column. Therefore, we use a mixture of organic solvent and buffer for the separation of carbonaceous materials in both reference samples and base soluble portions of archaeological charcoal. In this research, we use the same mobile phase compositions described in reference [8]. This allows us to make direct comparisons with the earlier data.

Figure 5.3 compares the UV-Vis spectra of SRHA in different liquids. We should note that there is no residual or precipitant in the supernatants that we measured. The result shows that different solvents change the spectral features of SRHA. For example, SRHA in water/methanol shows two peaks at 210 and 260 nm, while SRHA

in ammonium acetate/methanol depicts a sharp peak at 210 nm. SRHA dissolved in potassium phosphate/methanol shows a shoulder near 210 nm. SRHA shows two peaks near 210 and 270 nm when it is dissolved in water/methanol, compared with only a shoulder near 210 nm in the presence of buffer. It seems buffer changes SRHA in a way that UV features are affected.

It is known that changes in the polarity of solvents affect the energy levels between  $\pi^* \leftarrow \pi$  and  $\pi^* \leftarrow n$  [10]. The more polar solvent, the lower the energy between  $\pi^* \leftarrow \pi$ , which causes redshift in the UV spectrum. In contrast, polar solvents increase the energy between  $\pi^* \leftarrow n$  electron transitions and cause a blue shift. Surprisingly, peak shape changes in our data rather than showing a peak shift.

### 5.3.2 aOG in acid and base

Figure 5.4 (top) shows photos of aOG suspensions before and after dilute (pH=11) and concentrated (pH=13) base treatments. They help to show what happens to aOG after each treatment and to illustrate what portion we measure in our UV-Vis data. aOG stays suspended after dilute base (pH=11) treatment with a little colour change from light to dark brown, while it reacts with a concentrated base (pH=13) and separates into two phases: GO residual and OD clear colourless suspension. We analyzed the uniform suspensions of the aOG (samples on the left and middle), and only the clear colourless portion of the concentrated base (pH=13) treated sample on the right.

Figure 5.4 (bottom) depicts UV-Vis spectra corresponding to each sample shown in the photo. We observe a peak at 230 nm and a shoulder near 300 nm for aOG after dilute base (pH=11) treatment. Unlike aOG and dilute base (pH=11) treated aOG suspensions, the clear colourless suspension of the concentrated base (pH=13) treated aOG does not show any peaks in the UV-Vis region. This is surprising because

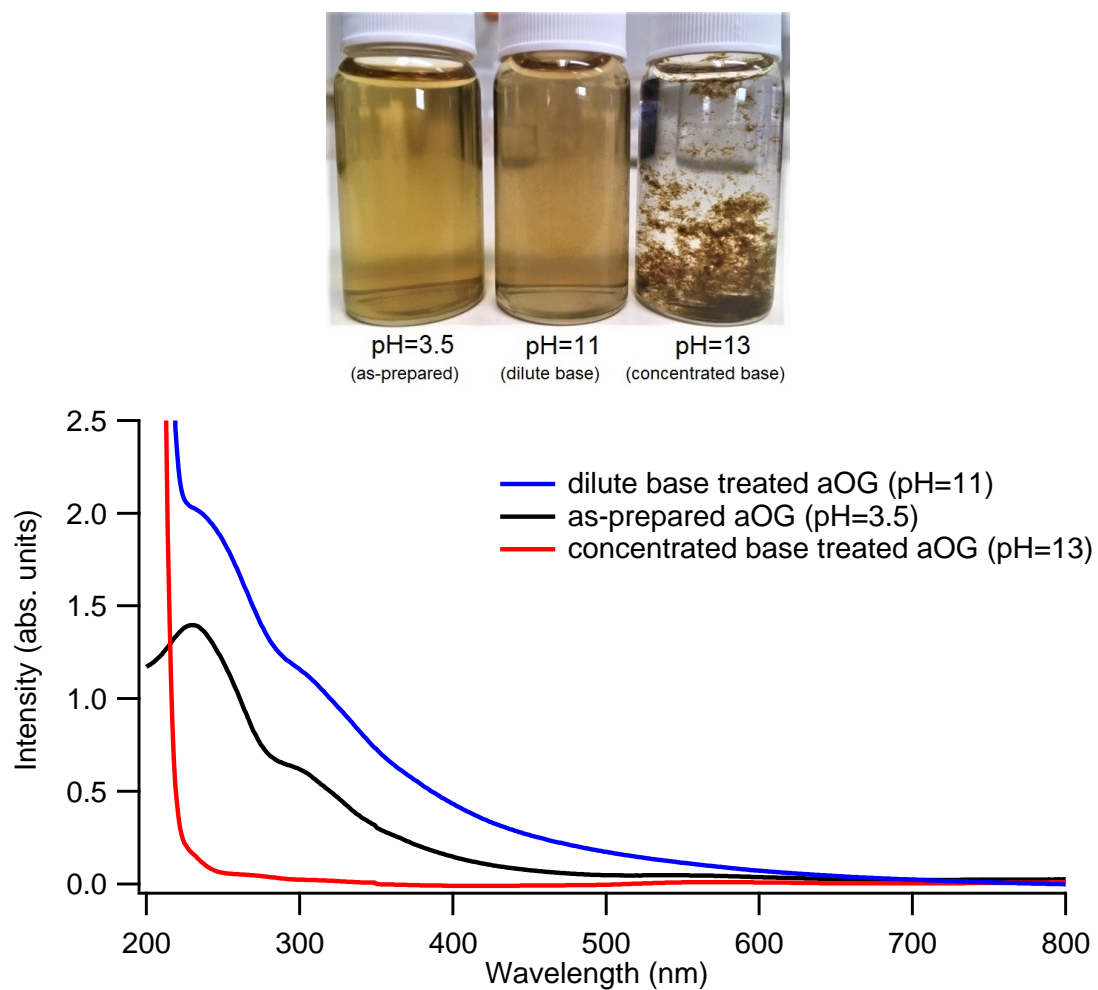


Figure 5.4: (top) Representative images of (left) aOG, (middle) dilute base (pH=11) treated aOG, and (right) concentrated base (pH=13) treated aOG suspensions. (bottom) UV spectra of (black) aOG, (blue) dilute base (pH=11) treated aOG, and (red) clear colourless portion of a concentrated base (pH=13) treated aOG suspensions.

this clear colourless suspension contains low molecular weight and highly oxidized materials that are responsible for the fluorescence of aOG [2,3]. It suggests that either there is not enough OD present in the sample or OD is trapped in the black residual. A threshold near 220 nm is also observed for both dilute and concentrated base (pH=11 and 13) treatments that is consistent with what we saw in the UV spectrum of the alkaline blank (Figure 5.2). Our results suggest that the most relevant pH for the analysis of oxidized graphenic materials using SEC-UV is approximately 11 because they are all suspended in this condition.

### 5.3.3 Archaeological charcoal in acid and base

Figure 5.5 (top) shows the supernatants of archaeological charcoal treated in concentrated acid, and dilute and concentrated base (pH=11 and 13). The suspensions of concentrated acid, and dilute and concentrated base (pH=11 and 13) treated archaeological charcoal are not able to stay suspended in the solution, like aOG, and they settle out quickly. Therefore, we decided to filter the suspensions and then do the UV-Vis measurements. Unlike the concentrated base (pH=13) treated aOG, archaeological charcoal did not separate into two phases (black residual and clear colourless suspension) after concentrated base (pH=13) treatment. If we imagine clear colourless OD came off the sample, it will not be observable due to strong brown colour of the suspension.

Figure 5.5 (bottom) compares the UV-Vis spectra of corresponding to each sample shown in the photo. All three supernatants show an absorption band near 500 nm. The higher the pH for the base treatment, the more brown materials come off, which results in higher absorption in the visible region. Among these supernatants, only dilute base (pH=11) treated archaeological charcoal shows a distinctive peak at 230 nm. This peak is known for  $\pi^* \leftarrow \pi$  electron transitions of oxidized graphite. This

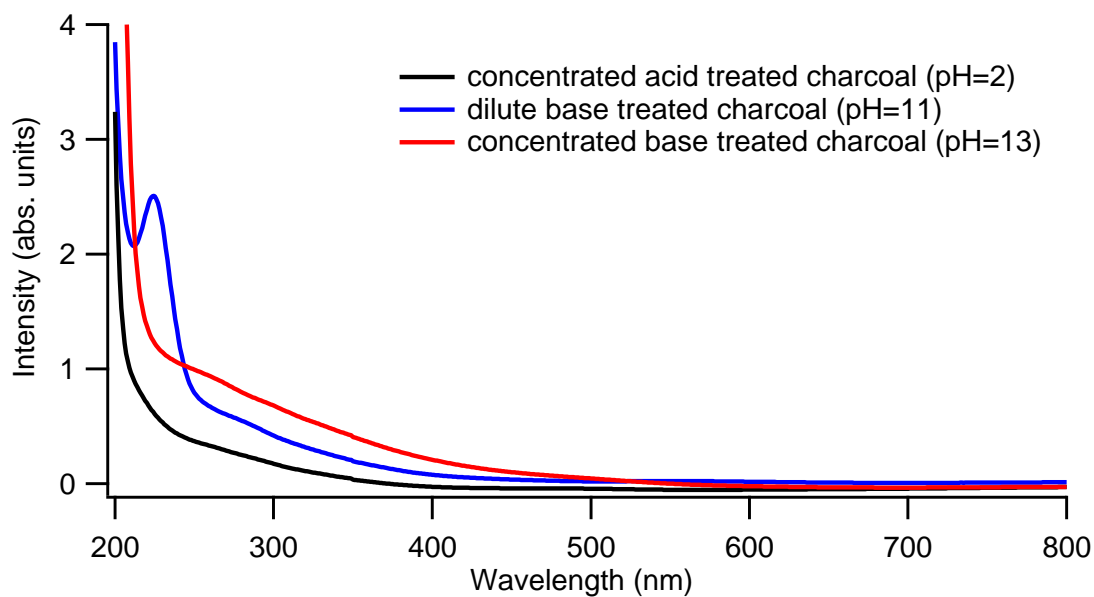
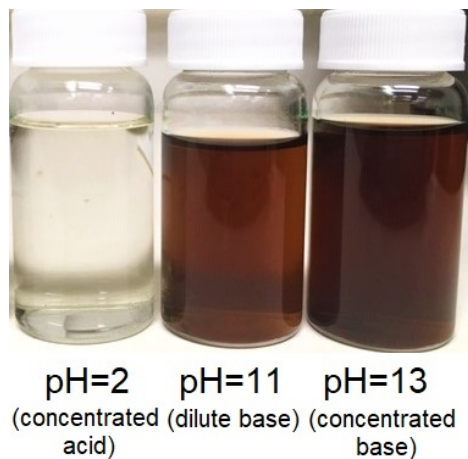


Figure 5.5: (top) Representative images of supernatants obtained from (left) acid treated, (middle) dilute base (pH=11) treated, and (right) concentrated base (pH=13) treated archaeological charcoal. (bottom) UV spectra of supernatants of archaeological charcoal treated in (black) 1M HCl, (blue) 0.1M NaOH, or (red) 1M NaOH.

peak is consistent with what we saw for the UV-Vis spectrum of the dilute base (pH=11) treated aOG suspension.

Our assessments on these liquid phase analyses by UV-Vis suggest that pH and solvent change the UV-Vis spectra of our analytes considerably. Our UV-Vis results also suggest that oxidized carbon materials exist in the supernatant of the dilute base (pH=11) treated archaeological charcoal. Hence, we try to use SEC-UV to separate these materials and differentiate the optical properties of oxidized graphenic materials and HA by looking at their UV responses, at specific wavelengths, as a function of retention time.

### 5.3.4 SEC Blank analysis

In liquid chromatography, a blank is injected before analyte to eliminate the effect of the blank from the chromatogram of the analyte. In this method, the blank chromatogram is commonly subtracted from the analyte. Figure 5.6 shows SEC-UV chromatograms of the blanks that were used to analyze reference and real samples at three wavelengths. Ammonium acetate/methanol is used as a blank for the analysis of SRHA and aOG, while a combination of NaOH/MeOH is measured to analyze dilute base treated (pH=11) archaeological charcoal. It is worth noting that we only did one run for each blank.

Before the analysis of blanks, we should note that the chromatograms shown in Figures 5.7 and 5.8, obtained from our analytes, have not been subtracted from their blanks due to different positive and negative peaks along with fluctuations in our blanks data. This is also because we are unsure what blanks work best for our samples, especially for lab synthesized aOG and dilute base (pH=11) treated archaeological charcoal. Therefore, we only try to ignore peaks observed in blanks to analyze our analytes.

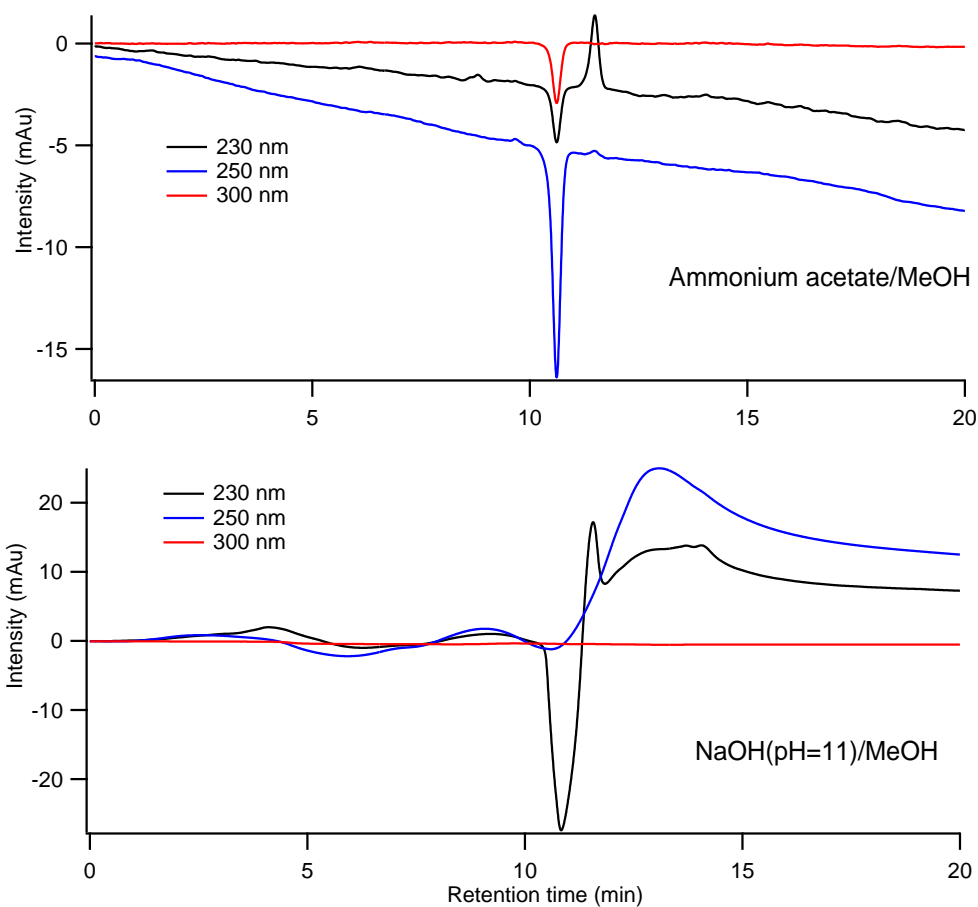


Figure 5.6: The SEC-UV chromatograms of (top) ammonium acetate/methanol and (bottom) NaOH/methanol at three different wavelengths (black) 230, (blue) 250, and (red) 300 nm.

There are some features in these blanks that concern us. Downward slopes at 230 and 250 nm are seen for acetate/methanol. The slow drift of the optics can happen in these systems, and the sloping baseline may reflect unstable power to the bulb. This type of baseline drift is common in liquid chromatography.

A negative peak for the chromatograms of ammonium acetate/methanol, just below 11 min at three wavelengths, and NaOH/methanol at 230 nm is observed. There are many reasons for getting a negative peak in liquid chromatography, including the wrong polarity of solvent and air bubbles through the system. Also, it might be due to the lower optical density of the sample compared with the mobile phase. In other words, this problem happens when the injection solvent elutes from the column even if the mobile phase and solvent compositions are similar.

The positive peaks just above 11 min obtained from both blanks, and the one at 13 min at 230 and 250 nm for NaOH/MeOH, can be due to the impurity of solvent or contaminant in the column. The analysis of blank before each measurement helps us to identify problems such as downward or upward slopes and negative or positive peaks in the real data.

Our further SEC-UV data show that many of these problems (sloping and wavy baselines) are not present. Thus, we decided to present uncorrected SEC-UV data of our analytes.

### **5.3.5 SEC-UV comparison**

Figure 5.7 (top) shows the absorption intensity as a function of retention time for SRHA at three different wavelengths. All three chromatograms depict two main peaks near 9 and 10 min. The peak at 9 min, which corresponds to the elution of larger molecules, increases as wavelength decreases. The SEC-UV results for SRHA is validated by the bulk UV-Vis data where the overall absorbance decreases as wavelength

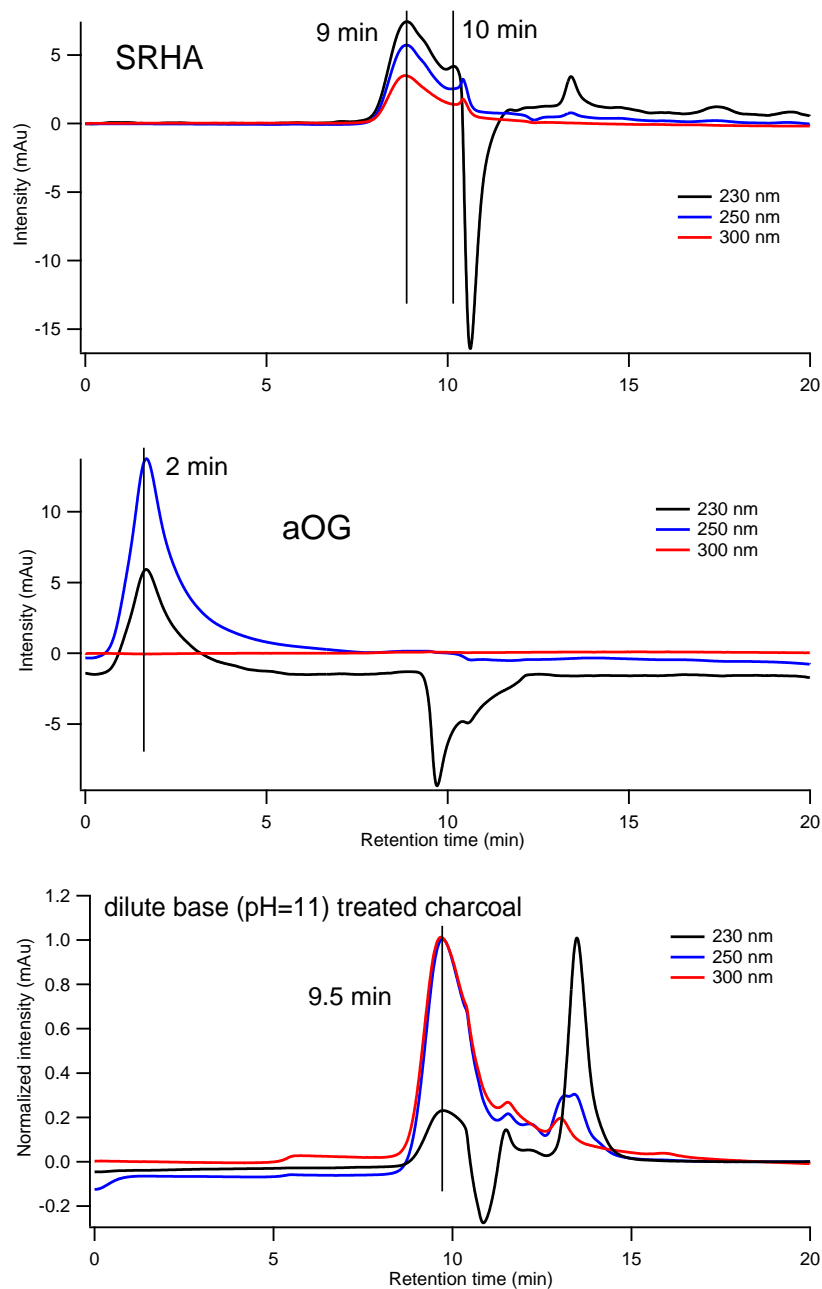


Figure 5.7: Representative (uncorrected) SEC-UV chromatograms of (top) Suwannee River Humic Acid (SRHA), (middle) as-prepared oxidized graphite, and (bottom) dilute base (pH=11) soluble portion of archaeological charcoal at three different wavelengths (black) 230, (blue) 250, and (red) 300 nm. The black vertical lines indicate the peak positions we assign to the elution of different groups of species (near 9 and 10 min, for SRHA, near 2 min, for aOG, and near 9.5 min for base treated charcoal.)

increases.

The SRHA chromatogram for 230 nm shows a negative peak near 11 min, which was already seen in the blank. Therefore, we can disregard this peak for the SRHA chromatogram. The peaks observed near 13 min can be associated with the elution of other species with smaller particle size in SRHA.

The SRHA chromatogram obtained at 300 nm looks comparable to the one reported by Di Lorenzo *et al.* [8]. They used 300, 365, and 405 nm as detection wavelengths for the analysis of SRHA. Their results demonstrate that the lower wavelength results in higher absorption for SEC-UV analysis of SRHA. This result is consistent with what we observe in our analysis.

Figure 5.7 (middle) shows the chromatograms of aOG at different wavelengths. Unlike SRHA, aOG chromatograms show only one peak near 2 min. A negative peak just below 10 min is observed for aOG at 230 nm. We are still unsure if this negative peak is due to the effect of blank or analyte itself.

Figure 5.7 (bottom) shows the chromatograms of the dilute base (pH=11) treated archaeological charcoal at 230, 250, and 300 nm. The three chromatograms show two peaks around 9.5 and 13.5 min. The negative peak near 11 min at 230 nm and small positive peaks around 11.5 min originate from the blank (NaOH (pH=11)/MeOH).

Our results suggest that aOG particles are bigger than the ones in SRHA and the dilute base (pH=11) soluble portion of archaeological charcoal. Our data also suggest that the particle size of species in the base soluble portion of archaeological charcoal is approximately similar to SRHA due to the same peaks near 9 min.

### 5.3.6 SEC-UV on archaeological charcoal

As a qualitative analysis, we compare UV-Vis spectra of the aOG, dilute base (pH=11) treated archaeological charcoal, and SRHA, which was dissolved in ammonium ac-

etate and methanol (1:1), to compare their optical absorbance properties (Figure. 5.8 (top)). All three spectra start absorbing light near 450 nm. aOG shows two main absorption peaks at around 230 and 300 nm, which were described in Chapter 2 (Section 2.3.4). A featureless absorption spectrum with a shoulder around 270 nm is observed for SRHA. Although the SRHA spectrum does not show a distinct peak at 230 nm like aOG, the overall absorption spectra look similar. The UV spectrum of dilute base (pH=11) soluble portion of archaeological charcoal shows the same peak near 225 nm compared with aOG.

These results suggest that oxidized graphite might exist in the dilute base (pH=11) treated archaeological charcoal. However, the differences in the UV results are not big enough to differentiate oxidized graphenic materials and HA, if any, in the base soluble portion of archaeological charcoal.

Figure 5.8 (bottom) compares SEC-UV chromatograms of aOG and SRHA (dissolved in ammonium acetate/methanol) with the base soluble portion of archaeological charcoal at 250 nm. aOG chromatogram shows a peak near 2 min. The other two chromatograms have characteristic peaks near 9 and 9.5 min. Our results show that either there is no oxidized graphite in the base soluble portion of archaeological charcoal or it is likely that these molecules are smaller than HA, and they elute at higher retention time like the peak at 13 min. It is assumed that the interactions between the column and analytes are negligible, but it has not been proved for our samples. If this assumption is not reliable, oxidized graphite in base soluble portion of archaeological charcoal will interact with column and elute at higher retention time. The interaction of HA and oxidized graphenic materials with each other should be studied since it might affect the retention time.

Recall that, aOG is made of highly oxidized low molecular weight compounds called OD and larger GO sheets. Results showed that water degrades aOG, breaking

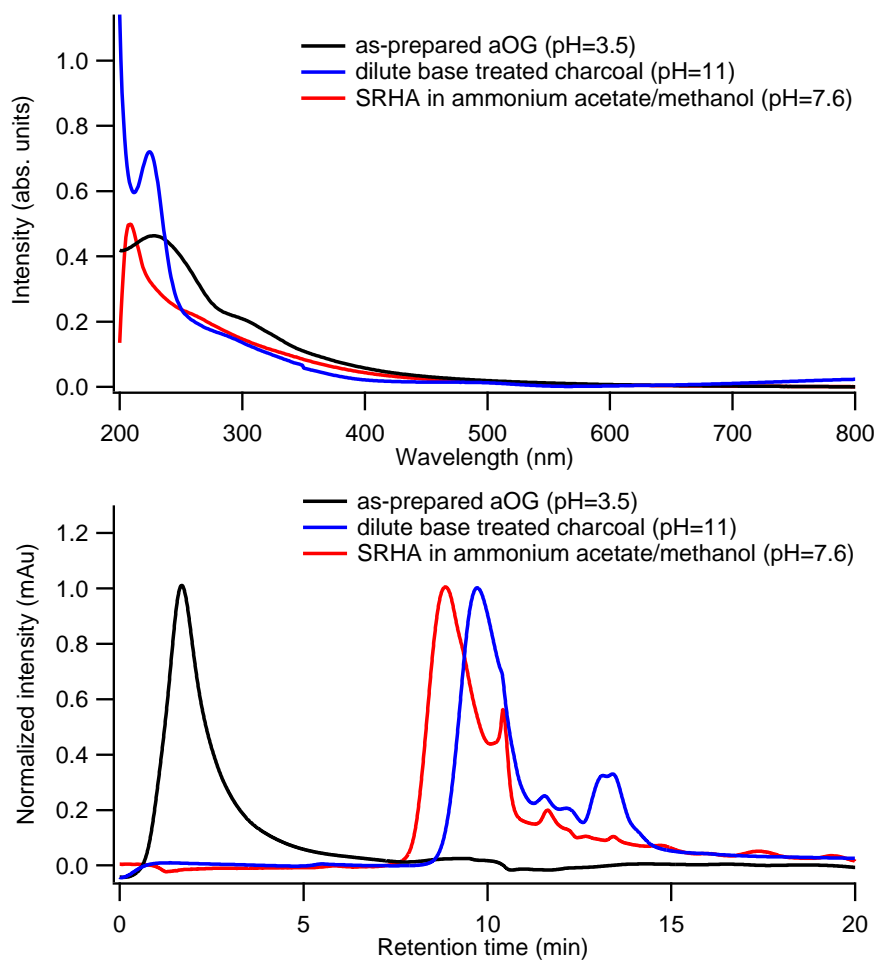


Figure 5.8: Representative UV-Vis spectra of (black) as-prepared oxidized graphite (aOG), (blue) dilute base (pH=11) treated archaeological charcoal, and (red) Suwannee River Humic Acid (SRHA) dissolved in ammonium acetate and methanol. Normalized chromatograms of aOG, dilute base (pH=11) treated archaeological charcoal, and SRHA dissolved in acetate and methanol at 250 nm.

it into smaller pieces through C-C bonds cleavage followed by an acidification process [11]. Therefore, we can also suggest that the peak at 13 min might be associated with the elution of OD. To confirm if this is true, one could do SEC-UV on the lab-prepared OD, and OD obtained from WSBA on archaeological charcoal, then compare the retention time and optical absorbance properties with the one we obtained here.

Our SEC-UV result for dilute base (pH=11) treated archaeological charcoal shows at least four separate components (Figure 5.8 bottom), while SEC-UV obtained from BrC depicts three components [8]. The absorption intensity of both BrC and dilute base (pH=11) treated archaeological charcoal increases as detection wavelength decreases. SEC-UV result for the dilute base (pH=11) treated archaeological charcoal depicts a front absorption starting near 8.5 min with the maximum absorption near 10 min (Figure 5.8 bottom). However, the SEC-UV result for BrC demonstrates absorbing species in which the absorption starts around 6 min with a maximum absorption peak approximately at 7 min [8]. It shows that atmospheric BrC particles are larger than terrestrial BrC in the dilute base (pH=11) treated archaeological charcoal.

## 5.4 UV analysis of graphenic materials

As explained in Chapter 1 (Section 1.3.2), acid and base (mild and strong pH) treatments cause significant damages to both reference and environmentally-altered sources of graphenic carbon materials. The acid and base treatments might cause these materials to come off the liquid supernatants. In this chapter, we also demonstrated that oxidized carbon might come off from archaeological charcoal after dilute alkaline (pH=11) treatment. Therefore, we decided to analyze liquid phases of graphite flakes and modern charcoal (as reference graphenic materials) along with coal and another fossil charcoal (as other environmentally altered graphenic sources) after acid (1M

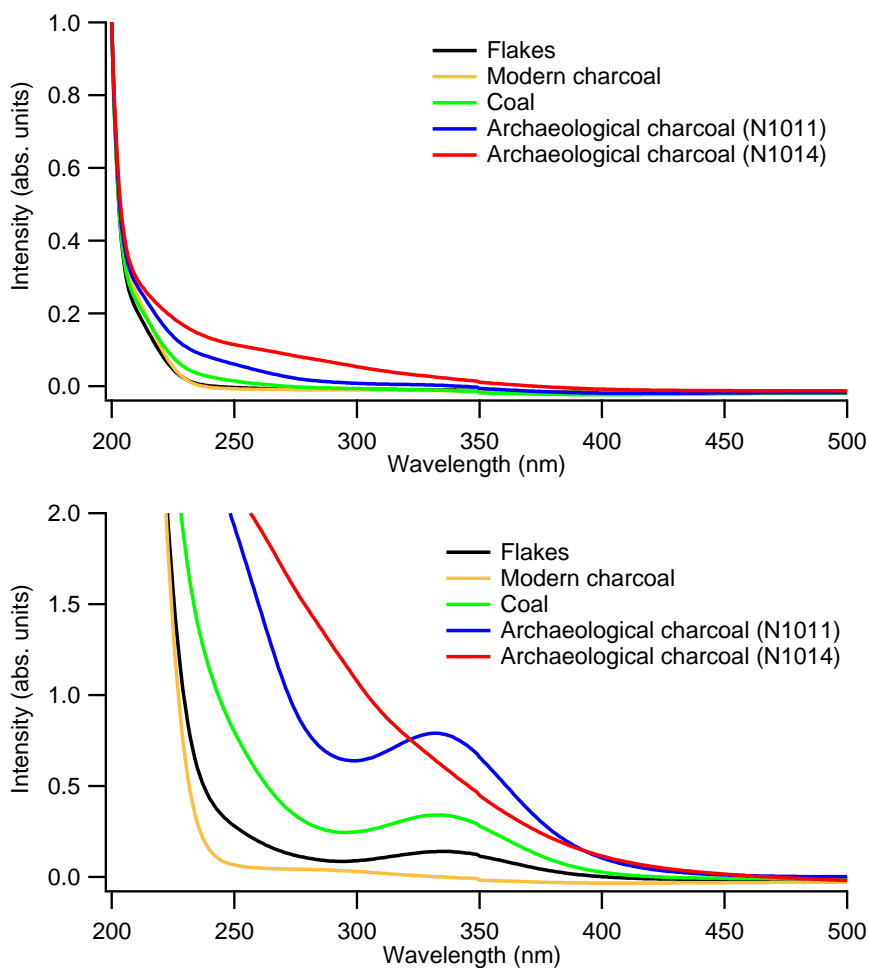


Figure 5.9: Representative UV-Vis spectra of (top) diluted and (bottom) non-diluted supernatants of acid treated graphite, modern charcoal, coal, and two different sources of archaeological charcoal.

HCl) and base (0.1 and 1M NaOH) treatments to monitor the effect of pH on UV-Vis spectroscopic features.

In this set of experiments, 0.4 g of graphite, modern charcoal, coal, and two different sources of archaeological charcoal were separately treated with 1M HCl at 40 °C for 1 hour under stirring condition (800 rpm). The suspensions were then centrifuged at 8,500 rpm for 15 min. The acidic supernatants were used for UV measurement, and the residuals were neutralized and prepared for the subsequent base treatments. The residual solid for each sample was divided into two portions.

The first portion was treated with 0.1M NaOH, while the second one was treated with 1M NaOH at 40 °C for 1 hour under stirring condition (800 rpm). The residuals and supernatants, for each portion, were separated by centrifuge at 8,500 rpm for 15 min. The dilute and concentrated alkaline (pH=11 and 13) supernatants were also analyzed by UV spectroscopy. It is worth noting that all the supernatants were diluted in nanopure water and then analyzed by UV.

Figures 5.9, 5.10, and 5.11 (bottom) show the original supernatants obtained after each treatment. This will help us to see a better resolution for weaker peaks and the difference in the starting absorption band of each analyte.

Figure 5.9 (top) shows UV-Vis results collected from the diluted acidic supernatants of graphite, modern charcoal, coal, and two different sources of archaeological charcoal. These spectra show no distinguishable peaks. UV-Vis spectra of two archaeological charcoal samples show absorption starting from 300 and 350 nm. This could be due to the removal of fulvic acid (FA) from the samples [5], but we have not attempted a direct spectral comparison. However, the concentrated supernatants of all samples demonstrate a peak around 330 nm except archaeological charcoal and modern charcoal (Figure 5.9 (bottom)). Researchers found that environmentally altered source of graphite-like coal is reacted with even diluted  $\text{HNO}_3$  or  $\text{H}_2\text{SO}_4$  that form carbon nanoparticles [12, 13]. These carbon-based nanostructures, with lateral dimensions less than 10 nm, are used to study photoluminescence property of carbon materials [14, 15]. Vinci *et al.* analyzed a mixture of carbon nanoparticles (CNPs) and proposed that Peaks below 300 nm could be assigned to  $\pi^* \leftarrow \pi$  electron transitions, whereas the bands above 300 nm are associated with  $\pi^* \leftarrow n$  of C=O bonding in a mixture of CNPs [16]. Although it is not clear whether the reaction of our samples with HCl can yield CNPs or GQDs, it shows that acid treatment removes materials that cause UV absorption.

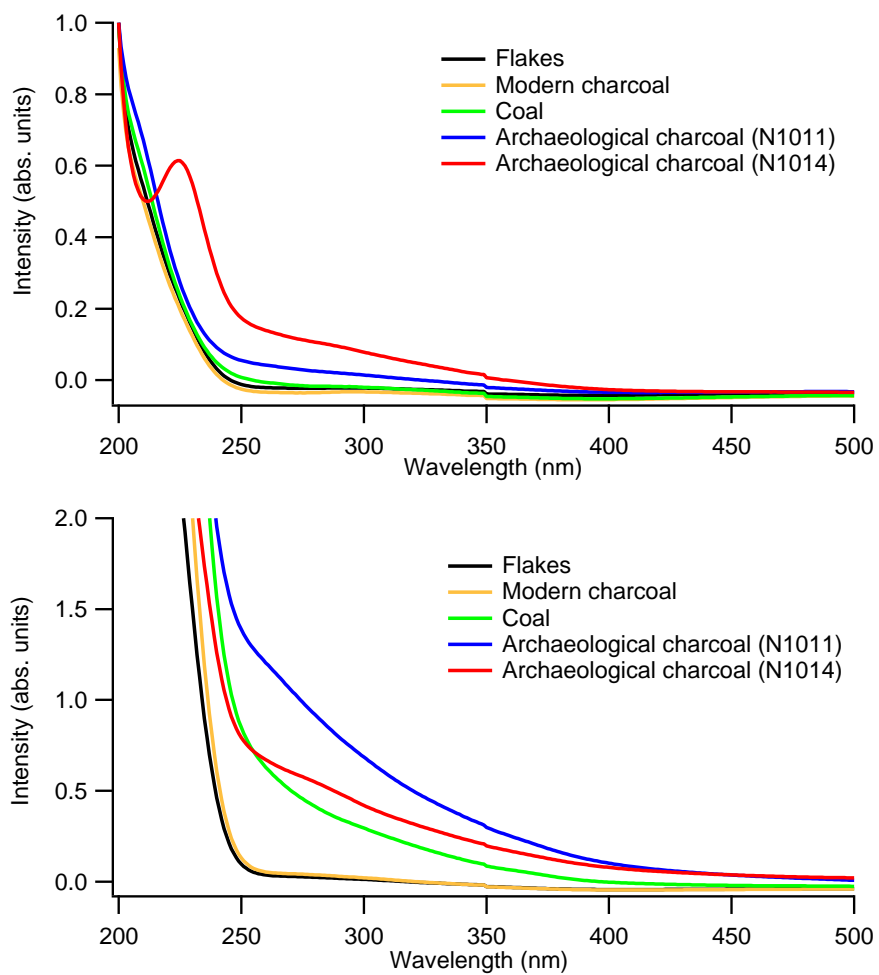


Figure 5.10: Representative UV-Vis spectra of (top) diluted and (bottom) non-diluted supernatants of base (0.1M) treated graphite, modern charcoal, coal, and two different sources of archaeological charcoal.

Additionally, we analyzed the dilute and concentrated base (pH=11 and 13) treated acid-washed samples by UV spectroscopy to monitor the impacts of mild and strong pH conditions on graphenic materials and see whether these conditions cause the removal of GO. Figure 5.11 (top) compares UV-Vis spectra of the base (0.1M) treated acid-washed archaeological charcoal we analyzed earlier with another fossil charcoal and sources of graphenic materials. Here, we observe that the coal and the second source of fossil charcoal show no peaks in the UV region, unlike the first archaeological charcoal sample. Figure 5.11 (bottom) demonstrates no absorption in UV-Vis regions for non-diluted graphite flakes and modern charcoal, while environmentally altered sources of graphite show absorption band starting from 450 nm due to the removal of fluorescent materials like humic substances [5].

On the other hand, the UV-Vis analysis of all base (1M) treated acid-washed graphenic materials do not show any distinguishable peaks (Figure 5.10 (top)), except strong absorption bands for environmentally-altered sources of graphite including coal and two sources of archaeological charcoal starting from 750 nm (Figure 5.10 (bottom)). Others have shown that concentrated alkaline (pH=13) solution removes humic substances from archaeological charcoal, leaving a dark brown supernatant behind [17].

Our results demonstrate that acid (1M HCl) treatment removes materials from both reference and environmentally altered sources of graphite. It also shows the emergence of oxidized carbon materials after dilute alkaline (pH=11) treatment of an archaeological charcoal sample.

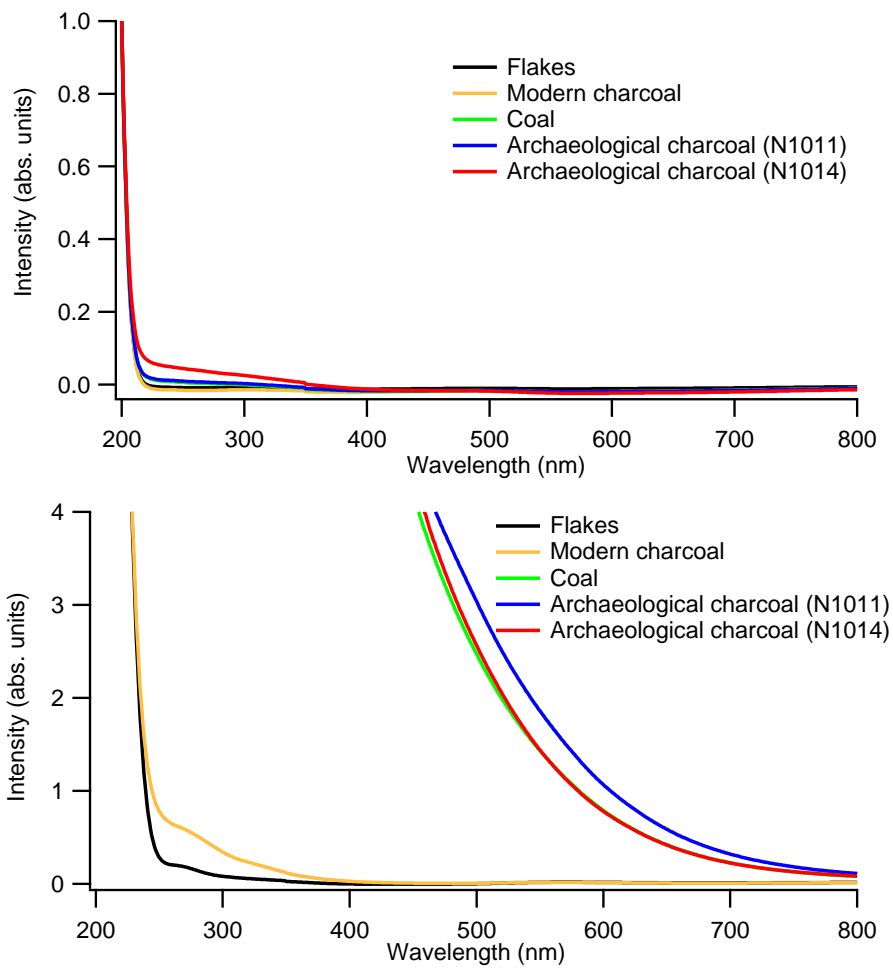


Figure 5.11: Representative UV spectra of (top) diluted and (bottom) non-diluted supernatants of base (1M) treated graphite, modern charcoal, coal, and two different sources of archaeological charcoal.

## 5.5 Conclusions

In this chapter, we show how pH (acidic or basic) affects the ability of aOG to stay suspended in the solution. We show that concentrated base (pH=13) separates aOG into a clear colourless suspension and dark brown residuals. Researchers believe that the clear colourless suspension contains lower molecular weight materials compared with the residual [3]. Thus, we expect pH adjustment has important implications for using SEC-UV to assess the size of suspended materials.

We also show that solvent composition can change the UV-Vis features of HA. Our SEC-UV results show that the dilute base (pH=11) soluble portion of archaeological charcoal has slightly shorter retention time (size) relative to a common HA standard and atmospheric BrC. We should note that buffer is used for all SEC-UV measurements, but we have not yet compared with bulk UV-Vis in buffered solutions.

## 5.6 Acknowledgments

As the first author, I did the size exclusion chromatography experiments in collaboration with Dr. Cora Young using the same experimental conditions as Di Lorenzo and Young [8]. I contributed to the collection and analysis of all experimental data.

## Bibliography

- [1] Edwin A. Olson and W. S. Broecker. Section of Geology and Mineralogy: Sample Contamination and Reliability of Radiocarbon Dates. *Trans. N. Y. Acad. Sci.*, 20(7 Series II):593–604, 1958.
- [2] Helen R. Thomas, Stephen P. Day, William E. Woodruff, Cristina Valles, Robert J. Young, Ian A. Kinloch, Gavin W. Morley, John V. Hanna, Neil R. Wilson, and Jonathan P. Rourke. Deoxygenation of Graphene Oxide: Reduction or Cleaning? *Chem. Mater.*, 25(18):3580–3588, 2013.
- [3] Jonathan P. Rourke, Priyanka A. Pandey, Joseph J. Moore, Matthew Bates, Ian A. Kinloch, Robert J. Young, and Neil R. Wilson. The Real Graphene Oxide Revealed: Stripping the Oxidative Debris from the Graphene-like Sheets. *Angew. Chem.*, 50(14):3173–3177, 2011.
- [4] Ayrat Dimiev, Dmitry V. Kosynkin, Lawrence B. Alemany, Pavel Chaguine, and James M. Tour. Pristine Graphite Oxide. *J. Am. Chem. Soc.*, 134(5):2815–2822, 2012.
- [5] Ki-Hoon Kang, Hyun Sang Shin, and Heekyung Park. Characterization of humic substances present in landfill leachates with different landfill ages and its implications. *Water Res.*, 36(16):4023 – 4032, 2002.
- [6] Gary D. Christian. *Analytical chemistry*. Wiley, New York, 2d ed.. edition, 1977.
- [7] Daniel C. Harris. *Quantitative chemical analysis*. W.H. Freeman ; Palgrave Macmillan, 6th edition, 2002.

- [8] Robert A. Di Lorenzo and Cora J. Young. Size separation method for absorption characterization in brown carbon: Application to an aged biomass burning sample. *Geophys. Res. Lett.*, 43(1):458–465, 2016.
- [9] Martin Rosillo-Lopez and Christoph G. Salzmann. A simple and mild chemical oxidation route to high-purity nano-graphene oxide. *Carbon*, 106:56–63, 2016.
- [10] Donald L. Pavia. *Introduction to spectroscopy*. Brooks/Cole, Cengage Learning, Australia ; Belmont, CA, 4th edition, 2009.
- [11] Ayrat M. Dimiev, Lawrence B. Alemany, and James M. Tour. Graphene Oxide. Origin of Acidity, Its Instability in Water, and a New Dynamic Structural Model. *ACS Nano*, 7(1):576–588, 2013.
- [12] Yu. Shchipunov, O. Khlebnikov, and V. Silantev. Carbon quantum dots hydrothermally synthesized from chitin. *J. Polym. Sci. B*, 57(1):16–22, 2015.
- [13] Yongqiang Dong, Jianpeng Lin, Yingmei Chen, Fengfu Fu, Yuwu Chi, and Guonan Chen. Graphene quantum dots, graphene oxide, carbon quantum dots and graphite nanocrystals in coals. *Nanoscale*, 6(13):7410–7415, 2014.
- [14] Alberto Bianco, Hui-Ming Cheng, Toshiaki Enoki, Yuri Gogotsi, Robert H. Hunt, Nikhil Koratkar, Takashi Kyotani, Marc Monthieux, Chong Rae Park, Juan M. D. Tascon, and Jin Zhang. All in the graphene family - A recommended nomenclature for two-dimensional carbon materials. *Carbon*, 65:1–6, 2013.
- [15] Sofia Paulo, Emilio Palomares, and Eugenia Martinez-Ferrero. Graphene and Carbon Quantum Dot-Based Materials in Photovoltaic Devices: From Synthesis to Applications. *Nanomaterials (Basel, Switzerland)*, 6(9), 2016.

- [16] John C. Vinci, Ivonne M. Ferrer, Steven J. Seedhouse, Allen K. Bourdon, Justin M. Reynard, Barbara A. Foster, Frank V. Bright, and Luis A. Colon. Hidden Properties of Carbon Dots Revealed After HPLC Fractionation. *J. Phys. Chem. Lett.*, 4(2):239–243, 2013.
- [17] N. R. Rebollo, I. Cohen-Ofri, R. Popovitz-Biro, O. Bar-Yosef, L. Meignen, P. Goldberg, S. Weiner, and E. Boaretto. Structural Characterization of Charcoal Exposed to High and Low pH: Implications for  $^{14}\text{C}$  Sample Preparation and Charcoal Preservation. *Radiocarbon*, 50(2):289–307, 2008.

# Chapter 6

## Conclusions

This work showed that a mixture of graphite and oxidized graphite can be separated using our protocol (water-sonication-base-acid (WSBA)) to yield oxidized graphenic materials like graphene oxide (GO) and oxidative debris (OD). A synergy between the chemistry involved in the separation of GO and OD from as-prepared oxidized graphite (aOG), and the radiocarbon dating cleaning procedure on graphenic carbon materials helped to design WSBA. We demonstrated that sonication near neutral conditions breaks aOG into smaller particles more easily than graphite. This process helped to separate aOG from graphite in a mixture. These findings help to understand the reasons why conventional ABA cleaning procedure sometimes breaks down poorly preserved charred graphenic materials. They are also promising and helpful to take a further step for the separation of oxidized graphenic materials from archaeological sources of charred graphenic materials.

A combination of analyses using vibrational spectroscopy (Raman and infrared) and pH measurements on the uncleaned archaeological charcoal suggests that a mixture of oxidized carbon materials are present in the sample. WSBA on archaeological charcoal helped to separate three groups of oxidized graphenic materials with different

levels of oxidation: the least, moderate, and the highest. For the future work, these materials can be used as potential sources for radiocarbon dating purposes, especially for poorly preserved charred graphenic materials where all sample sometimes diminish during the cleaning procedure, leaving no solid behind to be dated.

UV-Vis analyses on the supernatants of acid and base treated reference, and environmentally altered sources of graphenic materials demonstrate that pH plays an important role in the spectroscopic features of the samples. The pH of the blank itself shows different absorption features. It also causes graphenic samples to behave differently since it affects the way they suspend in the solution. UV-Vis spectroscopy shows the evidence of oxidized carbon in the supernatant of the base (0.1 M NaOH) treated archaeological charcoal, but it is not capable of differentiating it from contaminants like humic acid (HA). Size exclusion chromatography coupled with a UV detector (SEC-UV), on the base soluble portion of archaeological charcoal, showed compounds with similar UV response and retention time compared with HA.

In this thesis, I explored the presence of oxidized graphenic materials in archaeological charcoal as an environmentally-altered source of graphenic materials through several characterization techniques. However, there is also a possibility that carbonaceous contaminants like HA are present in the sample. These findings will help researchers who work with environmentally-altered graphenic carbon materials either for the chemistry or radiocarbon dating perspectives. This research provides information about handling a mixture of graphite and oxidized graphite to obtain oxidized graphenic materials. This helps archaeologists who deal with graphenic materials like charcoal to optimize their cleaning procedures for poorly preserved samples. The extraction of oxidized graphenic materials in archaeological charcoal has the potential to introduce other viable sources of graphenic carbon materials for radiocarbon dating.

# Appendix A

## Supporting information

In this appendix, I provide results for side projects.

### A.1 Effects of pH and temperature on the Raman spectra of coal

Researchers found that pH plays an important role in the chemistry of graphite-like materials. The concentrated acid rinse expands graphite layers and creates defects to remove intercalated counterions [1,2] and mineralized carbonates [3]. Base treatment at pH=11 not only removes humic substances, [3–5] but also exfoliates graphite layers [6]. Others found that soluble and sedimented fractions, obtained after ABA treatment, in fossil charcoal yield statistically similar dates [7]. This suggests that acid and base wash remove original carbon in fossil charcoal. Graphene oxide (GO) is hydrophilic and degrades gradually in water producing  $H^+$  ions [8,9]. When graphene oxide is treated with NaOH (1M), 35 percent of mass loss occurs due to the removal of oxidative debris (OD). Temperature is another contributing factor that affects graphite structure during the aqueous treatment. Eigler *et al.* showed that the struc-

ture of GO is not stable after base treatment at 40 °C.

Figure A.1 shows raw Raman spectra that are grouped according to acidic, basic, or water treatments. The most apparent differences are in the background intensity, which we assume are related to fluorescence, based on earlier work by Alon *et al.* [5]. It is a messy figure, but the colour groupings highlight an exciting trend. The coloured plots correspond to different treatment temperatures. Although base treatment at any temperature consistently reduces the background intensity, acid and water treatment introduce more variability in the background intensity. However, spectra obtained after aqueous treatments at different pH and temperatures on coal did not show any specific changes in D to G intensity ratio or peak positions to confirm graphite structural changes.

To do a precise analysis of the spectral changes of treated samples, I obtained the D to G intensity ratio and D-width for each spectrum and compared them with each other. Before showing the results, I give an example to describe how I analyzed the data to get the D/G intensity, D-width, and error bar from a raw spectrum. Figure A.2a shows a raw spectrum of acid treated coal at 23 °C. I obtained all necessary information about Raman peaks through analysis of a Raman spectrum using IGOR Pro with the "Multi-peak fitting 2" package applying polynomial baseline corrections and either Gaussian or Lorentzian peak shapes. Figure A.2b shows the fitted peak indicating the D and G peaks.

Figure A.3 compares D to G intensity against D width, grouped according to acidic, basic, or water treatments. There is considerable variability in the D to G intensity ratio and D width among spectra from different spots on the same sample. Earlier reports show that this is quite common, even for laboratory-produced graphene oxide [10]. Our results show that there is no significant difference after base treatment at 23 °C, while base treatments at higher temperatures tend to increase the width and

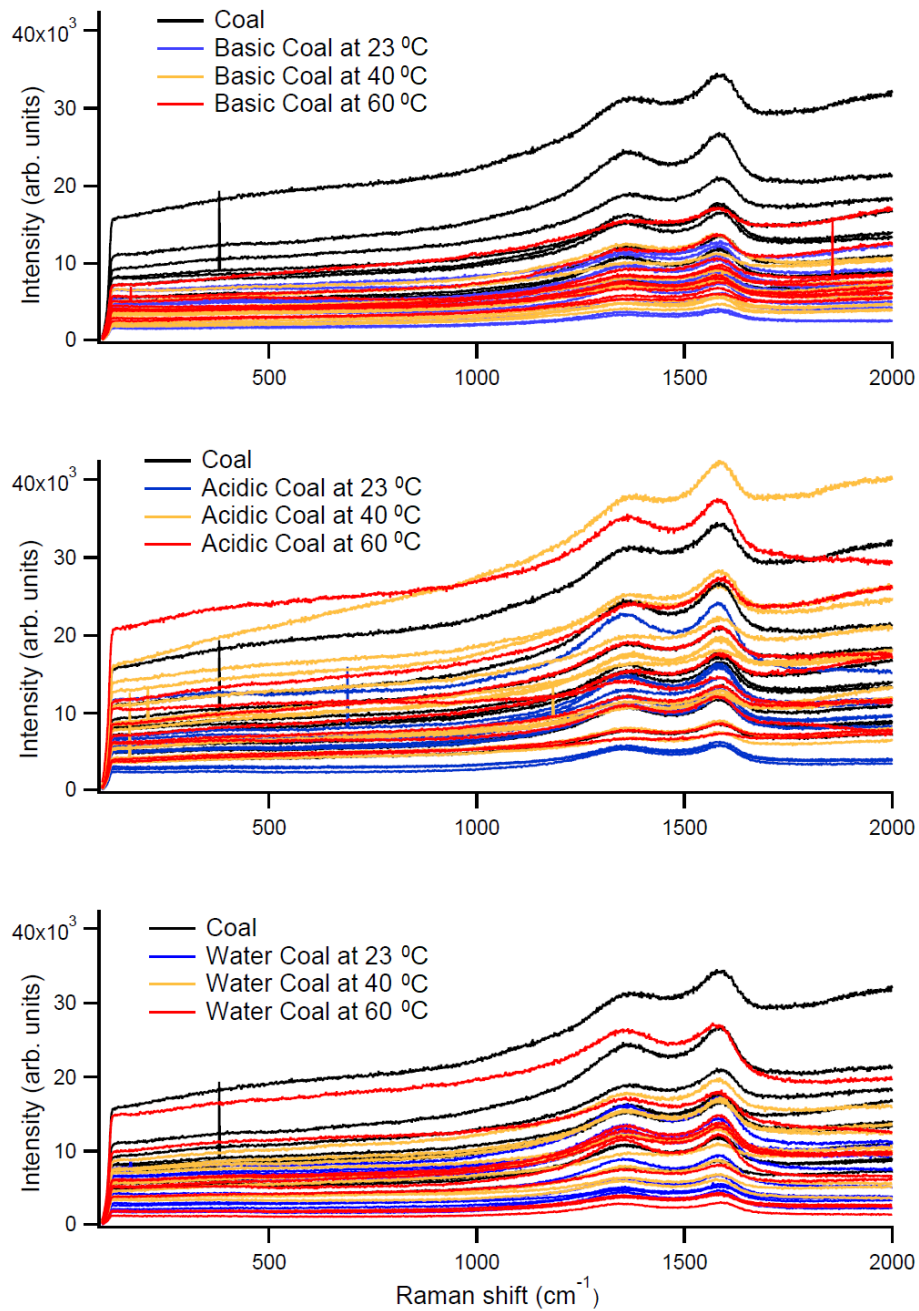


Figure A.1: The Raman spectra of coal before and after base (top), acid (middle), or water (bottom) treatments at different temperatures. The same original (before treatment) coal spectra are shown in black on all three plots.

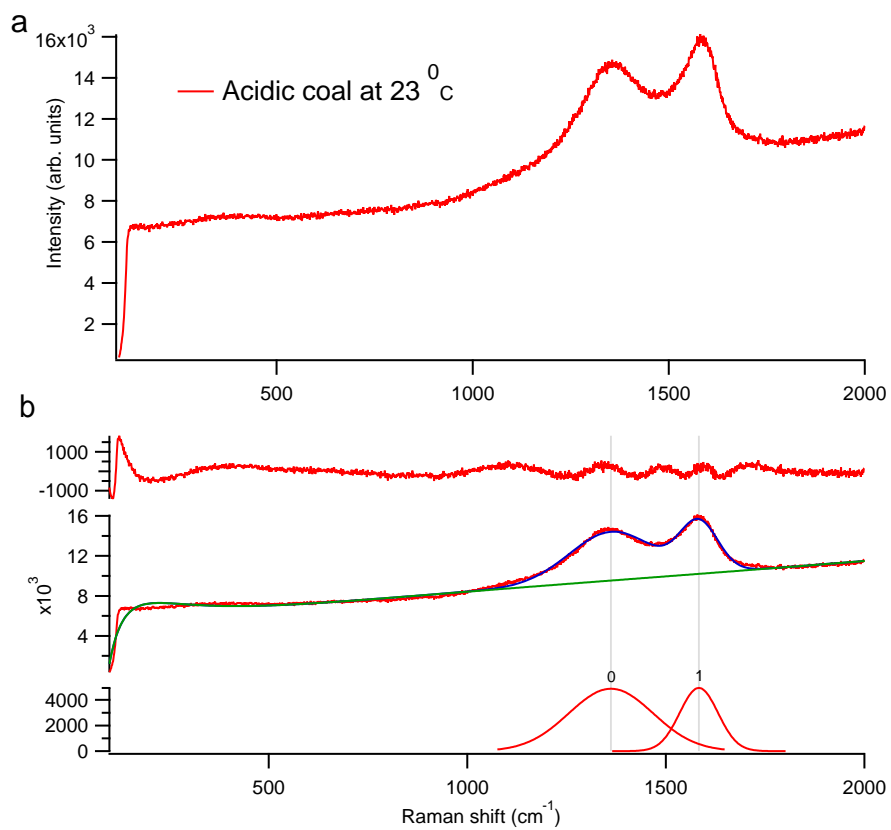


Figure A.2: Representative (a) raw and (b) analyzed Raman spectra of acidic coal at  $23^\circ\text{C}$ .

relative intensity of the D peak. We suspect this is due to the elimination of functional groups or cleavage of the oxidized graphite structure [10]. Acid treatment at high and low temperatures cause a larger spread in both width and relative intensity of the D peak. Studies have shown that even treatment of natural graphite with acid (HCl) expands graphite layers [2]. It was also observed that modern charcoal, even with optimal preservation and a higher proportion of crystalline graphite compared with fossil charcoal, experienced weight loss after HCl treatment [11]. Hence, we infer that acid (1M HCl) treatment leads to structural changes in the graphite-like materials structures in coal.

Water treatment shows an interesting effect: at all temperatures, water increases the relative intensity of the D peak but doesn't cause a significant change in the D peak width. Water can remove water-soluble materials such as oxidized graphite and humic substances from the sample.

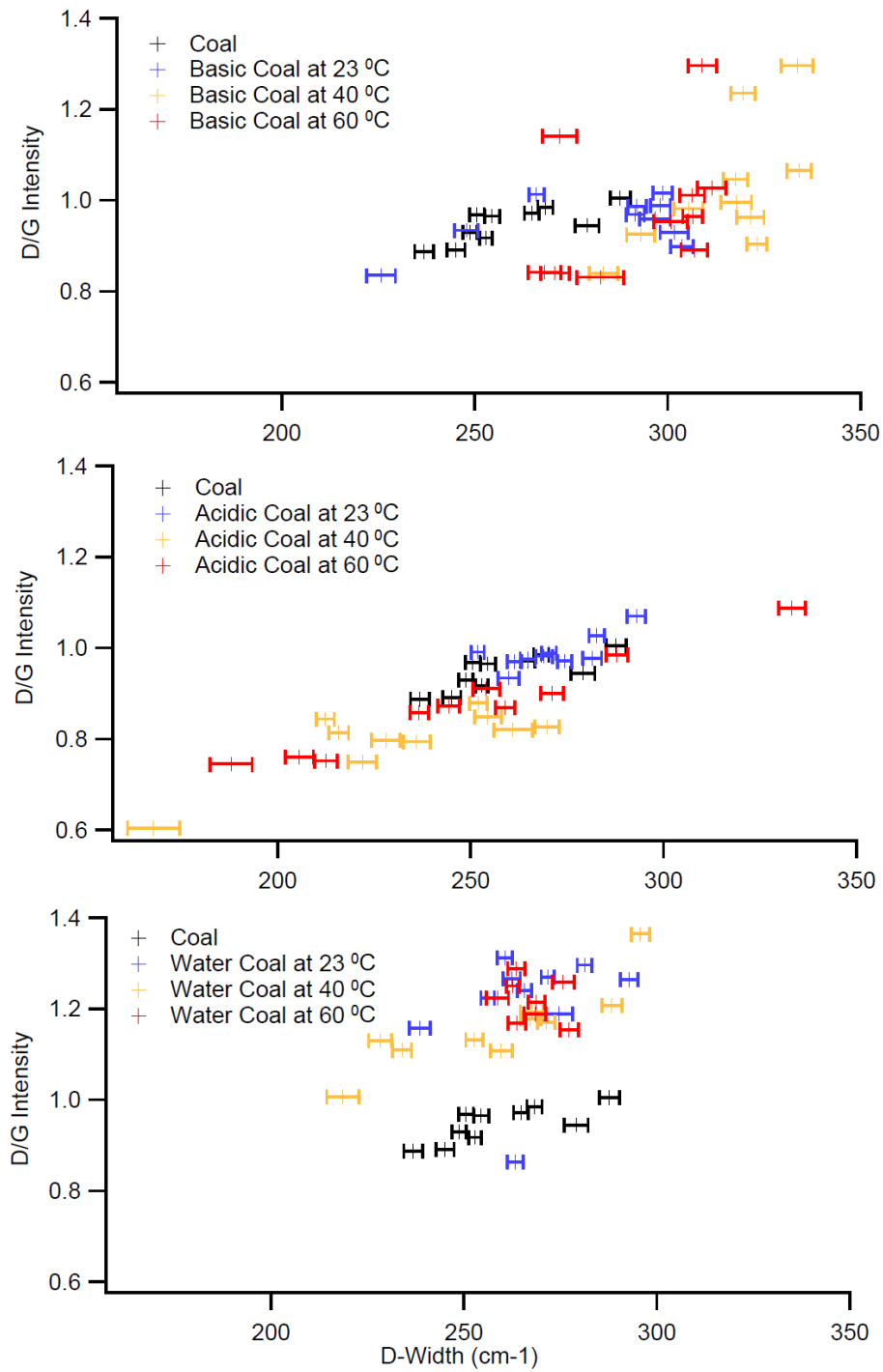


Figure A.3: Comparing D to G intensity *vs.* D peak widths before and after either a basic (top), acidic (middle), or water treatment. The same original (before treatment) coal values are shown in black on all three plots; coloured plots correspond to different treatment temperatures.

## A.2 Homogenization of oxidized materials

In Chapter 4, we suggested that a mixture of oxidized and non-oxidized graphite materials might be present in archaeological charcoal. Also, IR data from WSBA on the uncleaned archaeological charcoal confirmed that the least, moderate, and highly oxidized materials exist in the sample. Since oxidation levels of these oxidized materials are not uniquely defined, we oxidize archaeological charcoal to see if we can transform non-oxidized portion to a uniform oxidized materials like what we did for graphite flakes, then separate GO and OD from oxidized materials.

Surprisingly, the uncleaned archaeological charcoal does not undergo oxidation to get as-prepared oxidized graphite (aOG) like the graphite flakes (Figure A.4a). Results show that D and G peak positions remain the same after oxidation. However, background intensity decreases after the treatment that might be due to the removal of oxidizable carbon [12].

To find out whether it only occurs for one particular sample, we also oxidized uncleaned coal as another source of naturally occurring graphite materials. Figure A.4b compares the Raman spectra of a coal sample before and after oxidation. Like uncleaned archaeological charcoal, D and G peak positions do not change after the chemical oxidation.

These results suggest that the non-oxidized portion might not be accessible for oxidizing agents. Archaeological charcoal is a heterogeneous sample, which means that it contains a mixture of materials with non-uniform compositions. Dimiev *et al.* suggest that the morphology, size, and structural characteristics of flakes affects diffusion rate of oxidizing agents, which causes different oxidation degree [13]. They found that the formation of GO consists of three steps. In the first step, sulfuric acid intercalates graphite layers to make graphite intercalation compound (GIC), and then oxidizing agents penetrate between the layers to make pristine graphite oxide (PGO).

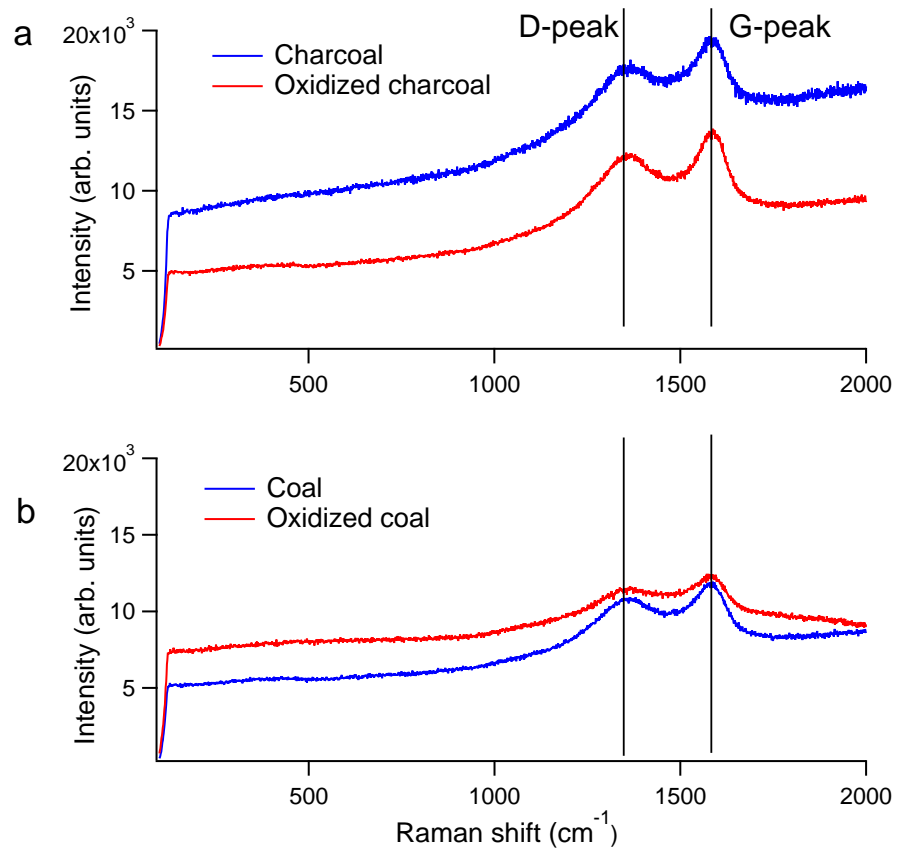


Figure A.4: Raman spectra of (top) archaeological charcoal and (bottom) coal samples (blue) before and (red) after chemical oxidation.

In the last step, water exfoliates graphite oxide to have single layer GO.

Our results confirm that the non-oxidized graphite, in archaeological charcoal, does not undergo chemical oxidation to yield GO the same as graphite flakes do. This might lead us to conclude the graphite in archaeological charcoal is already in an oxidized form.

## Bibliography

- [1] Emir Bouleghlimat, Philip R. Davies, Robert J. Davies, Rebecca Howarth, Jiri Kulhavy, and David J. Morgan. The effect of acid treatment on the surface chemistry and topography of graphite. *Carbon*, 61:124–133, 2013.
- [2] Feiyu Kang, Yang Leng, Tong-Yi Zhang, and Bensheng Li. Electrochemical synthesis and characterization of ferric chloride-graphite intercalation compounds in aqueous solution. *Carbon*, 36(4):383–390, 1998.
- [3] N. R. Rebollo, I. Cohen-Ofri, R. Popovitz-Biro, O. Bar-Yosef, L. Meignen, P. Goldberg, S. Weiner, and E. Boaretto. Structural Characterization of Charcoal Exposed to High and Low pH: Implications for  $^{14}\text{C}$  Sample Preparation and Charcoal Preservation. *Radiocarbon*, 50(2):289–307, 2008.
- [4] Edwin A. Olson and W. S. Broecker. Section of Geology and Mineralogy: Sample Contamination and Reliability of Radiocarbon Dates. *Trans. N. Y. Acad. Sci.*, 20(7 Series II):593–604, 1958.
- [5] Dani Alon, Genia Mintz, Illit Cohen, Steve Weiner, and Elisabetta Boaretto. The use of Raman spectroscopy to monitor the removal of humic substances from charcoal; quality control for  $^{14}\text{C}$  dating of charcoal. *Radiocarbon*, 44(1):1–11, 2002.
- [6] Karen B. Ricardo, Anne Sendeck, and Haitao Liu. Surfactant-free exfoliation of graphite in aqueous solutions. *ChemComm*, 50(21):2751–2754, 2014.
- [7] E. M. Wild, P. Steier, P. Fischer, and F. Hofmayer.  $^{14}\text{C}$  Dating of Humic Acids from Bronze and Iron Age Plant Remains from the Eastern Mediterranean. *Radiocarbon*, 55(02):599–607, 2013.

- [8] Ayrat M. Dimiev, Lawrence B. Alemany, and James M. Tour. Graphene Oxide. Origin of Acidity, Its Instability in Water, and a New Dynamic Structural Model. *ACS Nano*, 7(1):576–588, 2013.
- [9] Jonathan P. Rourke, Priyanka A. Pandey, Joseph J. Moore, Matthew Bates, Ian A. Kinloch, Robert J. Young, and Neil R. Wilson. The Real Graphene Oxide Revealed: Stripping the Oxidative Debris from the Graphene-like Sheets. *Angew. Chem.*, 50(14):3173–3177, 2011.
- [10] Siegfried Eigler, Michael Enzelberger-Heim, Stefan Grimm, Philipp Hofmann, Wolfgang Kroener, Andreas Geworski, Christoph Dotzer, Michael Rockert, Jie Xiao, Christian Papp, Ole Lytken, Hans-Peter Steinruck, Paul Muller, and Andreas Hirsch. Wet Chemical Synthesis of Graphene. *Adv. Mater.*, 25(26):3583–3587, 2013.
- [11] Ilit Cohen-Ofri, Lev Weiner, Elisabetta Boaretto, Genia Mintz, and Steve Weiner. Modern and fossil charcoal: aspects of structure and diagenesis. *J. Archaeol. Sci.*, 33(3):428 – 439, 2006.
- [12] M. I. Bird, L. K. Ayliffe, L. K. Fifield, C. S. M. Turney, R. G. Cresswell, T. T. Barrows, and B. David. Radiocarbon Dating of “Old” Charcoal Using a Wet Oxidation, Stepped-Combustion Procedure. *Radiocarbon*, 41(2):127–140, 1999.
- [13] Ayrat M. Dimiev and James M. Tour. Mechanism of Graphene Oxide Formation. *ACS Nano*, 8(3):3060–3068, 2014.